

**POLITECNICO DI TORINO**

**Master of Science in Mechanical Engineering**



Master's Degree Thesis

**Hard turning of Inconel DA 718 using PVD nanocomposite coatings for carbide insert: performance improvement and Three-Dimensional tool wear assessment**

**Supervisor**

Prof. Luca Settineri

Prof. Stephen Veldhuis

**Author**

Silvio Capasso

**Correlator**

Prof. Giovanni Belingardi

Dr. José Mario Fernandes Paiva JR.

September 2018



*To those who have always believed in me.  
I realized a dream,  
I kept a promise.*



# Abstract

Several current studies revolve around manufacturing components made by Inconel 718, one of the most used superalloys for crucial applications in modern aerospace and automotive industries, because its mechanical, chemical and physical properties lead to a complex and expensive machining of the material. The purpose of this research is to test PVD nanocomposite coatings for carbide tools made by Ti-Al-Cr nitrates in a Si-based amorphous matrix for turning direct-aged Inconel 718, under different cutting conditions.

According to the results of a developed analytical model for optimization and the current usage in industry, a range of cutting speeds have been experimentally tested. Tool wear evaluation and data analysis of efficiency parameters have been performed to determine the condition allowing most costs reduction and productivity improvements. The tool wear modes and mechanisms have been investigated by optical, Focus-Variable and scanning electron microscopes, in order to get information about flank wear as well as 3D-volume wear.

The traditional mono and the three-dimensional methodologies for defining the tool wear have been compared to find a correlation between the end of tool life limits. Thanks to the wide range of data, a predictive model for flank wear has been developed. Furthermore, since the 3D wear resembled to grow exponentially, a fitting model has been formulated to prove this tendency.



# Contents

<b>CHAPTER 1: INTRODUCTION .....</b>	<b>1</b>
1.1 DESCRIPTION OF THE PROJECT.....	1
1.2 OBJECTIVES .....	4
<b>CHAPTER 2: LITERATURE REVIEW .....</b>	<b>5</b>
2.1 INCONEL DA 718.....	5
2.2 MACHINING OF INCONEL DA 718.....	9
2.3 CUTTING TOOLS .....	11
2.4 TRIBOLOGY OF METAL CUTTING.....	21
2.5 EQUIPMENT SPECIFICATIONS .....	24
<b>CHAPTER 3: METHODOLOGY .....</b>	<b>27</b>
3.1 TOOLS ARCHITECTURE.....	27
3.2 PRELIMINARY CUTTING TESTS .....	30
3.3 DIGITAL MICROSCOPE ANALYSIS .....	33
3.4 OPTIMIZATION OF CUTTING PARAMETERS .....	35
3.5 EVALUATION OF PERFORMANCE .....	38
3.6 THREE-DIMENSIONAL TOOL WEAR ANALYSIS.....	42
3.7 SCANNING ELECTRON MICROSCOPE (SEM) ANALYSIS.....	44
<b>CHAPTER 4: RESULTS AND DISCUSSION .....</b>	<b>45</b>
4.1 TOOLS ARCHITECTURE.....	45
4.2 PRELIMINARY CUTTING TESTS .....	47
4.3 DIGITAL MICROSCOPE ANALYSIS .....	51
4.4 OPTIMIZATION OF CUTTING PARAMETERS .....	60
4.5 EVALUATION OF PERFORMANCE AND COMPARISON.....	65
4.6 THREE-DIMENSIONAL TOOL WEAR ANALYSIS.....	75
4.7 SCANNING ELECTRON MICROSCOPE (SEM) ANALYSIS.....	86
<b>CHAPTER 5: CONCLUSION .....</b>	<b>91</b>
<b>CHAPTER 6: FUTURE WORKS .....</b>	<b>93</b>



# List of Figures

FIGURE 2.1 – TOOL LIFE COMPARISON BETWEEN AN UNCOATED TOOL AND ALTiCrSiN-BASED COATED TOOL [34].....	12
FIGURE 2.2 – FLANK WEAR FOR A 50 M CUTTING LENGTH UNDER DIFFERENT $V_c$ AND COATING [38] 13	
FIGURE 2.3 – FLANK WEAR [42].....	16
FIGURE 2.4 – CRATER WEAR [42].....	17
FIGURE 2.5 – BUILT-UP EDGE WEAR [42] .....	18
FIGURE 2.6 – NOSE WEAR [42].....	18
FIGURE 2.7 – NOTCH WEAR [42] .....	19
FIGURE 2.8 – THERMAL CRACKS WEAR [42].....	19
FIGURE 2.9 – ISO 3685 STANDARDS TO DETERMINE THE TOOL WEAR FOR CARBIDE INSERTS [40] ....	20
FIGURE 2.10 – DIFFERENT TRIBOLOGICAL CONDITIONS ZONES IN MACHINING PROCESSES [40] .....	22
FIGURE 2.11 – OKUMA CROWN L1060 CNC LATHE .....	24
FIGURE 2.12 – ALICONA INFINITE FOCUS G5 .....	25
FIGURE 2.13 – TESCAN VEGA II LSU SEM .....	26
FIGURE 3.1 – GEOMETRY OF THE TOOLS ISO CNGG120408FS.....	27
FIGURE 3.2 – FROM LEFT TO RIGHT: RAKE FACE, 3D IMAGE, FLANK FACE, 3D-PRINTED SUPPORT ...	33
FIGURE 3.3 – EXAMPLE OF THE MEASUREMENT MADE WITH THE KEYENCE SOFTWARE TO EVALUATE THE FLANK WEAR AFTER A CERTAIN PASS.....	34
FIGURE 3.4 – EXAMPLE OF TCCL MEASUREMENT MADE WITH THE KEYENCE SOFTWARE .....	40
FIGURE 3.5 – EMBEDDED CHIP IN EPOXY RESIN TO MEASURE THE THICKNESS.....	41
FIGURE 3.6 – A GRAPHICAL EXPLANATION OF POST-PROCESS ANALYSIS OF THE 3D CAPTIONS.....	42
FIGURE 4.1 – SEM IMAGE OF THE NANOCOMPOSITE COATING CROSS SECTION .....	46
FIGURE 4.2 – ROUGHNESS OF THE SURFACE OF THE WORKPIECE DURING THE SUBSEQUENT PASSES OF THE CUTTING PROCESS WITH THE NANOCOMPOSITE MULTI-LAYERED COATING.....	48
FIGURE 4.3 – COMPREHENSIVE REPRESENTATION OF THE MACHINED WORKPIECE SURFACE ROUGHNESS ALONG THE TOOL LIFE AT DIFFERENT CUTTING SPEED .....	49
FIGURE 4.4 – THREE-DIMENSIONAL IMAGES OF THE CHIP SURFACE AFTER THE FIRST PASS .....	50
FIGURE 4.5 – TOOL WEAR MICROSCOPIC IMAGES AFTER THE FIRST PASS FOR KC5010 COATING, OBTAINED WITH 200X MAGNIFICATION .....	52
FIGURE 4.6 – TOOL WEAR MICROSCOPIC IMAGES AFTER THE FIRST PASS FOR TiAlCrN/TiCrAl52Si8N COATING, OBTAINED WITH 200X MAGNIFICATION .....	53
FIGURE 4.7 – TOOL WEAR MICROSCOPIC IMAGES AND AFTER $L = 600m$ FOR KC5010 COATING, OBTAINED WITH 200X MAGNIFICATION .....	55
FIGURE 4.8 – TOOL WEAR MICROSCOPIC IMAGES AFTER $L = 600m$ FOR TiAlCrN/TiCrAl52Si8N COATING, OBTAINED WITH 200X MAGNIFICATION .....	56

FIGURE 4.9 – TOOL WEAR MICROSCOPIC IMAGES AT THE END OF LIFE FOR KC5010 COATING, OBTAINED WITH 200X MAGNIFICATION.....	58
FIGURE 4.10 – TOOL WEAR MICROSCOPIC IMAGES AT THE END OF LIFE FOR TiAlCrN/TiCrAl52Si8N COATING, OBTAINED WITH 200X MAGNIFICATION .....	59
FIGURE 4.11 – MINIMUM COST AND MAXIMUM PRODUCTIVITY CUTTING SPEEDS.....	61
FIGURE 4.12 – TOOL WEAR MICROSCOPIC IMAGES FOR KC5010 COATING, OBTAINED WITH 200X MAGNIFICATION, FOR CUTTING SPEED $V_c = 97\text{ m/min}$ .....	63
FIGURE 4.13 – TOOL WEAR MICROSCOPIC IMAGES FOR THE MULTI-LAYERED NANOCOMPOSITE COATING, OBTAINED WITH 200X MAGNIFICATION, FOR CUTTING SPEED $V_c = 97\text{ m/min}$ .....	64
FIGURE 4.14 – TOOL WEAR RATE $TWR\ \mu\text{m}/\text{m}$ VARIATION ALONG THE TOOL LIFE, BASED ON THE VARIATION OF CUTTING SPEED $\text{m}/\text{min}$ FOR THE NANOCOMPOSITE MULTI-LAYERED COATING .....	65
FIGURE 4.15 – INDEX OF PERFORMANCE $IP\ \text{m}^3/\text{min}$ VARIATION ALONG THE TOOL LIFE, BASED ON THE VARIATION OF CUTTING SPEED $\text{m}/\text{min}$ FOR THE NANOCOMPOSITE MULTI-LAYERED COATING.....	67
FIGURE 4.16 – AVERAGE VALUES OF IP FOR TiAlCrN/TiCrAl52Si8N, BASED ON THE VARIATION OF CUTTING SPEED.....	67
FIGURE 4.17 – TCCL COMPARISON AT DIFFERENT CUTTING SPEED BETWEEN KC5010 AND NANOCOMPOSITE COATING .....	68
FIGURE 4.18 – $d_{re}$ MEASUREMENT .....	69
FIGURE 4.19 – TOOL LIFE CURVES COMPARISON BETWEEN KC5010 AND TiAlCrN/TiCrAl52Si8N .....	71
FIGURE 4.20 – FITTING FOR THE PREDICTIVE MODEL OF THE FLANK WEAR EXPERIMENTAL DATA FOR THE NANOCOMPOSITE COATING AT DIFFERENT CUTTING SPEED.....	72
FIGURE 4.21 – COMPARISON OF PERFORMANCE BETWEEN NANOCOMPOSITE AND KC5010, VARYING THE CUTTING SPEED.....	73
FIGURE 4.22 – 3D VOLUME WEAR EVOLUTION ALONG THE TOOL LIFE FOR KC5010 AND TiAlCrN/TiCrAl52Si8N .....	75
FIGURE 4.23 – COMPARISON BETWEEN FLANK WEAR AND 3D VOLUME WEAR TRENDS FOR THE NANOCOMPOSITE AND THE KC5010 COATINGS .....	77
FIGURE 4.24 – 3D VOLUME WEAR EXPONENTIAL FITTING FOR THE NANOCOMPOSITE AND KC5010 COATED TOOLS .....	78
FIGURE 4.25 – BUE EVOLUTION ALONG THE TOOL LIFE FOR KC5010 AND TiAlCrN/TiCrAl52Si8N .....	80
FIGURE 4.26 – 3D FIGURES OF THE WORN COATED TOOLS AFTER $L = 130\text{m}$ .....	81
FIGURE 4.27 – 3D FIGURES OF THE WORN COATED TOOLS AFTER $L = 600\text{m}$ .....	81
FIGURE 4.28 – 3D FIGURES OF THE WORN COATED TOOLS AT END OF TOOL LIFE.....	82
FIGURE 4.29 – 3D VOLUME WEAR TOOL LIFE CURVES AT $V_c = 120\text{ m/min}$ .....	83

FIGURE 4.30 – 3D VOLUME WEAR EXPONENTIAL FITTING FOR THE COATED TOOLS AT $V_c =$ 120 $m/min$ .....	84
FIGURE 4.31 – 3D FIGURES OF THE WORN AT $V_c = 120 m/min$ .....	85
FIGURE 4.32 – SEM IMAGES WITH TWO DIFFERENT MAGNIFICATION AT THE END OF LIFE AT $V_c =$ 80 $m/min$ .....	86
FIGURE 4.33 – SEM IMAGES WITH TWO DIFFERENT MAGNIFICATION AT THE END OF LIFE AT $V_c =$ 120 $m/min$ .....	87
FIGURE 4.34 – EDS ANALYSIS AT THE END OF LIFE FOR KC5010 AT $V_c = 80 m/min$ .....	88
FIGURE 4.35 – EDS ANALYSIS AT THE END OF LIFE FOR NANOCOMPOSITE AT $V_c = 80 m/min$ .....	89
FIGURE 4.36 – EDS ANALYSIS AT THE END OF LIFE FOR KC5010 AT $V_c = 120 m/min$ .....	90
FIGURE 4.37 – EDS ANALYSIS AT THE END OF LIFE FOR NANOCOMPOSITE AT $V_c = 120 m/min$ .....	90



# List of Tables

TABLE 2.1 – CHEMICAL COMPOSITION OF INCONEL 718, CONFORMED TO AMS SPECIFICATIONS [25]	5
TABLE 2.2 – PHYSICAL CONSTANTS AT ROOM TEMPERATURE OF INCONEL DA 718 [26] [28] [29]	6
TABLE 2.3 – MECHANICAL PROPERTIES AT ROOM TEMPERATURE OF INCONEL DA 718 [26] [29]	7
TABLE 3.1 – DIMENSION OF THE STANDARDIZED INSERT ISO CNGG120408FS	27
TABLE 4.1 – HARDNESS, ELASTIC MODULUS AND PLASTICITY INDEX FOR THE NANOCOMPOSITE COATINGS	45
TABLE 4.2 – SURFACE ROUGHNESS OF THE CHIP $Sa$ [ $\mu m$ ]	49
TABLE 4.3 – AVERAGE VALUES OF TWR FOR TiAlCrN/TiCrAl52Si8N, BASED ON THE VARIATION OF CUTTING SPEED	66
TABLE 4.4 – CCR RESULTS	70
TABLE 4.5 – CUTTING LENGTH AT THE END OF LIFE (MAXIMUM TOOL LIFE) FOR TiAlCrN/TiCrAl52Si8N, BASED ON THE VARIATION OF CUTTING SPEED	71
TABLE 4.6 – STANDARD DEVIATION, MEAN, AND COEFFICIENT OF VARIATION CALCULATED BETWEEN TESTS AT DIFFERENT $Vc$ FOR SOME OF THE COMPARISON PARAMETERS	74
TABLE 4.7 – VALUES OF THE COEFFICIENTS $a$ AND $b$ FOR THE FITTING WITH EXPONENTIAL CURVES OF THE EXPERIMENTAL DATA	78
TABLE 4.8 – $a$ AND $b$ COEFFICIENTS FOR THE EXPONENTIAL CURVES FITTING OF THE EXPERIMENTAL DATA AT $Vc = 120 m/min$	84



# Chapter 1: Introduction

## 1.1 Description of the Project

Nowadays, the aerospace industry generates essential demands for materials with properties that can be employed in complex environments which require high melting temperature and high corrosion resistance. Metallic alloys such as titanium and nickel-based alloys, also known as heat-resistant superalloys (HRSA) are the principal group of materials recommended for this application, by the fact to retain their mechanical and corrosion/oxidation properties at elevated temperatures [1] [2]. Besides that, Inconel 718, which is also considered an HRSA has many additional advantages such as high toughness, thermal fatigue, oxidation resistance, corrosion resistance, low thermal conductivity, lightweight, and ability to retain its properties at high temperature [3]. These characteristics make Inconel 718 attractive for applications in turbine engine discs, turbine blades, and drive-shafts components in the aircraft industry. However, Inconel 718 is also known as difficult-to-machine material [4], and it is still considered a challenge to be machined [5]. During machining, this superalloy presents the ability to strain hardening. Low thermal conductivity results in the built-up edge (BUE) associated with the heat generated in the cutting zone. This combination leads to the thermal stresses at the cutting tool, resulting, therefore, in rapid tool wear [5] [6] [7]. As a consequence, flank, notch, crater wear, plastic deformation, and chipping are the predominant wear modes caused by the combination of the presence of abrasive particles in its microstructures, and chemical affinity towards tool wear [8] [9] [10].

In order to mitigate the issues found during the machining of Inconel 718, an adequate selection of the cutting tool is needed. In this way, many researchers developed exhaustive research projects considering tool geometry, tool material, tool surface engineering, coatings and different cutting conditions [4] [10] [11] [12] as a solution to reduce machining costs and improving the machining process of Inconel 718. So far, the most significant solutions found to improve machining of Inconel 718 are throughout surface engineering modification of the cutting tools,

using Physical Vapor Deposited (PVD) coatings [13]. PVD coatings have particular characteristics such as mechanical properties, reduced friction coefficient, and thermal conditions that reflect favourably on the performance during the cutting and, as a consequence, the tool life, which directly affects the cost of machining and product quality, is increased [14].

However, there is still a challenge to be addressed, which is to improve machining process and reduce machining costs maintaining a machined workpiece with excellent surface integrity (better surface roughness and low levels of surface stresses) even once a tool wear ending criterion have been reached [4] [15] [16]. As it is well known, the surface quality of the machined parts will always be a core task for heat resistant super alloys employed in particular in aerospace industry [15] [17]. One of the ways suggested by [6] [15] [18] to control the surface's state during machining of Inconel 718, is throughout the monitoring of the tool wear using real industrial conditions and evaluating the levels of the tensile residual stresses at the workpiece surface generated at different stages of the tool wear. Other researchers suggest rising the cutting speed to increase chip flow, and as a consequence to obtain better surface integrity on the machined workpiece [17]. Higher cutting speeds results in elevated temperatures on the cutting zone with the consequence of a decrease in workpiece mechanical properties, as well as inferior tool life [16].

Literature also describes the effects of the several PVD coatings studied during machining. Results show improvement in tool life and surface integrity due to the coatings that present a number of positive characteristics once machining aerospace alloys: high corrosion resistance, high hardness, high thermal and chemical stability and good surface quality, which improve friction conditions, compared to uncoated carbide tools [19] [20] [21] [22]. The literature also reports that PVD nanocomposite coatings have shown improved performance compared to the state of the art PVD coatings [23]. Therefore, the use of PVD coated tool increase the production and product quality. To increase the productivity and the quality of the machined parts for aerospace industry applications it is needed a better management and understanding on the effect of the machining conditions (cutting parameters, PVD coated tool, and the combination of the cutting tool - machine tool - workpiece). To

address these operating conditions, it is fundamental the evaluation of PVD nanocomposite coatings against to the state of the art PVD coatings in terms of tool wear monitoring and prediction of tool wear, which is still lacking.

Therefore, to understand the tool wear characteristics during machining of nickel-based superalloys, in this research, a predictive model for flank wear based on the experimental data obtained from several tests at different cutting speed has been developed. Comparing this outcome with the analysis of many indicators as the material removal rate (MRR) and the tool wear rate (TWR), a wide vision of the turning process has been obtained, allowing to perform a productivity improvement. Furthermore, since observations with the optical microscope showed that the main tool wear modes have been chipping and BUE, deeper wear analyses were needed. An innovative investigation of the three-dimensional tool wear evolution permitted to definitely determine whether or not the employment of hard PVD nanocomposite coatings have been advantageous for the protection of the carbide substrate.

## 1.2 Objectives

This research aims to study two different physical vapour deposited (PVD) carbide tools' coatings for turning Inconel DA 718. One coating is made by a mono-layered nanocomposite film of Ti<sub>20</sub>Cr<sub>20</sub>Al<sub>52</sub>Si<sub>8</sub>N and the other has a TiAlCrN/TiCrAl<sub>52</sub>Si<sub>8</sub>N multi-layered architecture. Employing a set of different cutting conditions in terms of cutting speed, the two structures will be deeply compared with a benchmark (KC5010 by Kennametal) in the next chapters.

Several indicators will be investigated, as tool wear curves, the material removal rate (MRR), the tool wear rate (TWR), the index of performance (IP), the minimum cost and the maximum production speeds. Submitting these coefficients to numerical analysis, it will be possible to evaluate the performance of the turning process for finishing cutting conditions, obtaining a comprehensive characterization of the inspected coatings. In this way, optimized cutting parameters will be established, based on the tool wear partners and mechanisms that will occur in many cases. Moreover, a tool life predictive model will be developed for the coatings under evaluation.

To achieve the main objectives, it is necessary to investigate the tribological and wear performances of the coatings, examining the tool wear modes and mechanisms that the superalloy causes on the surface of the designed tools. The tests will permit making some considerations about the influence of cutting conditions on tool life, tracking the flank wear according to the ISO 3685 normative. Furthermore, advanced technologies as a Focus Variation Microscope (FVM) will be also employed, allowing deep tool wear modes evaluation and 3-dimensional measurements of 3D-volume wear (chipping) and BUE. At last, through roughness measurements, also the quality of the machined workpieces' surfaces will be a result of the study, because the components made by Inconel DA718 are crucial parts of several applications, therefore they should respect restrictive quality levels.

A Scanning Electron Microscope (SEM) study with annexed EDS will be employed to validate some of the considerations extracted from the obtained results.

## Chapter 2: Literature Review

### 2.1 Inconel DA 718

Inconel DA 718 is an age-hardened austenitic Nickel superalloy. In the following paragraphs, the general stats of the material and the most common applications will be explained.

#### *2.1.1 Microstructure and Chemical composition*

The grain size of Inconel DA 718 ranges from 2 to 10  $\mu\text{m}$  [24]. As it can be seen from the Table 2.1, the content of Nb in weight percentage is high. Sometimes (particularly in the case of welded or cast Inconel) it happens that Niobium segregates in the interdendritic regions, because of the low tendency of the element in diffusion. As a result, brittle and full of microvoids Laves  $(\text{Ni-Fe-Cr})_2(\text{Nb-Mo-Ti})$  phases are formed in these areas, leading to a leak in mechanical properties and an incremented risk of fragile trigger of breakage. In order to balance the distribution of elements and to obtain a more homogeneous structure, an ageing process is recommended.

<b>Element</b>	<b>Ni</b>	<b>Mn</b>	<b>P</b>	<b>S</b>	<b>Si</b>	<b>Cr</b>	<b>C</b>	<b>Mo</b>
<b>Weight %</b>	50÷ 55	<0.35	<0.015	<0.015	<0.35	17÷ 21	<0.08	2.80÷ 3.30

<b>Element</b>	<b>Nb</b>	<b>Ta</b>	<b>Ti</b>	<b>Al</b>	<b>Co</b>	<b>B</b>	<b>Cu</b>	<b>Fe</b>
<b>Weight %</b>	4.75÷ 5.50	<0.05	0.65÷ 1.15	0.20÷ 0.80	<1.00	<0.006	<0.30	Bal.

*Table 2.1 – Chemical Composition of Inconel 718, conformed to AMS specifications [25]*

During the heating treatment, the partial precipitation of the  $\gamma'$  ( $\text{Ni}_3\text{Al}$ ) and  $\gamma''$  ( $\text{Ni}_3\text{Nb}$ ) phases can be observed. The  $\gamma''$  precipitate is metastable, therefore during the process part of it is transformed in the  $\delta$  ( $\text{Ni}_3\text{Nb}$ ) stable phase, which segregates at the grain boundaries, avoiding the movement of dislocations and consequently the grain growth phenomena. It results in the improvement of the resistance to creep

and stresses, important characteristics requested for the applications of the alloy [26] [27].

### *2.1.2 Physical properties*

A research based on the data sheets for Inconel 718 from the main manufacturers was conducted. A summary related to the typical constants at room temperature, interesting for the application studied in this document, is shown in the following Table 2.2:

Density	$\rho$	8.22	[g/cm <sup>3</sup> ]
Melting Temperature Range	$T_m$	1260÷1336	[°C]
Specific Heat	$c$	435	[J/(kg K)]
Thermal Conductivity	$\lambda$	11.39	[W/(m K)]
Thermal Expansion Coefficient	$\alpha$	14.38 <sup>1</sup>	[K <sup>-1</sup> ]
Young's Modulus	$E$	199.95	[GPa]
Poisson's Ratio	$\nu$	0.294	-

*Table 2.2 – Physical constants at room temperature of Inconel DA 718 [26] [28] [29]*

It is noteworthy that, even if on average the physical properties of the superalloy are similar to most of the steels, thermal conductivity is low compared to other iron-based alloys. This peculiarity is one of the challenging reasons why it is hard to find an efficient methodology to machine Inconel 718; in fact, it results in a difficulty in heat dissipation while machining.

Corrosion resistance is another fundamental characteristic of this superalloy, but it is not particularly interesting for the research.

---

<sup>1</sup> Value obtained as an average between data of a wide temperature range

### *2.1.3 Mechanical properties*

Mechanical properties of Inconel 718 are divergent depending on the various treatments applied to the material. In this research, the chosen alloy is aged with a  $925^{\circ} - 1010^{\circ}\text{C}$  annealing and, after remaining at  $720^{\circ}\text{C}$  for  $8h$ , it is furnace cooled at  $50^{\circ}\text{C}/h$  to  $620^{\circ}\text{C}$  and kept for  $8h$  at  $620^{\circ}\text{C}$ ; at the end, it is air cooled down to room temperature [27]. This is considered as the optimal process to get the best mechanical features of the steel [26]. Table 2.3 shows the minimum values of the main properties at room temperature (note that the superalloy has the great advantage of maintaining these competitive features also at high temperature).

Tensile Strength	$UTS$	1275	[MPa]
Yield Strength	$\sigma_y$	1034	[MPa]
Elongation %	$\varepsilon$	12	[%]
Reduction of Area %	$A\%$	15	[%]
Brinell Hardness	$HB$	331	-
Charpy V-Notch Impact Strength	$CVN$	27.8	[J]
Fatigue Strength for $2 * 10^6$ cycles	$\sigma_{lim}$	531	[MPa]

*Table 2.3 – Mechanical properties at room temperature of Inconel DA 718 [26] [29]*

It is worth noticing that the alloy has high yield strength as well as ultimate tensile strength, despite having a good level of elongation %, which ensures that it is also not brittle.

Additionally, as explained in the paragraph describing the microstructure, also the creep resistance is advanced.

### *2.1.4 Applications in the Industry*

Inconel 718 is widely used for several advanced applications, such as high-temperature casings, cryogenic tankage (thanks to the low ductile to brittle transition temperature) or gas turbines for the aerospace industry, as well as liquid-fuelled

rockets [26]. As an example, about 30% of the CF6 engine (General Electric) is made by this superalloy [28].

Such a vast employment of the material is due to the good behaviour in various working conditions, in terms of corrosion resistance, toughness, ductility and mechanical strength, in a large range of temperature, which guarantees a significant creep resistance.

Some of the most remarkable implementations in automotive and aerospace industries are:

- Formula One and NASCAR exhaust systems, obtaining the advantage of being able to enlarge the temperature working range and reducing the weight of the vehicles;
- Tesla Motors Model S battery pack contactor, in which Inconel allows to work with higher temperatures, then higher current so that the car can accelerate faster;
- Turbines of EcoBlue diesel engines by Ford Motor Company;
- Space X several utilizations, including the engine manifold of the Falcon 9 rocket and a large number of other components for their vehicles;
- Studs made of Inconel connected to frangible-sealed to the platform nuts, which had to explode at the moment of the launch to let the Space Shuttle take off [30].

## 2.2 Machining of Inconel DA 718

The high impact of various applications of Inconel DA 718 implies the necessity of performing properties of the machined parts. For example, to guarantee fatigue strength, in ideal conditions it is necessary to have a defect-free surface (in terms of tears and cracks) [24].

However, because of the superalloy bad machinability, finding an appropriate tool which ensures a good finish of the machined workpiece and at the same time a long tool life is very hard. In addition, although the ageing process provides a better quality of the finished component and improved properties, it also involves a loss of tool life [26].

In particular, the main issues related to the machinability this superalloy could be summarised as:

- Excellent mechanical properties such as yield strength maintained even if the component is heated up to 950°C, which causes powerful forces on the parts in contact [31];
- Extremely abrasive carbide particles, with the consequence of abrasions on the tool surface [32];
- Scarcity in thermal conductivity, that implies a rise of the temperature during the process, with the consequence of increasing the risk of welding (built-up edge) and adhesion among the insert and the workpiece (adhesive wear). Furthermore, elevated temperature causes more likely plastic deformation and, in some cases, if there is a chemical affinity between 718 and elements contained in cutting tools or in the atmosphere, diffusion and oxidation wear may be observed [32];
- Work hardening characteristics during the chip formation of Inconel, which contributes together with elevated temperatures in the deformation and chipping of the cutting edge because of the high-stress area [26] [13].

In order to limit these effects, it is necessary to adopt coatings made by hard, not affine with Inconel materials with low friction coefficient (in fact, little friction is

associated to curly chips, smooth surfaces and long tool life [33]), and even a designed kind and amount of lubricant. Another adjustment to control the efficiency is using proper cutting conditions.

## 2.3 Cutting Tools

In last years, advanced machine tools have permitted to improve machining performance of the workpieces. Nevertheless, to ensure good results, performing cutting tools are required. This issue becomes more critical if the material to treat is in itself problematic to be machined: that is the case of Inconel DA 718.

For the reasons mentioned above, chemical, physical and mechanical characteristics of cutting tools are widely studied for machining the Nickel superalloy, in order to find the best results in terms of both tool life and quality of the machined parts under different working conditions [32].

### *2.3.1 Coated tools with PVD coatings*

A way to make possible an efficient processing of difficult to machine materials for the aerospace industry as Inconel DA 718 is to protect tools with hard physical vapour deposited (PVD) coatings. The technique is realised in a vacuum atmosphere in order to reduce the chemical reactions between vaporised particles and to make the film more homogeneous.

Inconel, as mentioned above, is characterised by high strength maintained also at elevated temperature, as well as extreme work hardening and low thermal conductivity. Furthermore, the microstructure of the superalloy is abrasive for the tool surface. PVD coatings have the task to resist against these aspects that lead to a quick tool wear (across different modes explained in the following paragraphs) and thus to the expensive manufacturing of the material. As a result, tool life will be improved.

The main benefits provided from the method are improved features at both low and high temperature of oxidation resistance, strength, fatigue life and hardness (in fact, in PVD the impacting particles on the surface create a compression state in the external layer which makes it harder). Moreover, in some cases, PVD coatings are able to dissipate vibrations during the microplastic deformation, preserving the surfaces from cracking. Many coatings have also low thermal conductivity, a positive peculiarity in that it ensures the protection of the tool from overheating.

Another feature is that, thanks to the typical high percentage of aluminium in the microstructure of the coatings, a passivation layer is usually formed on the surface: for instance, alumina  $Al_2O_3$  is a very stable oxide that prevents eventual further oxidation of the tool. In last years, nanocomposite coatings have been developed; many of them are more performing than classic coatings, because of their high-temperature lubricity associated with a better response against the tool wear mechanism of adhesion [33].

### ***2.3.1.1 Mono-layered Nanocomposite Coatings***

Employing nanocomposites for covering carbide tools for machining of hard to cut aerospace alloys is one of the most beneficial methods to optimize the performance of the process. Past research have demonstrated that coatings made by nanocomposite material have significantly improved mechanical strength, in respect of uncoated or standardly coated tools. Strength is a fundamental aspect to pursue a better machining process of Inconel 718, achieving a significantly longer tool life, as also shown in Figure 2.1:

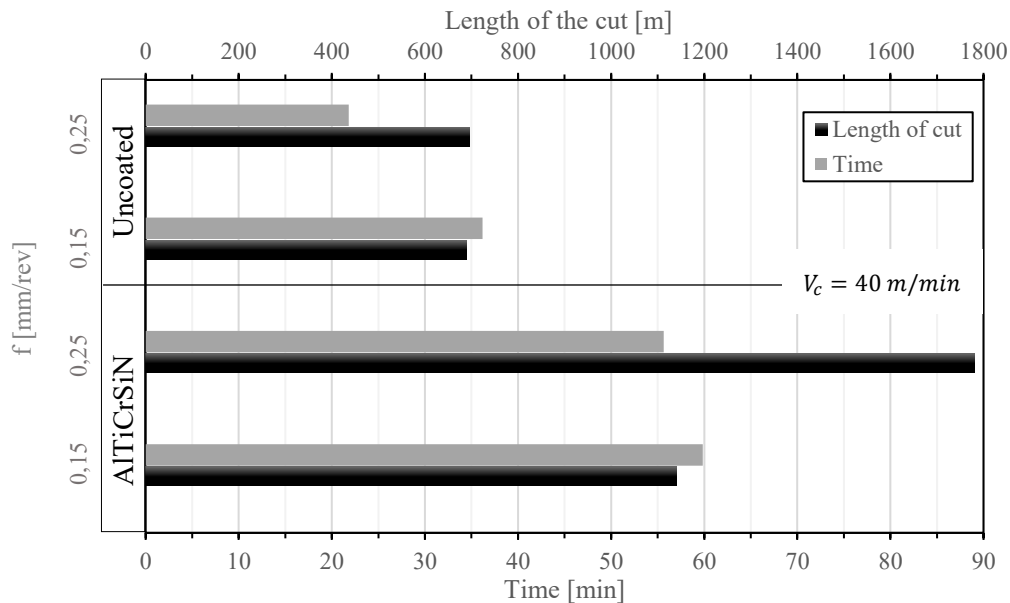


Figure 2.1 – Tool life comparison between an uncoated tool and AlTiCrSiN-based coated tool [34]

The mainly used kind of nanocomposite is formed by many nanometric scattered particles in an amorphous strong monolithic matrix that avoids the motion of

nanoparticles under external stresses. In particular, widespread combinations are ternary and quaternary nanostructures made by different quantities of elements as Ti, V, N, Al, Cr and Si [35].

### **2.3.1.2 Multi-layered Nanocomposite Coatings**

Multi-layered coatings are formed by a variable number of mono-layer films, in order to satisfy the necessary physical and chemical properties. The result is the obtainment of improved characteristics in comparison with the behaviour of singular layers, in terms of higher crack resistance, as well as mechanical, thermal and chemical resistance to tool wear, leading to a tool life higher by 40% in comparison to the average of the previously adopted structures.

It is essential to employ bonding films, to ensure the fixed attachment between layers and delay (or reduce) the crack propagation. Furthermore, sometimes the multi-layered coating is treated after the deposition, to activate the desired properties [35]. Regarding the coating material and structure, as also expressed by Figure 2.2, the minimum tool wear can be obtained by using AlTiCrN-based layers under a TiSiN-based top layer [36]. This is justified by the high hardness and oxidation resistance of the material even at high temperatures (above 900 °C), because of the formation of a stable alumina Al<sub>2</sub>O<sub>3</sub> tribofilm [37].

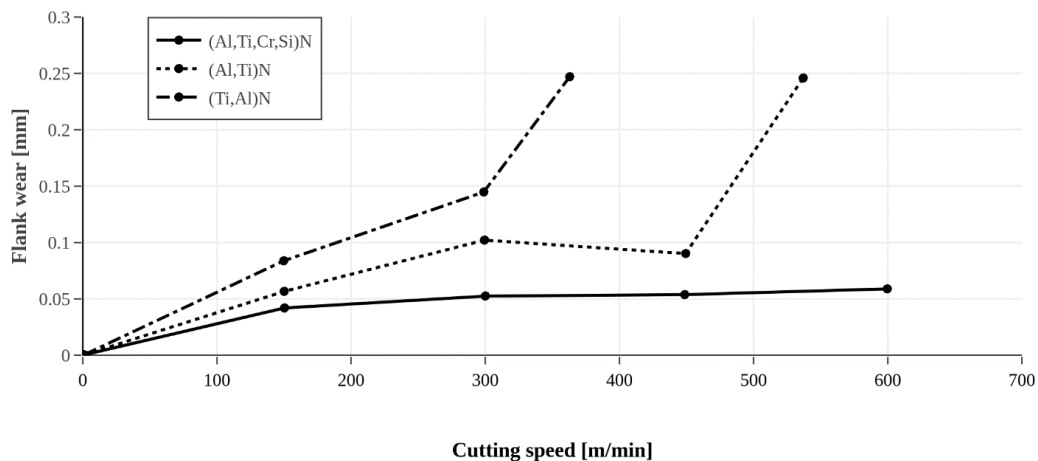


*Figure 2.2 – Flank wear for a 50 m cutting length under different  $V_c$  and coating [38]*

With aggressive cutting conditions, as for example high cutting speeds, the adhesion of the coatings tends to be compromised. These facts suggest conducting tests over

the multiple parameters, in order to find the best balance between reduced production costs (directly related to tool wear) and productivity.

### *2.3.2 Tool wear*

The quality of an instrument for machining purposes is measured through its reaction to varying tribological circumstances. High temperatures, repetitive impacts and aggressive chemical conditions are examples of dangers for tool life and surface integrity while machining. These factors are determined according to the chosen materials, the kind of machining process (and the related cutting conditions as feed rate, cutting speed and depth of cut) and the coolant/lubricant employed. Therefore, to improve the efficiency and efficacy of the activity so that costs and productivity can be optimized, deep studies are needed.

A tool can be damaged in two ways, which are not ever well distinguished: wear and fracture. The former consists of a continuative loss of tool body and it is the most worth analysing because it interests effects ranging from the molecular to the macroscopic magnitudes, while the latter is the instantaneous breakage of the insert [39].

A first manner to recognise the tool wear pattern is to distinguish the one which influences the rake face from the flank face one. In the following paragraph, the most noticeable tool wear mechanism and associated modes are described [40].

#### *2.3.2.1 Wear mechanisms*

It is fundamental to explain the driving principles for tool wear because they are responsible for the different type of deterioration influencing the insert.

Wear mechanisms may be sorted as [39] [41]:

- *Abrasive wear*, due to rough hard particles that might be found in the metallic matrix, able to progressively remove material from the tool by sliding on the surface. Both the workpiece and the sawtooth external border of the chip (in hard machining processes) can abrade the surface of the instrument. It is the main factor for flank wear on the tools, causing several scrapes and notches on the tool side. The effect is even increased in hostile working conditions,

including high temperature and continuative cutting. To prevent tools from abrasive wear, one of the principal solutions is adopting resistant coatings with good behaviour even when a large amount of heat is released.

- *Adhesive wear*, which is a thermally activated phenomenon. Adhesion interests not only flank wear, indeed it is one of the main mechanisms producing crater wear as well, owing to the repetitive sticking and detachment cycle between work material and surface of the tool, especially at low cutting speed. This effect is caused by the formation of bonds among the parts in contact: in the case in which these links result to be stronger than the localized strength of one material, a little fragment from the weaker one can be transferred to the surface of the other. Over time, an entire chip portion (cluster of several particles) will be released from the system. The same mechanism leads also to the BUE wear mode that is discussed in the next paragraph.
- *Diffusion wear*, also known as solution wear, which is thermally activated, as adhesive wear is. At high cutting speeds, especially when the temperature reaches considerable levels and in high solubility conditions, it plays the main role in the rise of tool wear rate. The decomposition of the external part of the microstructure of the components can be observed, due to motion induced by the heat released in the working area. Subsequently, microparticles establish solid solutions with the removed material. Therefore, the surface of the tool becomes weak and crater wear is thus accelerated. The main issue of diffusive usury is that it is not reliant by mechanical properties, so the chemical characteristics of the chosen tools must be as well appropriately selected, for the whole range of temperature in which it will work.
- *Tribo-chemical wear*, which involves oxidation and corrosion wear phenomena, with the result of notching of the edges of the tool. This wear mechanism happens at a temperature high enough that the reaction between the metallic atoms and the oxygen contained in the atmosphere may be activated. Oxidized tool portions are brittle and poor in mechanical

resistance, so they can be easily abraded by the generated chip. Regarding corrosion wear, it is mainly caused by extreme pressure (EP) additives free of S and Cl in the cutting lubricant.

- *Fatigue wear*, particularly fretting wear. The cause is the continuous sliding of the chip on the tool surface and the oscillating force due to the repetitive contacts with the workpiece. The outcome is the origin of the propagation of several subsurface microcracks, that joined together induce the external delamination of the tool.
- *Plastic deformation*, that is caused by insufficient yield strength of the tool substrate in comparison to the workpiece's one. The tool-tip blunting affects the precision of the process, so it must be kept under control. This phenomenon gets worse as the temperature increases (creep failure), reducing the tool life expectations.

#### **2.3.2.2 Tool wear modes**

The tool wear modes affecting the study of the alloy are classified in different categories [33] [39] [40]:

- *Flank wear*, which gives one of the major contributions to the leak in tool life for nickel superalloys machining, is manifested with an almost uniform damaged lateral surface. It is caused by abrasion from Inconel hard carbides and adhesion between the surfaces during high speed (and thus temperature) machining. Flank wear can be modelled using Taylor's equation, that helps to forecast the maximum duration of the tool in base on the cutting speed.

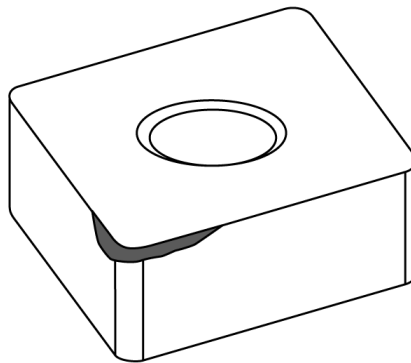


*Figure 2.3 – Flank wear [42]*

- *Crater wear*, which occurs particularly at low-speed machining on the rake face, has a little impact on tool life. In fact, very deep craters are needed to make this phenomenon leading to the tool failure by reaching the cutting edges. It is due to several effects correlated to high temperature. At first, the subsequent adhesion and separation of work material on the tool with the result of chipping wear is one of the most effective. Another significant mechanism for cratering is diffusion. It results in irregular and striped surfaces. Crater wear can be considered into Taylor's equation for tool life, but it has a minor effect because, even though craters formation is faster than flank wear development, the former affects processes quality less than the latter does.

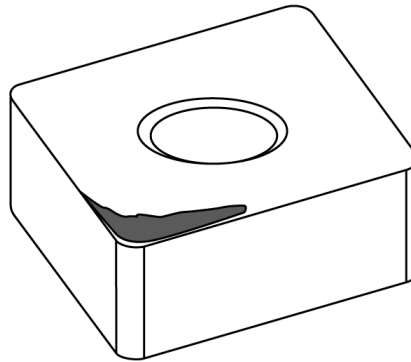


*Figure 2.4 – Crater wear [42]*

- *Wear due to intensive Built-up edge (BUE) formation*, which, even if in general involves materials with low melting temperature, also strongly affects this process, because of the leak in heat dissipation. It happens when a welding between the chip and the tool tip occurs, due to the adhesive wear mechanism. Therefore, BUE can take place typically at low cutting speeds (or the ideal conditions to obtain attritional wear). Additionally, it is possible to get built-up edge wear in case of wrong selection of lubricant and coolant fluids, that must have sufficient anti-weld properties. The consequence of this mode is the chipping of the tool side and a bad quality of the machined workpiece surface.

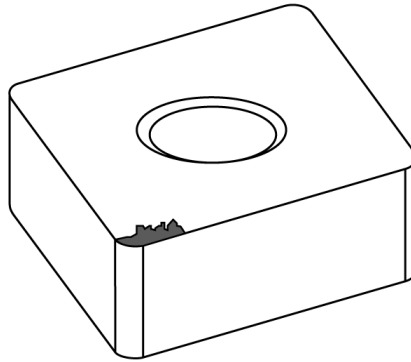


*Figure 2.5 – Built-up edge wear [42]*

- *Nose wear*, which is also called tool-tip blunting, may be seen particularly at elevated temperature, where the phenomenon of plastic deformation is more likely to happen.

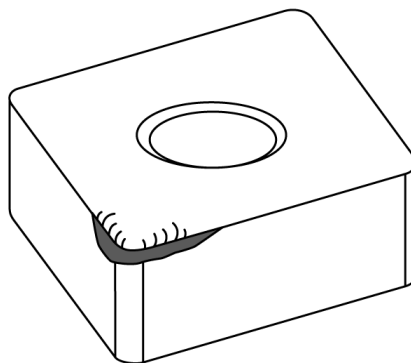


*Figure 2.6 – Nose wear [42]*

- *Notching*, that is a kind of wear that involves the formation of a notch at the depth-of-cut. As easily suggested by intuition, the primary cause is the abrasion of the side of the insert by the chip generated during the process. Thus, the effect is greater if the workpiece material is harder and abrasive, with a high tendency to work-hardening and low thermal conductivity, as it is for Inconel 718. Moreover, notching is associated with the local oxidation of the tool. To decrease this effect, it is possible to employ rounded or blunt edges of the inserts. Because of notch wear, the machined surface can appear badly finished.

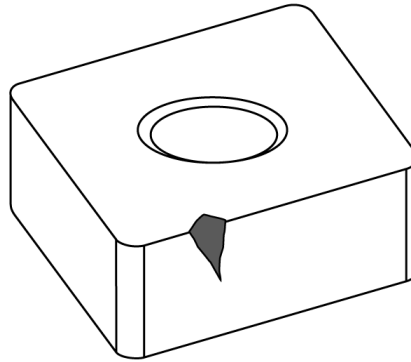


*Figure 2.7 – Notch wear [42]*

- *Thermal cracks*, which consist of a continuously variable temperature cycle, causing thermal stresses in the component that, with time, lead to the development of cracks. The temperature variation is usually correlated with interrupted cut under wet conditions of cooling, at low cutting speed.

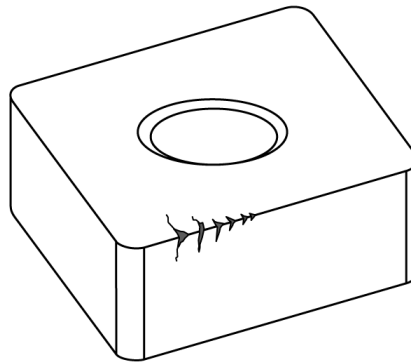


*Figure 2.8 – Thermal cracks wear [42]*

### **2.3.2.3 Tool wear measurement according to the ISO 3685**

The most critical wear patterns from the list described above can be quantified employing the normative ISO 3685, which defines several indicators referred to dimensional characteristics, in order to make comparable the wear affecting two or more inserts from different processes [40].

For the tools chosen in this research, the main measurable parameters according to the standardized regulation can be resumed in Figure 2.9.

**Geometrical indicators of tool wear**

$VB_B$  – average flank wear land width

$VB_{Bmax}$  – maximum flank wear land width

$VB_N$  – width of notch wear

$VB_C$  – width of flank wear at tool corner

$VB$  – flank wear

$BW$  – width of groove backwall wear

$BL$  – length of groove backwall wear

$KT$  – depth of groove backwall wear – crater depth

$SW$  – width of secondary face wear

$SD$  – depth of secondary face wear

$N$  – nose wear

$NL_1$  – notch wear length on main cutting edge

$NW_1$  – notch wear width on main cutting edge

$NL_2$  – notch wear length on secondary cutting edge

$NW_2$  – notch wear width on secondary cutting edge

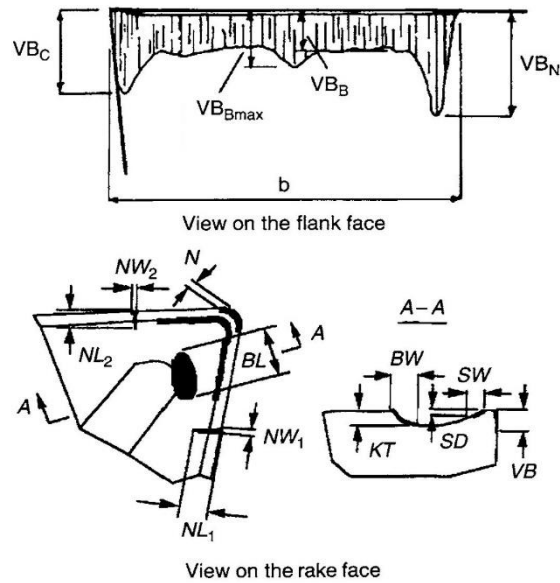


Figure 2.9 – ISO 3685 standards to determine the tool wear for carbide inserts [40]

For carbide tools, the life is assumed as terminated if one of the following conditions occurs:

- $VB_B = 0.3 \text{ mm}$  ;
- $VB_{Bmax} = 0.6 \text{ mm}$  (if the flank appears irregularly worn and it is possible to observe extended notches);
- $KT = 0.06 + 0.3f$  , in which  $f$  is the feed rate;
- Delamination (or the detachment of the coating from the surface of the insert in case of coated tools).

## 2.4 Tribology of Metal Cutting

Tribology is the engineering science that studies the trinomial of friction, wear and lubrication. Hence, it is applied to every mechanical phenomenon, including the metal cutting. Tribological conditions are one of the crucial factors affecting the quality of a process, so they are deeply investigated by many researchers, with the aim of finding the optimal balance of the effects.

The tribological status of a system during the cutting process is compounded by the aspects listed below [40]:

- Highly reactive chip;
- Intensive loads concentrated in a reduced area, which lead in some cases to high stresses reaching peaks of  $1600\text{ MPa}$  for the normal strain  $\sigma$  and  $1000\text{ MPa}$  for the shear strain  $\tau$ ;
- Much heat released during cutting, especially in high-speed machining, that together with the large plastic deformation of the worked material can cause melting and welding of the asperities of the two parts in contacts;
- Difficulties in the penetration of lubricant and cooling liquids in the cutting area during high-speed working conditions because of friction;
- Variable friction due to the geometrical variation correlated with tool wear.

In machining processes, according to some models found in literature, it is possible to recognize three zones in which tribological status is different, as represented in Figure 2.10 [40]:

- *A*: named sticking area (plastic frictional contact). It involves parts of flank as well as rake tool faces. In this region, workpiece material is almost completely in contact with the tool surface; indeed, the ratio between the real contact area and the ideal one is around 100%. Hence, working conditions are locally dry and the surfaces in contact constantly change.
- *B*: named sliding area (elastic frictional contact). It is a transition zone, between *A* where there is a complete contact and *C* where the components

are fully separated. A thin lubricating layer can be formed in the region if lubricant is provided.

- *C*: named narrow area. As anticipated above, it is less interesting for tribology, because the tool is not in contact with the workpiece.

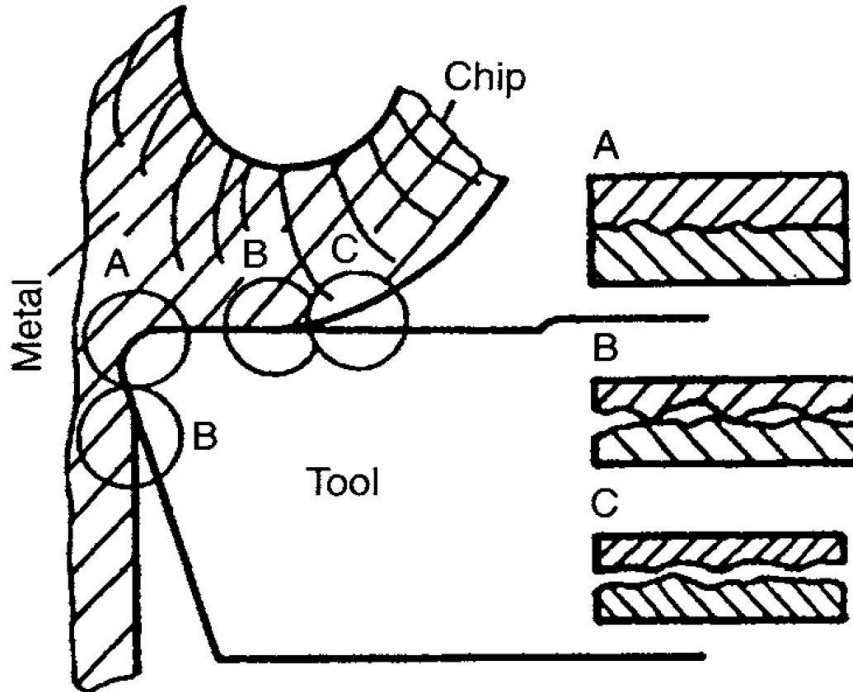


*Figure 2.10 – Different tribological conditions zones in machining processes [40]*

Some authors proposed models to predict the range of sticking area. As an example, according to the Abuladze expression [40], it is possible to analytically evaluate the extent of the sticking area:

$$l_{st} = h \left[ CCR * (1 - \tan\gamma_0) + \frac{1}{\sin\gamma_0} \right]$$

In which  $l_{st}$  expresses the length of the sticking region (A),  $h$  is the depth of the cut,  $CCR$  is a ratio between the deformed and undeformed chip thickness (chip compression ratio) and  $\gamma_0$  is the rake angle.

Another important quantity, easy to evaluate experimentally, is the tool-chip contact length  $TCCL$ , that is the maximum distance of contact between the tool and the workpiece material, from the tool tip to the end of the sliding area (B).

### *2.4.1 Effects of Coatings on tribological conditions*

The presence of coatings on cutting tools affects the tribology of metal cutting: it is the main reason because of many research activities revolve around the characterization of innovative coatings.

Varying the coating architecture influence several aspects of machining:

- *Contact*: the friction between the surfaces is altered; thus, it follows that heat generation and chip flow can be improved to refine the efficiency of the process.
- *Wear*: tool life is nearly 100% dependant on wear. A suited coating allows to reduce the impact of mechanisms as abrasion, adhesion and diffusion, with a result of decreasing the tool wear phenomena effect.
- *After work*: the aim of a cutting process is to preserve the tool integrity (especially superficially) and to obtain an accurate finish on the workpiece. A careful attention in selecting the coating helps with these factors.

## 2.5 Equipment specifications

### 2.5.1 Okuma Crown CNC Lathe

Since the main objectives of the research are to analyse the tool wear and the surface quality of the machined parts, the employed workpieces are reduced in dimensions and the operations relatively simple. Therefore, this 2 axes CNC machine was suited to perform all the turning tests on Inconel DA 718. The main instructions and safety rules were found in a proper manual provided by the manufacturer.



*Figure 2.11 – Okuma Crown L1060 CNC lathe*

It is powered by a 13.4 kW electric motor, able to work in a spindle speed range between 75 and 3500 rpm. Regarding the feed rate, it is continuously variable from 25 to 10000 mm/min [43].

Furthermore, the lathe is equipped with a 12 positions servo-turret, a coolant system and a chip conveyor that help to keep clean the working area.

The programming language is standard G code, with the possibility to build the program on the onboard controller or separately using a PC.

### *2.5.2 Alicona Infinite Focus G5 FVM*

The Alicona Infinite Focus G5 optical microscope was helpful during the cutting tests, allowing to get a first understanding of the tool wear in all the analysed cases. It is a focus variation microscope (FVM), classifiable as a white light interferometer. Thanks to the 3D measurement system, many aspects have been investigated, as the three-dimensional volume wear of the inserts and the roughness of both chip and machined workpieces, according to the ISO 4288 normative.



*Figure 2.12 – Alicona Infinite Focus G5*

The microscope has also the ability to scan larger areas of the items, thanks to the horizontal automatic movement along X and Y axes (image stitching).

The vertical resolution is  $10nm$ , while the lateral one is  $400nm$  [44].

### *2.5.3 Tescan VEGA II LSU SEM*

A scanning electron microscope Tescan VEGA II LSU SEM has been employed to deeply observe the machined workpiece and the tool surface after the processes. In this way, more accurate considerations have been expressed.



*Figure 2.13 – Tescan VEGA II LSU SEM*

The microscope allows to variate the vacuum level in a range from 150 (high) to 500 Pa (low) in the measuring chamber and is equipped with mechanic suspension.

VEGA II LSU has a standardized secondary electron (low energy) detector Everhart-Thornley and a back scattered electron (high energy) detector. Regarding the electron gun, it has a tungsten filament type.

To make EDS analysis, an EDS Oxford X-MAX equipment is assembled on the main body [45].

# Chapter 3: Methodology

## 3.1 Tools architecture

For all the employed tools, as substrate, the cemented carbide K313 by Kennametal has been selected, a hard-low bound WC/Co with fine grain (%Co = 6, HRA = 93).

The tools geometry follows the ISO CNGG120408FS. Referring to Figure 3.1, the related dimensions are shown in the Table 3.1 [46]:

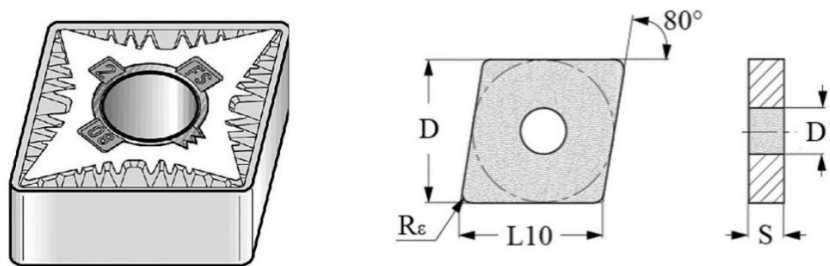


Figure 3.1 – Geometry of the tools ISO CNGG120408FS

D [mm]	L10 [mm]	S [mm]	R <sub>ε</sub> [mm]	D1 [mm]
12.70	12.90	4.76	0.8	5.16

Table 3.1 – Dimension of the standardized insert ISO CNGG120408FS

### 3.1.1 Coatings characterization

For the research, a PVD coated carbide tool KC5010 by Kennametal has been employed as a benchmark, since it is widely used in modern industry. Both the mono Ti20Cr20Al52Si8N and multi-layered TiAlCrN/TiCrAl52Si8N coatings have been deposited on a carbide substrate by KOBELCO Advanced Coating industry (same substrate of the KC5010), using an SFC (Super Fine Cathode) physical vapour deposition. This method, in comparison to standard PVD procedures, involves reduced and controllable internal stresses, thin films (up to 20nm) and homogeneous distribution of the material. The result is longer tool life in the cases of stainless steel and superalloys turning and milling tests [47].

To examine the thickness of the coatings, SEM analyses have been conducted on the cross-sections of the tools, that have been obtained by fragile breakage, in order

to do not alter the geometry as can happen while sectioning the material by cutting. However, because of the strength of the tools, half of the body has been cut and then the remained part brittlely broken through an impulse.

### **3.1.1.1 Benchmark KC5010**

Nowadays, KC5010 is one of the most widespread coated tools for hard turning, since its behaviour results to have higher tool life and maximum cutting speed of many other available coatings, especially under finishing cutting conditions.

The structure of the PVD coating is composed by an Aluminium-Titanium-Nitrate layer deposited over the carbide main body, allowing to reach higher temperature during the process, preserving the tool from wear and thus improving the tool life also in case of high-speed machining [48].

### **3.1.1.2 Nanocomposites $Ti_{20}Cr_{20}Al_{52}Si_8N$ and $TiAlCrN/TiCrAl_{52}Si_8N$**

The coatings have been deposited using a bias voltage of 150V for the PVD deposition process. The supposed full thickness of the coatings is averagely 2 $\mu$ m.

The structure of the nanocomposite is made by nc-Al/Ti/Cr-N nanofillers scattered in a Si<sub>3</sub>N<sub>4</sub> amorphous matrix. The result of employing nanoparticles is a fine crystalline structure, a positive aspect explicable by the Hall-Petch effect, which states that the hardness of the material  $H(d)$  increase when the grain dimension  $d$  is reduced:

$$H(d) = H_0 + Kd^{-\frac{1}{2}}$$

The estimation of grain size is around 10nm, that together with other effect guarantees a high hardness, around 40GPa. Therefore, the coatings are included in the category of superhard coatings.

Silicon not only contributes to the hardness of the coating, but also confers to the system many other positive properties:

- Firstly, the ceramic material has the characteristic of low heat conduction. In this way, the heat will be confined in a restricted area of the coating and will not move on the substrate, delaying the degradation of the insert.

- Another peculiarity of Si is the high lubricity, which involves low friction coefficient and thus the obtainment of curly and smooth chip and better surface finish.
- Moreover, the silicon nitrate  $\text{Si}_3\text{N}_4$  allows a good level of sliding of nanoparticles, which implies a relatively good toughness in respect of most of the superhard nanocomposite materials.

However, the amount of Si is limited, to avoid the precipitation of second phases, leading to an increase in brittleness.

The amount of aluminium in the material is higher than titanium and chromium, because Al addresses two main functionalities:

- At first, due to the phenomenon of passivation, the formation of a thin layer of aluminium oxide (alumina  $\text{Al}_2\text{O}_3$  tribofilms) at high temperature, that protect the material from further oxidation and involves high lubricity.
- Secondly, aluminium has the task to take part in the spinodal decomposition at high temperature together with chromium and titanium (between  $800^\circ\text{C}$  and  $1000^\circ\text{C}$ , range in which the temperatures reached while machining Inconel DA718 are included). This process consists in the segregation of coexisting and thermally-stable phases of fcc-AlN, fcc-CrN and fcc-TiN, that limit the movement of dislocation. This is justified by the fact that having different phases implies different sliding systems of dislocations and complex grain boundaries. Moreover, grain boundaries are strengthened by the solid-state chemical affinity between the segregations, involving the advantage of having a small number of voids and vacancies.

Titanium and chromium confer to the system oxidation resistance thanks to the formation of stable tribofilms. Furthermore, tribofilms preserve the coating and the tool body by overheating thanks to their low thermal conductivity and confer lubricity to the tool. At last, in past research, Ti showed also improvements in terms of toughness [49].

## 3.2 Preliminary cutting tests

The first step of the study is performing cutting tests with the previously described Okuma Crown L1060 CNC lathe, adopting a variable range of cutting speed and different coated tools.

Three cutting speed during turning of Inconel have been analysed for all the insert taken into consideration:

- $V_c = 60 \frac{m}{min}$ ;
- $V_c = 80 \frac{m}{min}$ ;
- $V_c = 120 \frac{m}{min}$ .

All the other cutting parameters were instead maintained constant through the trials.

The chosen depth of the cut was  $d = 0.25mm$  and a feed rate of  $f = 0.1225 \frac{mm}{rev}$  was selected. The machining processes have been wet, cooled and lubricated with CommCool™ HD semi-synthetic metalworking fluid [50].

In order to compare the results obtained by machining at different cutting speed, tracking the time of the cut to define the tool life is not appropriated, so the length of the cut has been selected as reference parameter:

$$L = \sum l_i = \sum \frac{\pi D_i * l_{1_i}}{1000f}$$

In which  $L$  is the total length of the cut,  $l_i$  is the cutting length for every pass (on average  $120m$ ),  $D_i$  represent the diameter of the workpiece in millimetres after the pass,  $l_{1_i}$  is the linear length of the considered pass in millimetres and  $f$  is the feed rate in millimetres per revolution.

The tool life curve has been traced by frequently interrupting the cutting process and measuring the tool wear pattern with the optical microscope. Considering an average tool life of  $1000m$ , a reasonable cutting length of  $120m$  has been selected as the most suitable for every step, in order to get a complete approximation of the tool life curve, without introducing too much discontinuities (interrupted cut), that could lead in an alteration of the process.

### *3.2.1 Workpiece and Chip Roughness*

After each pass, the roughness of the workpiece surface along the tool life has been measured through a mean of 3 values acquired by a Mitutoyo SJ-201 portable profilometer.

To ensure the reliability of the results, the portable roughness measurer has been compared with the high-accuracy Mitutoyo Formtracer Extreme CS-5000 profilometer by testing standard surface roughness samples (certified from Flexbar Machine Corporation), with variable  $Ra$  from  $0.05\mu m$  to  $12.5\mu m$ . For every sample, 10 measurements have been executed. At the end of the procedure, the reliability of the SJ-201 has been confirmed by an ANOVA analysis in the range  $0.05\mu m \leq Ra \leq 3.2\mu m$  (the null hypothesis  $H_0$  of equal results between the two profilometers has not been rejected, with a level of significance  $\alpha = 5\%$ ), while there have been discrepancies for higher  $Ra$ .

Moreover, to evaluate the chip roughness, the Alicona focus variation microscope was used. This measurement is fundamental to determine whether or not the nanocomposite coatings give an advantage, considering that having a system with higher lubricity leads in smoother chip.

### *3.2.2 Preparation of the workpiece*

Before starting the first pass with a fresh corner, the surface of the workpiece must be cleaned with a cleaning tool, to minimize the work hardening effect from the last pass and ensure the desired diameter of the cylinder. In fact, when the previously tested corner reached the end of life, the diametral dimension indicated in the G-code was not effectively respected in real, due to the altered geometry of the insert.

Using this strategy, the tests have been standardised, avoiding systematic causes of error and variance between the processes that may distort the results.

### *3.2.3 First pass*

After the first pass of every corner, a sample of the chip has been stored, to allow eventual further analyses on the chip geometry and microstructure.

### *3.2.4 End of the tests*

For every trial, in this part of the project, the normative ISO 3685 has been considered for the end of life of the corners.

### 3.3 Digital Microscope Analysis

To plot the tool life curves, pass-by-pass superficial analysis of cutting tools have been carried out initially using a 200x magnification with a Keyence VHX Digital microscope, to obtain data related to the average and maximum flank wear (respectively  $V_{BB}$  and  $V_{Bmax}$ ). In order to extract more reliable measurements, an optical microscope has been also used to check the results.

Before the beginning of every tool life test, the corner under evaluation has been preliminarily observed under the microscope, to ensure the absence of defects on the coating distribution as chipping or delamination. Indeed, the tested coatings are under experimental development, so the chance of surface irregularities is high.

In order to remove residual powders that could avoid the correct measurements, a sticky patty (plasticine) has been gently tapped on the corner of interest before every microscopical scan.

#### *3.3.1 Set-Up Equipment*

The 3D-printed support showed in Figure 3.2 has been utilized for standardizing the orientation of every recorded image. This allows making comparisons between the different insert and passes.

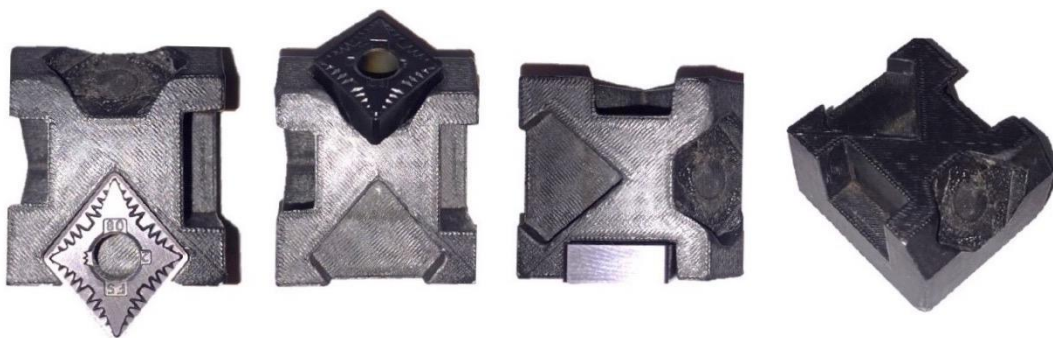


*Figure 3.2 – From left to right: Rake face, 3D image, Flank face, 3D-printed support*

Three images per pass have been taken:

- 3-Dimensional: it permits to have a general and comprehensive view of the tool wear;

- Rake face: crater wear and adhesion of Inconel are highlighted from this perspective;
- Flank face: the flank interested by the wear has been in this way analysed, allowing the measurements of  $V_{BB}$  and  $V_{Bmax}$ .

### *3.3.2 Flank wear measurement*

$V_{BB}$  and  $V_{Bmax}$  has been evaluated directly from a tool available in the Keyence software. In the following image an example of the result is shown. In the figure  $V_{BB} = 71\mu m$ , while  $V_{Bmax} = 197\mu m$ :

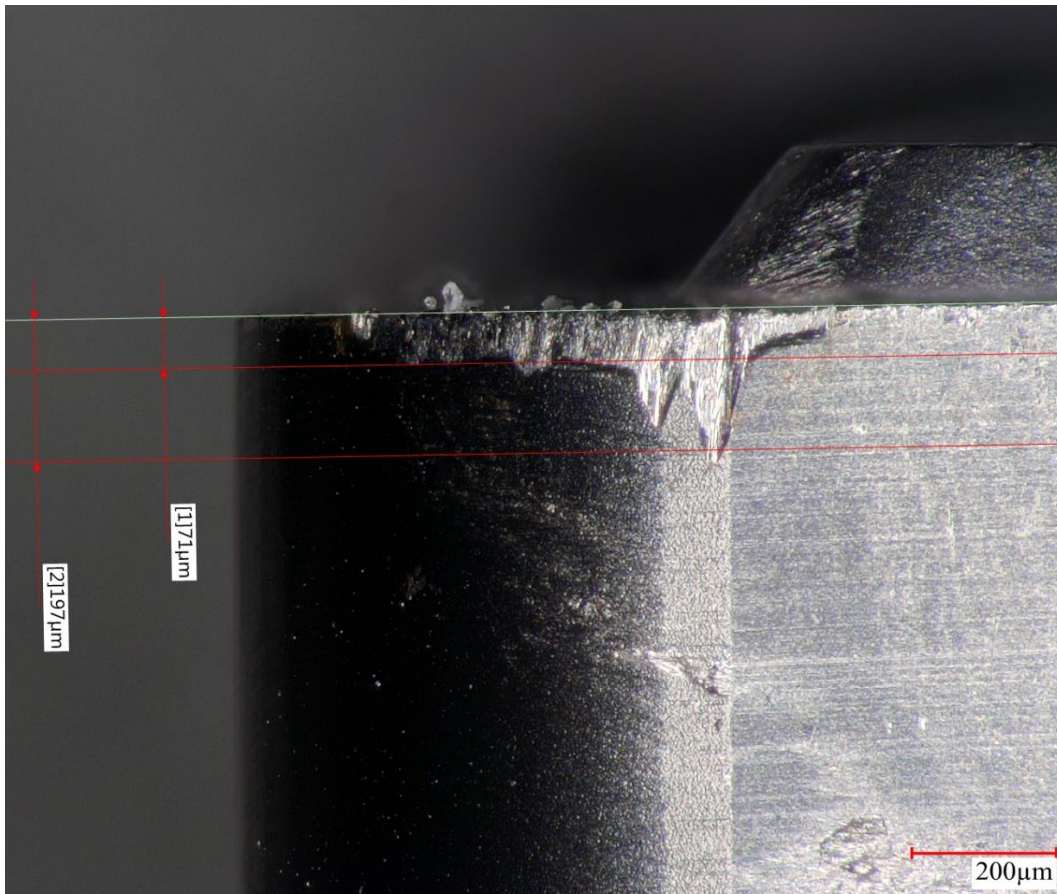


*Figure 3.3 – Example of the measurement made with the Keyence software to evaluate the flank wear after a certain pass*

## 3.4 Optimization of cutting parameters

### 3.4.1 Minimum cost speed

It is known that the total unit cost  $u$  [\$/pt] of a turning operation can be estimated as:

$$u = C_p \left( t_p + t_m + t_c * \frac{t_m}{T} \right) + C_t \frac{t_m}{T}$$

Where:

- $C_p$  [\$/min] is the unit cost of the workplace, including the labour cost and all the direct machining costs. Since the measure of this quantity is complex and variable from company to company, it will be evaluated as a mean of data available in literature for turning the superalloy;
- $C_t$  [\$] is the cost per cutting edge. Considering  $C_h$  [\$] as the cost of the holder (that is supposed to last about 400 times more than a cutting edge),  $C_i$  [\$] as the cost of the insert and  $N$  the number of cutting edges, on average  $C_t$  could be evaluated as [51]:

$$C_t = \frac{C_h}{400} + \frac{C_i}{0.75N} ;$$

- $t_p$  [min/pt],  $t_m$  [min/pt],  $t_c$  [min/pt] and  $T$  [min] are respectively the passive time (setup), machining time, tool replacement time and tool life.

The machining time can be expressed as:

$$t_m = \frac{L}{n * f} = \frac{\pi * D * L}{1000 * f * V_C}$$

In which:

- $L$  [mm] is the length of the cut;
- $n$  [rpm] is the spindle speed;
- $D$  [mm] represents the diameter of the part to be machined.

Moreover, it is remembered that Taylor's equation for tool wear is:

$$V_C * T^n = C$$

Where  $n$  and  $C$  are coefficients dependant on material and cutting conditions that can be experimentally evaluated. To find these values, a method is to perform several tool life tests at different cutting speeds (for example choosing 5 values of  $V_C$  around the theoretically optimal one), record the tool life  $T$  in minutes for every trial and then fit the constants  $n$  (that should be between 0.3 and 0.6) and  $C$  that best respect the general equation.

It is now possible to find the minimum cost tool life, substituting the expressions of  $t_m$  and  $T$  (since they are the only two terms depending from the cutting speed) in  $u$  and solving the derivative expression:

$$\frac{du}{dV_C} = 0$$

The resulting minimum cost speed is:

$$V_{C_e} = \frac{C}{T_e^n}$$

Where  $T_e$  is the cheapest tool life and it can be calculated as:

$$T_e = \left(\frac{1}{n} - 1\right) \left(t_c + \frac{C_t}{C_p}\right)$$

### *3.4.2 Maximum productivity speed*

Similarly to the minimum cost speed, to find the cutting speed which maximizes the productivity, it is helpful to write the expression representing the full time of the machining process per unit  $t$  [min/pt]:

$$t = t_p + t_m + t_c * \frac{t_m}{T}$$

Then, by substituting Taylor's equation in the relation above and deriving:

$$\frac{dt}{dV_C} = 0$$

The result in term of maximum productivity speed is:

$$V_{C_p} = \frac{C}{T_p^n}$$

In which  $T_p$  is the associated optimal tool life:

$$T_p = \left(\frac{1}{n} - 1\right) t_c$$

To calculate the minimum cost and maximum productivity cutting speeds, since the fitting of the parameters  $n$  and  $C$  was needed, a script has been implemented in Mathworks Matlab.

If coherent, the cutting speeds so calculated will be tested and compared with the results of the preliminary cutting tests.

## 3.5 Evaluation of performance

### *3.5.1 Tool Wear Rate TWR*

Since the core of the study is to evaluate the cutting performances for turning Inconel DA 718 in many different conditions, it is fundamental to employ some comparison parameters that express the ability of the coated systems to protect the insert from degradation.

For this purpose, the following equation is proposed for defining the average tool wear rate:

$$TWR = \frac{VB_B}{L} \left[ \frac{\mu m}{m} \right]$$

Where  $VB_B$  is the average flank wear in microns, while  $L$  is the considered length of the cut in metres.

Another measure for the TWR is the incremental one, that represents the local information of the tool wear rate, for a certain pass  $i$  of the tool life curve:

$$TWR_i = \frac{VB_{B_i} - VB_{B_{i-1}}}{l_i} \left[ \frac{\mu m}{m} \right]$$

Considering passes of the same cutting length,  $l_i \cong const \forall i$ , so the average TWR results to be:

$$TWR = \frac{\sum TWR_i}{n}$$

Where  $n$  is the total number of passes for the full tool life of the corner under test.

Together with the flank wear – length of the cut diagrams, in this way it is possible to obtain a more complete vision of the quality of the processes.

### *3.5.2 Material Removal Rate MRR*

MRR is also important for making considerations about performances. In fact, in order to take into account economic factors, investigating how fast is the turning operation in removing material and relating it to TWR is crucial.

The known expression for material removal rate is:

$$MRR = d * f * V_c * 1000 \left[ \frac{mm^3}{min} \right]$$

In which  $d$  represents the depth of the cut in millimetres,  $f$  the feed rate (in terms of millimetres per revolution) and  $V_c$  the cutting speed in metres per minute.

MRR is independent from the cutting length, thus, the value results to be unique during the whole tool life.

### *3.5.3 Index of Performance IP*

Another parameter to compare different processes is the index of performance (IP), defined as the ratio between the MRR and the TWR:

$$IP = \frac{MRR}{1000 * TWR} \left[ \frac{m^3}{min} \right]$$

The value should be as high as possible. Indeed, higher IP means that the TWR is relatively small, or that the tool is wearing slower, and (or) at the same time that the MRR is elevated so that the process is faster.

Using this index allows investigating the entire cutting process synthetically and therefore to rapidly differentiate the efficiency between several results.

A final comparison between all the outcomes of the study has been made using both Matlab and Excel, in order to qualitatively determine the best one to employ for the next part of the research.

### *3.5.4 TCCL and CCR*

As lasts, tool-chip contact length and chip compression ratio have been experimentally evaluated. Thanks to these quantities, important information about the lubricity of the coating and the deformation of both tool-tip and workpiece can be extracted. Thus, interesting considerations will be executed to differentiate not only the coatings, but also the cutting speeds.

### 3.5.4.1 Tool Chip Contact Length TCCL

TCCL has been measured as shown in the example in Figure 3.4: on the rake face, it represents the perpendicular maximum distance from the tool-tip interested by the worn area, after the first pass. In the figure,  $TCCL = 247\mu m$ .

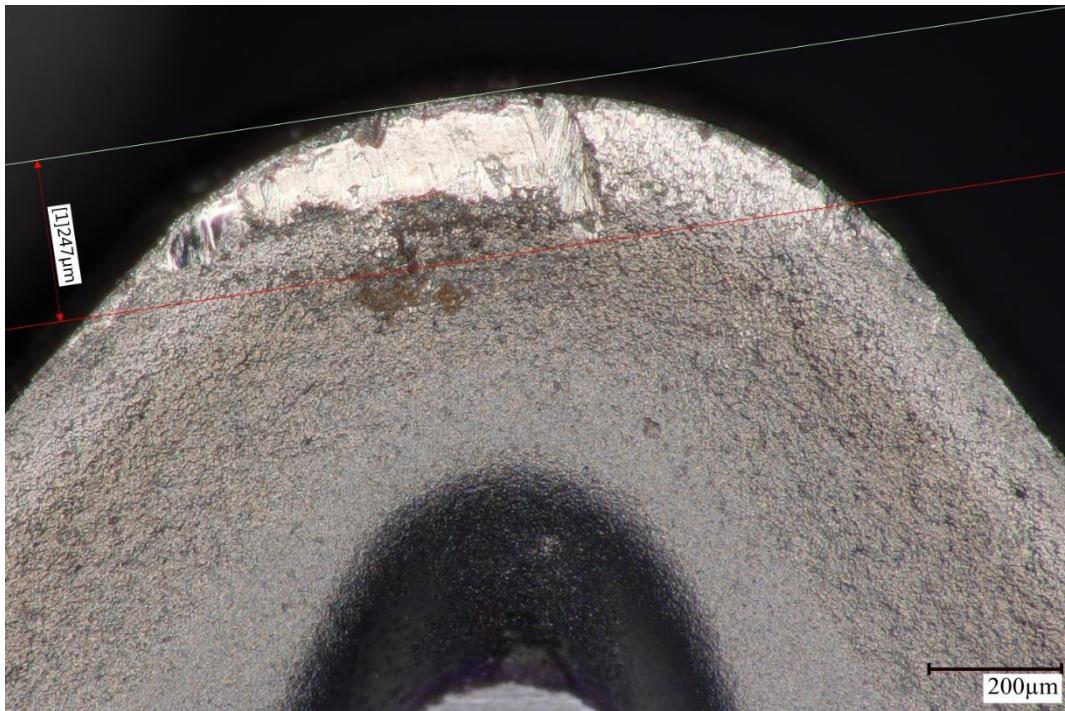


Figure 3.4 – Example of TCCL measurement made with the Keyence software

As much the TCCL is higher, as lower is the lubricity of the system, because it means that the sticking and sliding areas of contact between chip and tool rake face are more extended.

### 3.5.4.2 Chip Compression Ratio CCR

The CCR has been evaluated through the equation:

$$CCR = \frac{d_{re}}{d}$$

In which  $d_{re}$  is the thickness of the deformed chip after the first pass and  $d$  is the thickness of the undeformed chip, or the depth of the cut.

To investigate the  $d_{re}$  values, at first, the chip cross sections have been treated with a cold mounting (or embedding) in epoxy resin; than it has been polished (Figure 3.5).



*Figure 3.5 – Embedded chip in epoxy resin to measure the thickness*

In this way, the cross sections have been positioned orthogonally to the observing direction. Then,  $d_{re}$  have been measured through the software of the Keyence microscope and the values have been calculated through an average of 5 measurements.

### 3.6 Three-Dimensional Tool Wear Analysis

The second part of the project has been focused on the comparison of the 3D volume wear and the built-up edge evolution along the tool life between the KC5010 and the nanocomposite multi-layered coated tools.

All the tests have been performed using the most convenient cutting speed, according to the research described in the previous sections.

To execute these analyses, the FVM Alicona Infinite Focus G5 has been used. A description of the followed procedure is expressed below.

#### 3.6.1 Scanning and Post-processing procedures

These scansions with FVM, are practically pretty similar to the ones performed with the Keyence digital microscope to analyse the flank wear, therefore the same support has been employed and a similar procedure with the microscope has been followed to caption the 3D images.

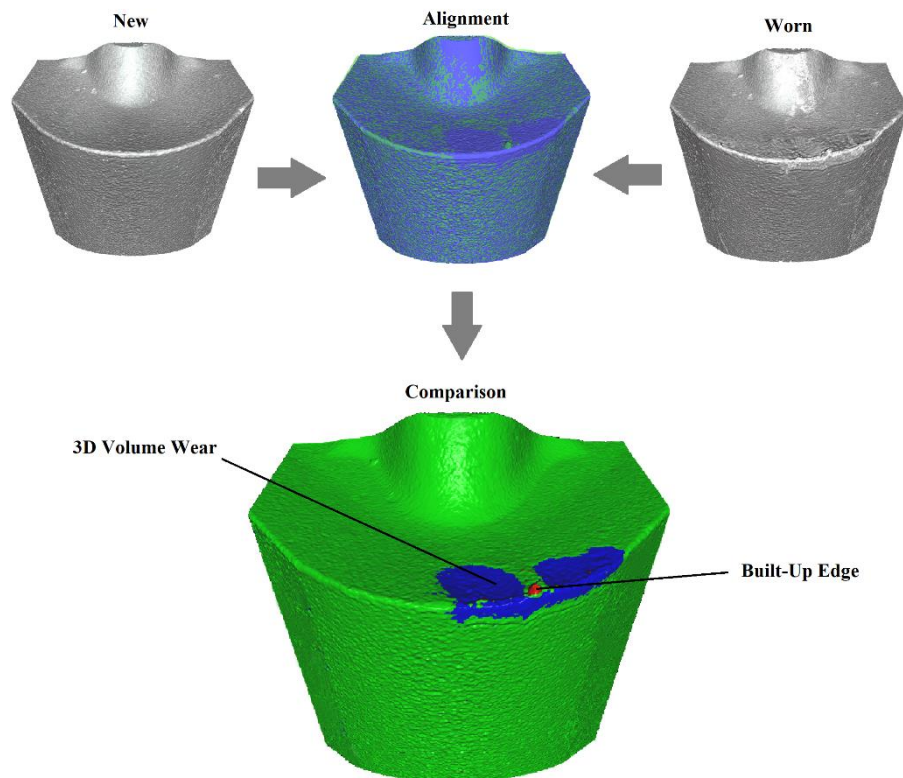


Figure 3.6 – A graphical explanation of post-process analysis of the 3D captions

Before the start of the machining process, every corner under examination has been captured, in order to have a comparison figure to calculate the 3D volume wear and to estimate the amount of built-up edge after every pass.

Subsequently, after every pass (around 130m of cutting length), the 3D associated figure has been aligned and compared with both the one from the previous pass and the original image of the unworn insert.

The resulting parameters that are extracted from the process using the Alicona software are:

- *Peaks Volume  $V_p$* : the total volume of material exceeding the reference surface of the original insert;
- *Valleys Volume  $V_v$* : the total volume of material below the reference surface of the original insert;
- *Incremental Peaks Volume  $V_{p_{discr}}$* : the total volume of material exceeding the reference surface delimited by the previous pass;
- *Incremental Valleys Volume  $V_{v_{discr}}$* : the total volume of material below the reference surface delimited by the previous pass.

$V_p$  and  $V_{p_{discr}}$  allow the estimation of the BUE on the tool edge, while  $V_v$  and  $V_{v_{discr}}$  help to evaluate the 3D volume wear.

## 3.7 Scanning Electron Microscope (SEM) analysis

Employing the Tescan Vega II LSU SEM, further observations of the worn tool-tips can be captured in high quality. That images allow confirming the already evaluated chipping, abrasion and BUE wear modes and mechanisms.

Moreover, through the Oxford X-MAX system, also Energy Dispersive X-ray Spectrometry (EDS) have been performed. EDS is useful for determining the chemical elements distribution around the tool corners and consequently making assumptions about the diffusion mechanisms.

## Chapter 4: Results and Discussion

### 4.1 Tools architecture

The nanocomposite coatings show, as supposed, high hardness and elastic modulus. Furthermore, the plastic index ( $\sim H/E$ ) is lower than 0.6: in case of contact, most of the asperities are deformed elastically, while plastic deformation occurs only under high contact pressures. In opposition to the nanocomposites, the microhardness obtained for KC5010 through nanoindentation is around 20 GPa.

The data are expressed in Table 4.1:

<i>Coating</i>	<i>Hardness H [GPa]</i>	<i>Elastic Modulus E [GPa]</i>	<i>Plasticity Index</i>
<i>Ti20Cr20Al52Si8N</i>	$37.3 \pm 4.6$	466.01	0.40
<i>TiAlCrN/TiCrAl52Si8N</i>	$38.7 \pm 4.5$	517.21	0.42

Table 4.1 – Hardness, elastic modulus and plasticity index for the nanocomposite coatings

#### 4.1.1 Coatings characterization

In Figure 4.1 an SEM image of the nanocomposite coating cross-section after brittle breakage is displayed. The thickness is around 2 microns, composed by alternate TiAlCrSi8N and TiAlCrN nano-layers of about 20 nm thick.

Regarding the nanocomposite mono-layered coating, the cross-sectional SEM investigation has not been performed, since the result of the cutting tests (discussed in the next paragraphs) have been not relevant. The declared data of the coating thickness from Kobelco industry is of 3 microns.

From past research [52], it is known that the KC5010 is structured with a single PVD AlTiN 3 microns thick layer. The average grain size is 1 micron.

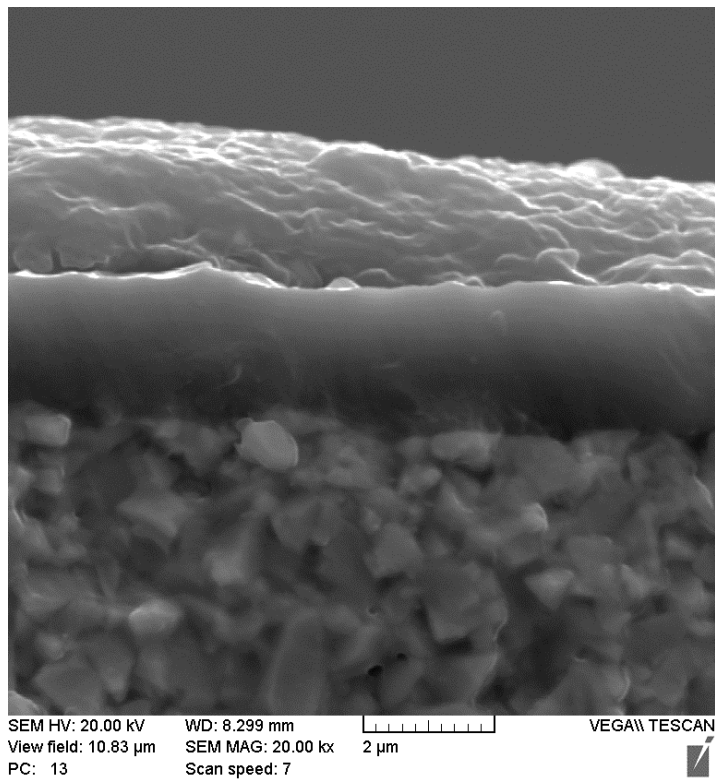


*Figure 4.1 – SEM image of the nanocomposite coating cross section*

## 4.2 Preliminary cutting tests

The first cutting test has been held at  $60\text{ m/min}$  of cutting speed for the three coatings, while for the next trials at  $80\text{ m/min}$ ,  $120\text{ m/min}$  and then at  $97\text{ m/min}$  (calculated minimum cost cutting speed), just the benchmark coating KC5010 and the multi-layered nanocomposite TiAlCrN/TiCrAl<sub>52</sub>Si<sub>8</sub>N coating have been tested, since the results obtained for the mono-layered nanocomposite Ti<sub>20</sub>Cr<sub>20</sub>Al<sub>52</sub>Si<sub>8</sub>N coating have been unsatisfactory, so it is possible to state that this system is not suitable for machining Inconel DA 718, at least with the chosen cutting parameters.

### *4.2.1 Workpiece and Chip Roughness*

The roughness of the workpieces has been checked after every pass in the tests at  $80$ ,  $97$  and  $120\text{ m/min}$  and the trends for these measures are showed in Figure 4.2.

From all the curves, it is clear that the main tendency is similar in all cases. There are three distinguished zones in the roughness curves:

- Initially, correspondently to the first area of the tool life curves (Figure 4.17),  $R_a$  is relatively high in respect of the other two zones. This is justified by two main factors. At first, during the initial passes, the tribofilms are forming and not yet developed, so the lubricity of the coating is not elevated and therefore the friction between tool and chip is still high, with the consequence of worse surface finish. Furthermore, at the beginning, the tool corner is sharp and the radius small.
- In the second zone the tribofilms are well developed and at the same time the tool is not greatly worn; thus, the coating has high lubricity. Moreover, a small tool wear might be advantageous for the roughness, because the geometry of the corner is modified by the wear in itself, that tends to increment the tool tip radius.
- Lastly, the tool results to be intensively worn. There is no coating anymore on some areas and therefore neither protective nor high-lubricious tribofilms. Another issue is the presence of chipping and BUE on the tool edge, that confer bad surface finish on the workpiece.

**Results and Discussion**  
**4.2 Preliminary cutting tests**

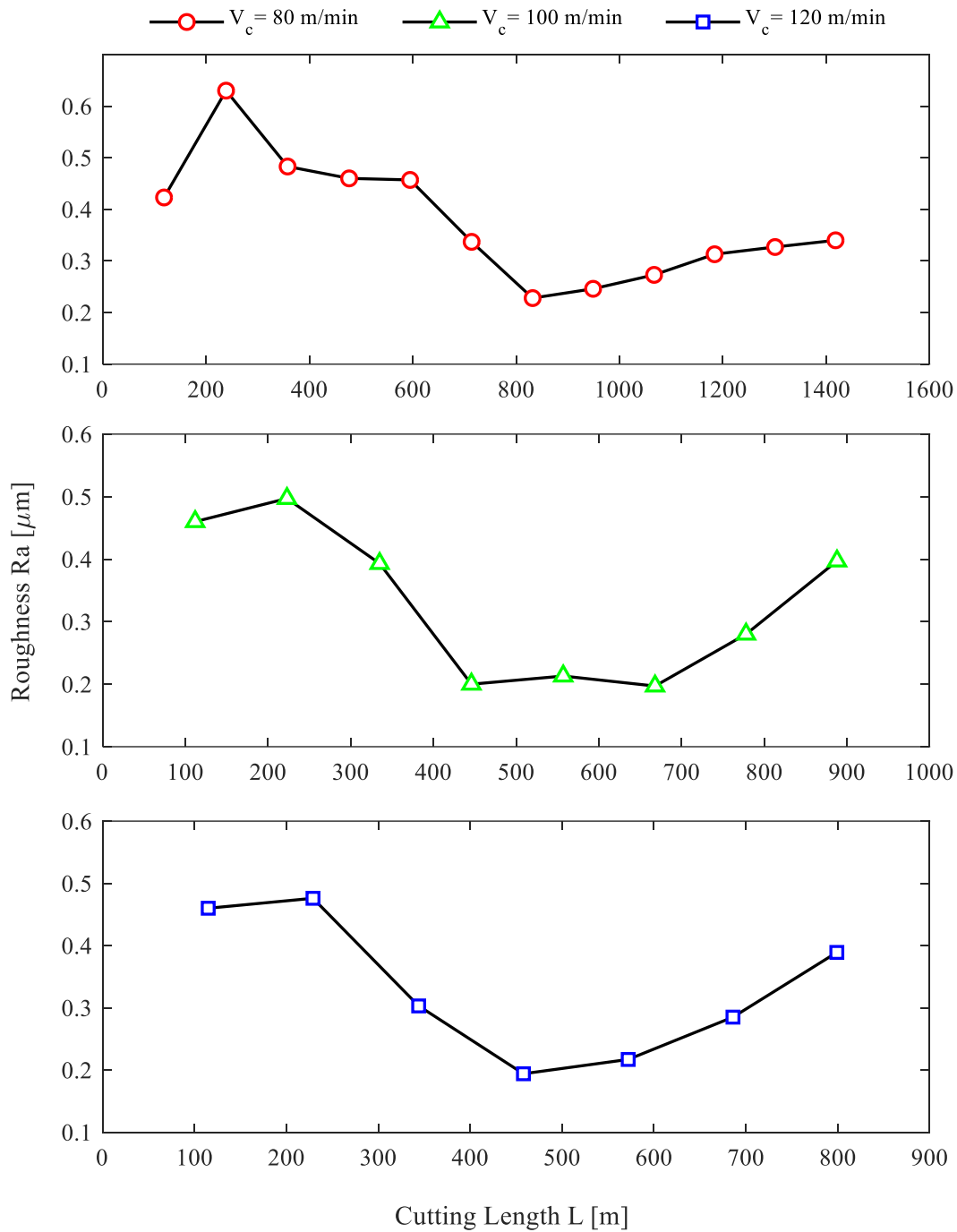


Figure 4.2 – Roughness of the surface of the workpiece during the subsequent passes of the cutting process with the nanocomposite multi-layered coating

On average, Figure 4.3 confirms that higher cutting speed ensure better quality of the surface, especially at the beginning of the tool life, while lower cutting speed have better results around the half of the tool life (starting from 500m). This outcome can be justified by the tribofilms formation, that happens earlier as much

as the speed is increased. The diagrams below are limited to the minimum tool life of every insert at one of the studied cutting speeds, because of problems of representation.

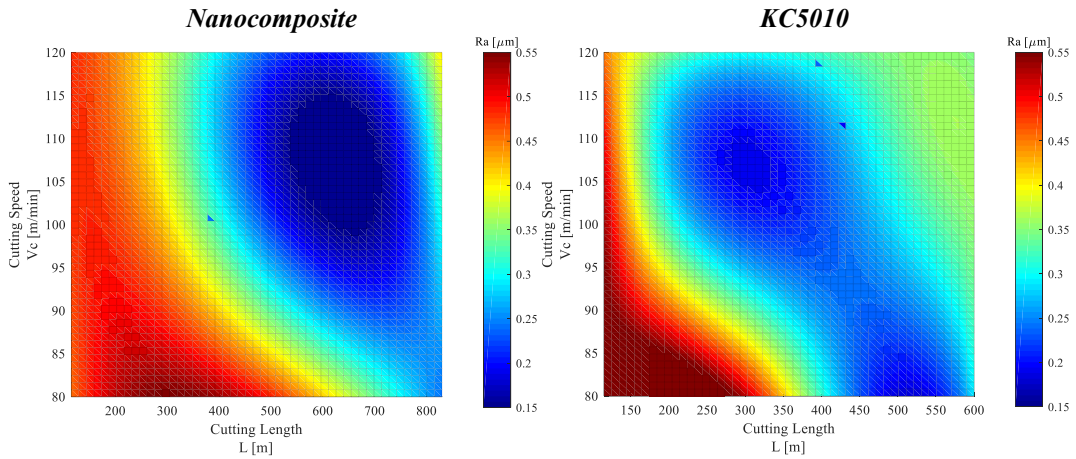


Figure 4.3 – Comprehensive representation of the machined workpiece surface roughness along the tool life at different cutting speed

Regarding the chip roughness, the results gotten by the Alicona software are showed in Table 4.2. As it can be seen from the table, the surface roughness indicator  $Sa$  were studied, in that it gives a more accurate description of the whole superficial area. Overall, the roughness is around  $0.3 \mu m$  for the nanocomposite, versus an average of  $0.7 \mu m$  for the benchmark. These measures of the chip smoothness prove the better lubricity of the nanocomposite coating.

$V_c \left[ \frac{m}{min} \right]$	$Sa \left[ \mu m \right]$	
80	0,34	0,32
100	0,26	0,84
120	0,34	0,82
	<i>Nanocomposite</i>	<i>KC5010</i>

Table 4.2 – Surface roughness of the chip  $Sa \left[ \mu m \right]$

Figure 4.4 is the result of scanning of the chip surface after the first pass, varying the cutting speed. It shows that using a fresh corner, initially, a lower cutting speed implies smoother chip. This result is coherent with the values of surface roughness

of the machined workpiece after the first pass, that can be observed looking the values close to the vertical axes in Figure 4.3. Furthermore, the nanocomposite coating produces more regular chip, with shallow grooves and scratches in the machining direction.

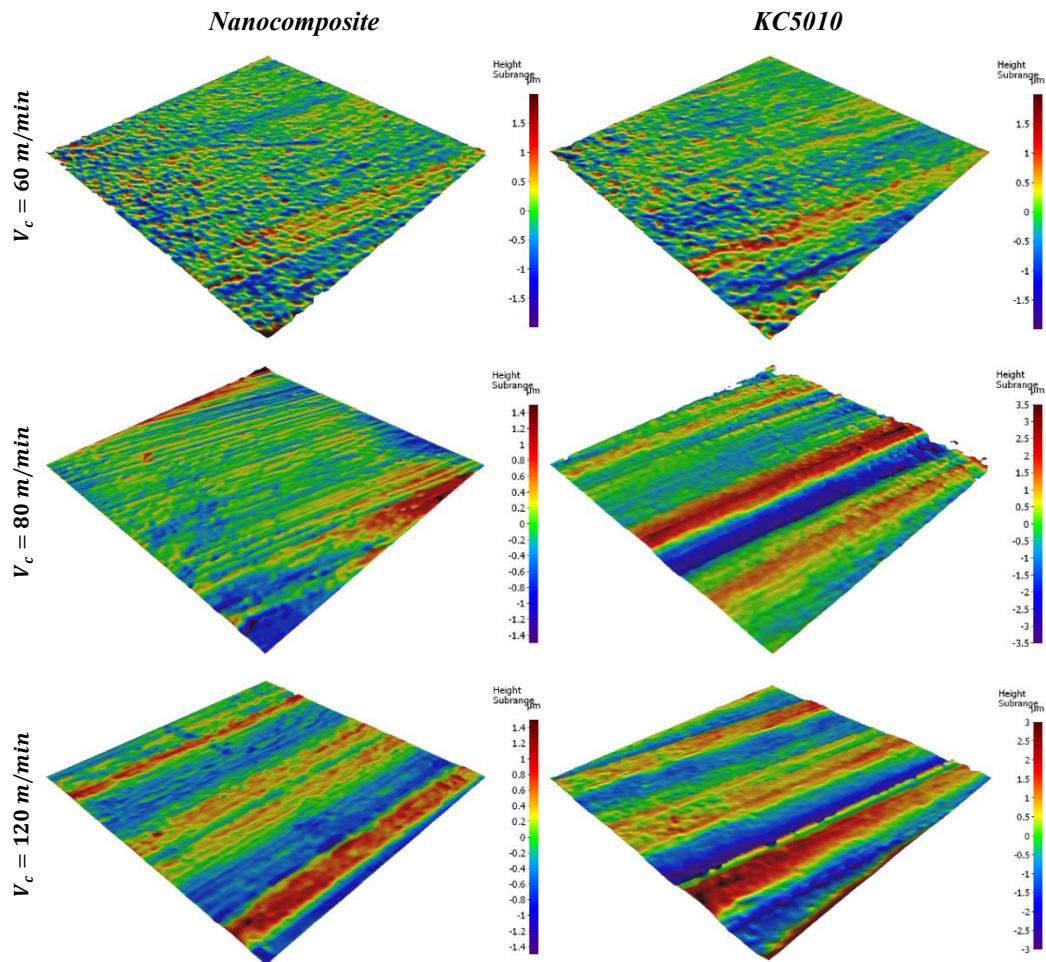


Figure 4.4 – Three-Dimensional images of the chip surface after the first pass

## 4.3 Digital microscope analysis

### *4.3.1 Microscopic Figures*

In the following, the most significant results of the preliminary cutting tests are presented. The selected cutting lengths are approximately  $L = 130m$  (after the first pass – first zone of the tool life curve),  $L = 600m$  (representing typically a cutting length in which the increasing of flank wear is almost linear – second zone of the tool life curve) and the  $L$  corresponding to the end of life for the considered corner at the evaluated  $V_c$ .

#### **4.3.1.1 $L = 130m$**

Considering the benchmark KC5010, as shown in Figure 4.5, noteworthy is the fact that for  $V_c = 60 m/min$ , the main tool wear mode is notching. Indeed, secondary notches and a wide and deep depth-of-cut notch can be noticed. This is justified by the relatively high ductility of Inconel DA 718: at low cutting speed, the superalloy tends to be deformed by the tool, with the consequence of material accumulation at the depth-of-cut that implies an increase in the notching phenomenon. Raising the cutting speed to  $80 m/min$ , higher temperature and strong adhesion lead to the formation of BUE. As a consequence of this tool wear mode, also the roughness of the machined workpiece is higher in respect of the other cases. At  $V_c = 120 m/min$ , elevated contact forces are responsible to crater wear. However, thanks to the formation of alumina, the crater has been not deep at this stage.

Regarding the multi-layered coating (Figure 4.6), at  $60 m/min$ , the behaviour of the system is pretty similar with the benchmark, for the same reasons explained above, but the notching is more limited and the rake face seems to be less worn. When  $V_c$  is raised to  $80 m/min$ , flank wear and notching are very limited, but microchipping on the rake can be seen, perhaps due to micro welding and successive detachment of material. The best behaviour is observed instead at  $V_c = 120 m/min$ , where BUE, notching, flank wear and crater are prevented by the formation of tribofilms thanks to the high temperatures.

**Results and Discussion**  
4.3 Digital microscope analysis

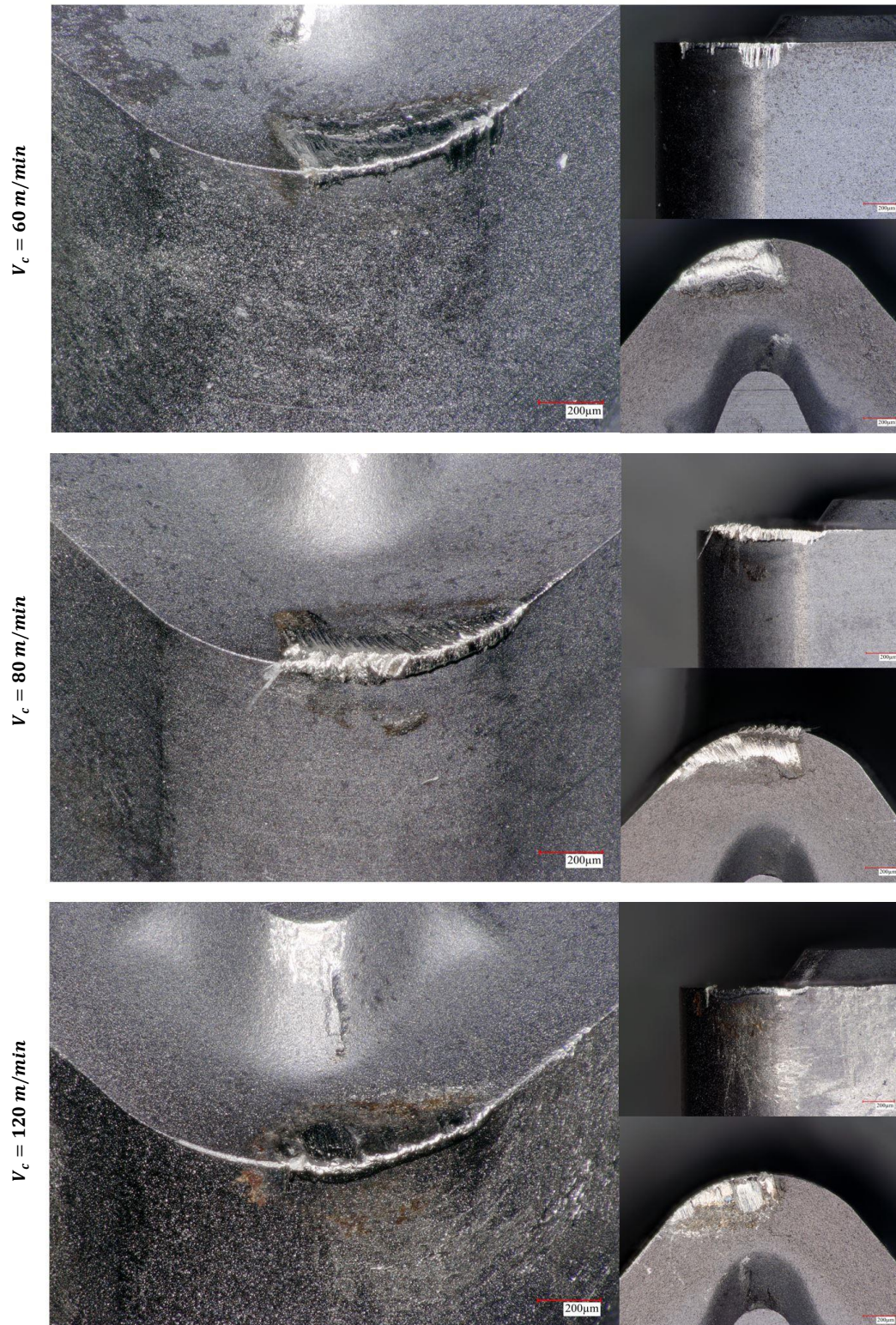


Figure 4.5 – Tool wear microscopic images after the first pass for KC5010 coating, obtained with 200x magnification

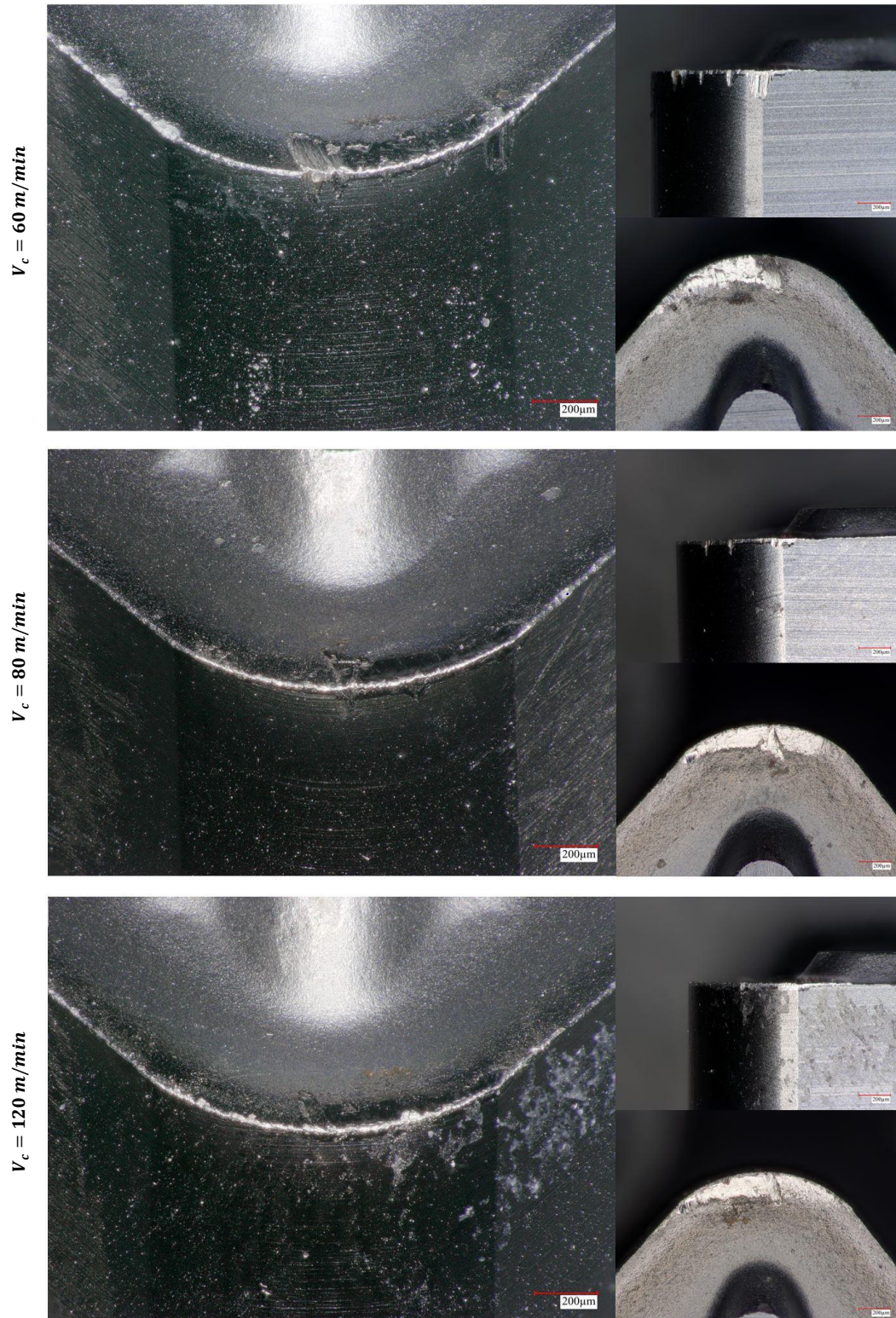


Figure 4.6 – Tool wear microscopic images after the first pass for TiAlCrN/TiCrAl52Si8N coating, obtained with 200x magnification

#### **4.3.1.2 $L = 600m$**

The following Figure 4.7 and Figure 4.8 show microscopic pictures relative to the 3D, flank and rake views after 600m of cutting length.

For KC5010, the notch has become wider for the cutting speed of 60 *m/min*, counting now as almost half of the flank wear extension. With regards to the 80 *m/min* and 120 *m/min* cutting speeds, in both cases chipping took place. This phenomenon is explained by the continuous adhesion and detachment of material on the surface, that tends to remove material from the tool body. It is more remarkable at higher  $V_c$ , because of the combination of elevated forces and temperatures.

The behaviour of the nanocomposite coating has been generally better in this stage. Particularly, at low cutting speed, notching is less expanded on the flank face. It is worthwhile to give attention to the 80 *m/min* edge: the flank wear appears homogeneous and the crater shallow. This  $V_c$  is clearly an advantageous balance between the main effects. Indeed,  $V_c = 80 \text{ m/min}$  is enough to provide an effective formation of tribofilms and spinodal decomposition (thanks to the high reached temperatures) and it is also not too much elevated to lead in chipping and catastrophic failure, as instead it tends to be at 120 *m/min* (comparable with the result of using KC5010 at  $80 \div 120 \text{ m/min}$ ).

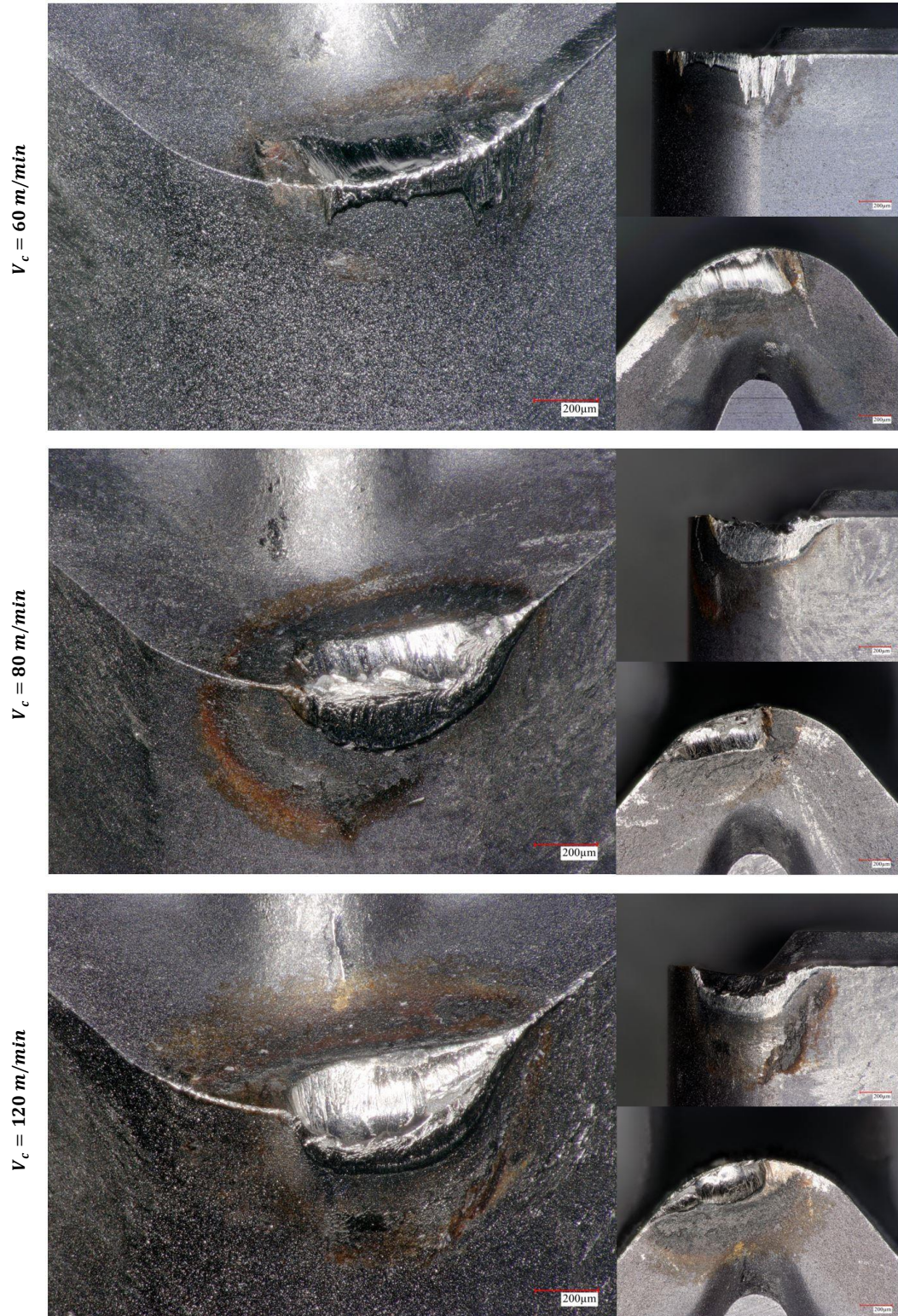


*Figure 4.7 – Tool wear microscopic images and after  $L = 600m$  for KC5010 coating, obtained with 200x magnification*

*Results and Discussion*  
*4.3 Digital microscope analysis*

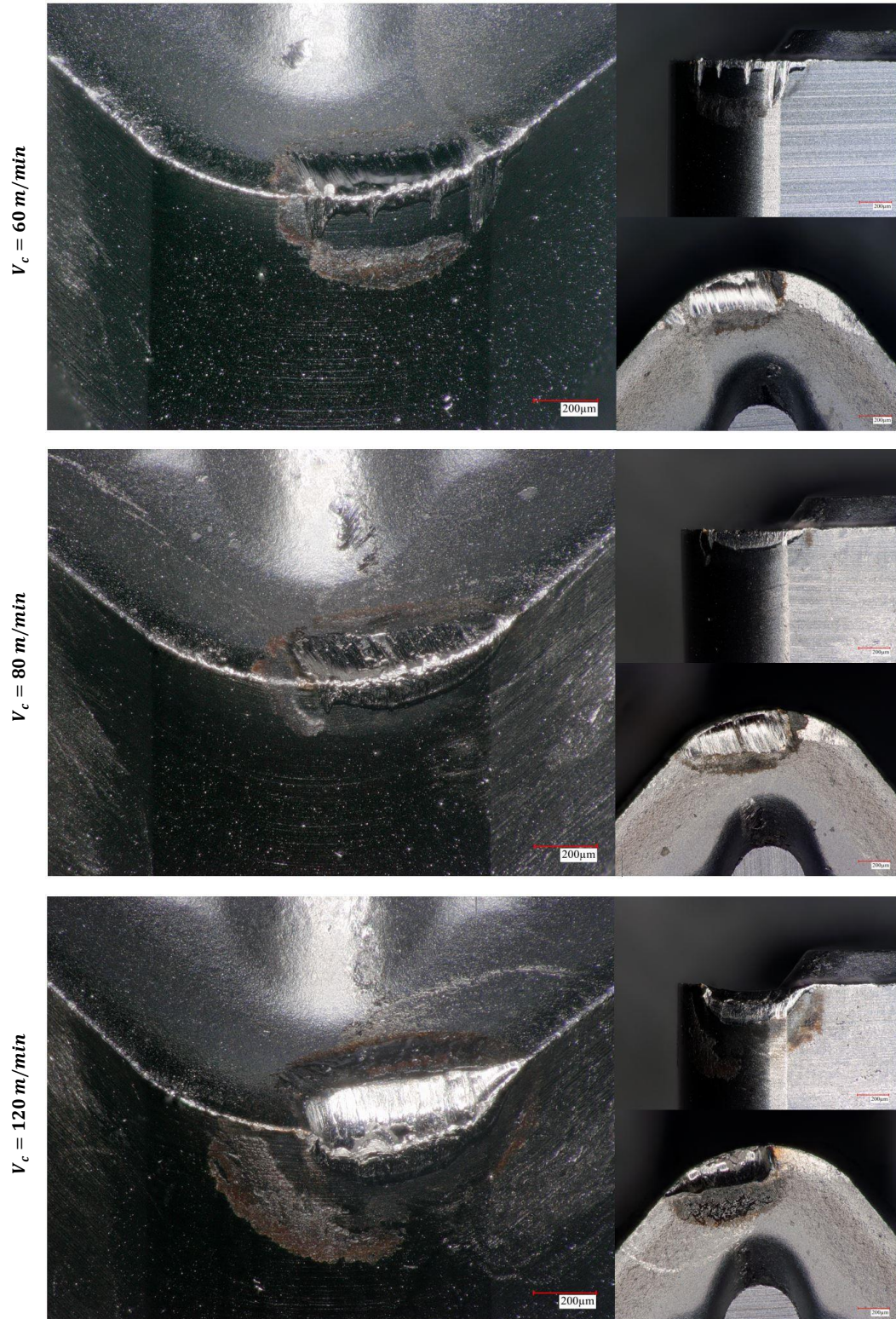


Figure 4.8 – Tool wear microscopic images after  $L = 600\text{m}$  for  $\text{TiAlCrN/TiCrAl52Si8N}$  coating, obtained with 200x magnification

#### ***4.3.1.3 End of Life***

As demonstrated in Figure 4.9, KC5010 reached the end of life by three different conditions. At 60 *m/min* the flank wear, result of abrasion and wide notching, overtook the limit of  $V_{BB} = 300\mu m$ . Increasing  $V_c$ , delamination has been occurred in the case of 80 *m/min*, while at 120 *m/min*, because of greater machining forces, adhesions and detachments led in catastrophic failure.

The failures of the nanocomposite TiAlCrN/TiCrAl52Si8N coating have been happened mainly according to the same criteria of KC5010: abrasion and notching for low  $V_c$  and chipping in case of greater cutting speed (worse results have been collected at 120 *m/min* in comparison to 80 *m/min*)

To get better results, a proposed idea from some researchers is to perform the first pass at high speed and then to speed down (for example, from 80 to 60 *m/min*). In this way, a resistant layer of tribofilms and – in case of the chosen nanocomposites and similar compositions – spinodal decomposition can be initially obtained and then exploited to resist against abrasion and notching. However, this practice is not ever recommended because not easy to employ in a manufacturing company where the time spent for this procedure could be disadvantageous.

**Results and Discussion**  
4.3 Digital microscope analysis

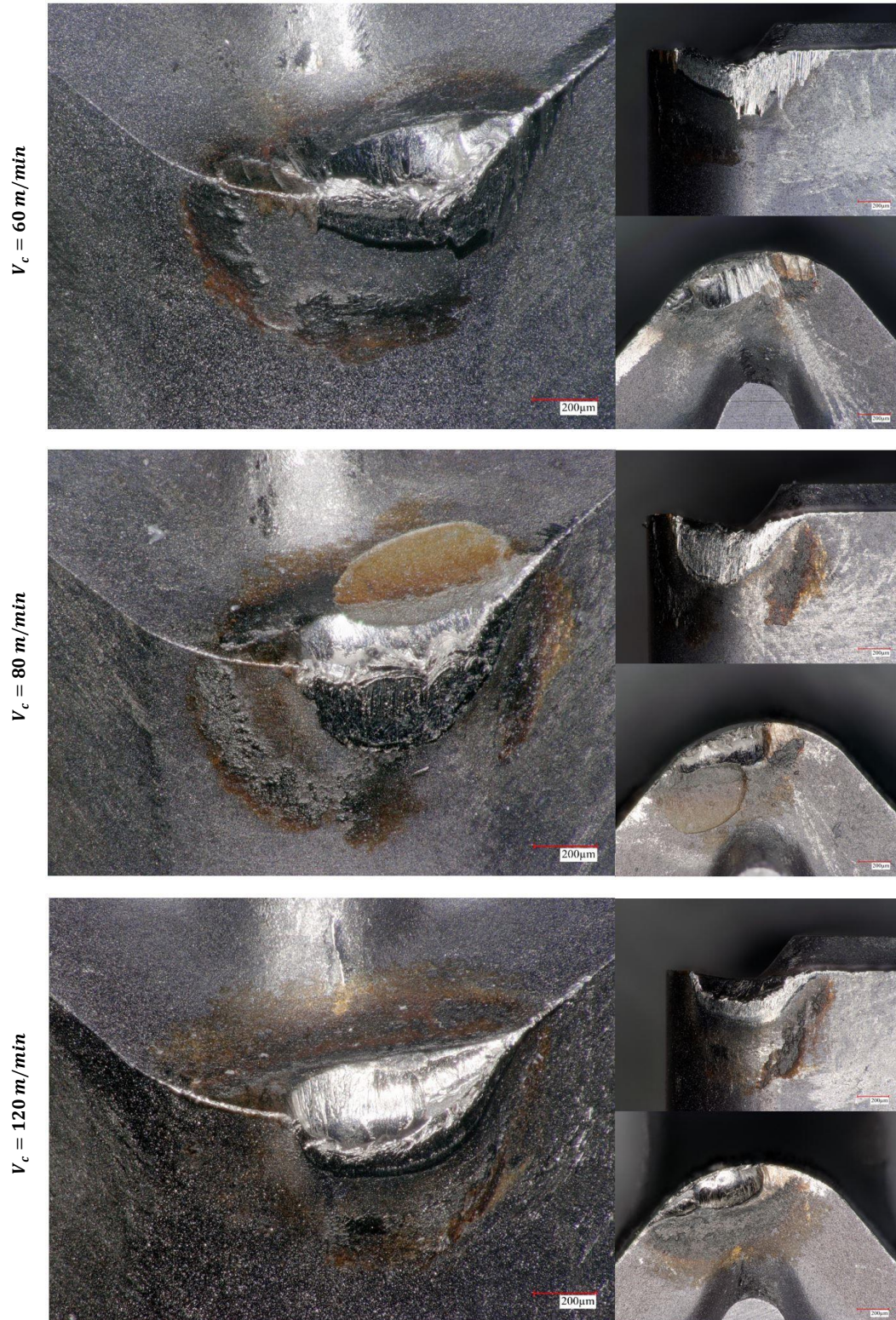


Figure 4.9 – Tool wear microscopic images at the end of life for KC5010 coating, obtained with 200x magnification

*Results and Discussion*  
*4.3 Digital microscope analysis*

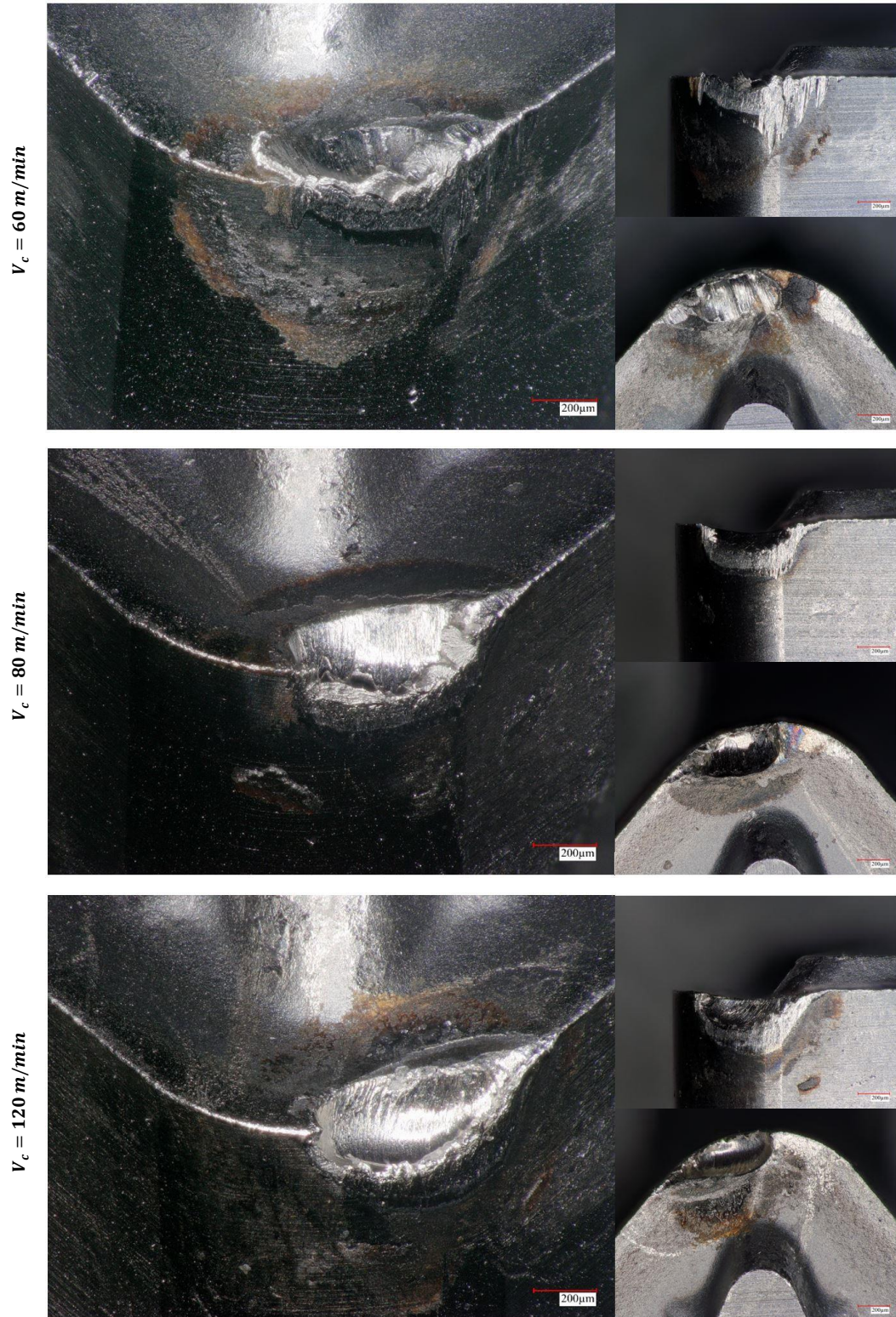


Figure 4.10 – Tool wear microscopic images at the end of life for TiAlCrN/TiCrAl52Si8N coating, obtained with 200x magnification

## 4.4 Optimization of cutting parameters

### 4.4.1 Computation

As mentioned above, a Matlab script has been developed to optimize the cutting parameters by fitting Taylor's curve with the experimental data obtained from the preliminary cutting tests.

Initially, after defining a vector containing all the cutting speeds of the preliminary trial, the length of the cut to reach the end of life  $L$  has been expressed in terms of time ( $T$  [s]):

```
Vc = [60 80 120]; %[m/min]
```

```
T = [1386/Vc(1)*60 1418/Vc(2)*60 799/Vc(3)*60]; %[s]
```

After that, the known constants have been defined:

```
tc = 30; %[s]
```

```
Ch = 71.60; %[€/toolholder]
```

```
Ci = 23.38; %[€/insert]
```

```
Ct = Ch/400+Ci/(0.75*4); %[€/edge]
```

```
Cp = 0.0138; %[€/s]
```

After monitoring it experimentally,  $t_c$  (or the time to change corner) has been estimated as 30s. The cost of the toolholder is the currently available on the Kennametal website [53], while the cost of the insert is the proposed by Kobelco industry. To assess the sum of the costs directly dependant on the machining operation  $C_p$ , the cost estimator by CustomPartNet has been employed [54]. Indeed, the value of  $C_p$  is different between countries, sector, as well as companies in themselves; therefore, generally thinking, using a cost estimator is a reasonable strategy. Then, the same study can be also applied on a particular industrial plant, to get the real value of the considered company.

The next step has been defining a general function describing the calculation of the cutting speed through Taylor's equation with unknown values of the constants  $C$

$(x(1))$  and  $n(x(2))$  and another function representing the quadratic error between the experimentally employed and the Taylor's cutting speed. Then, the optimal values of  $C$  and  $n$  have been found using the function `fminsearch`, through a fitting of the experimental data.

```
Vc_fun = @(x) x(1)./T.^x(2);
```

```
Vcerr_fun = @(x) sum((Vc-Vc_fun(x)).^2);
```

```
[x_opt fval_Vc] = fminsearch(Vcerr_fun, [90/1000^0.45  
0.45]); % [C n]
```

Then, applying the equations related to the minimum cost speed and maximum productivity speed described in the Methodology chapter, the optimized cutting speeds have been calculated. The results are showed in Figure 4.11:

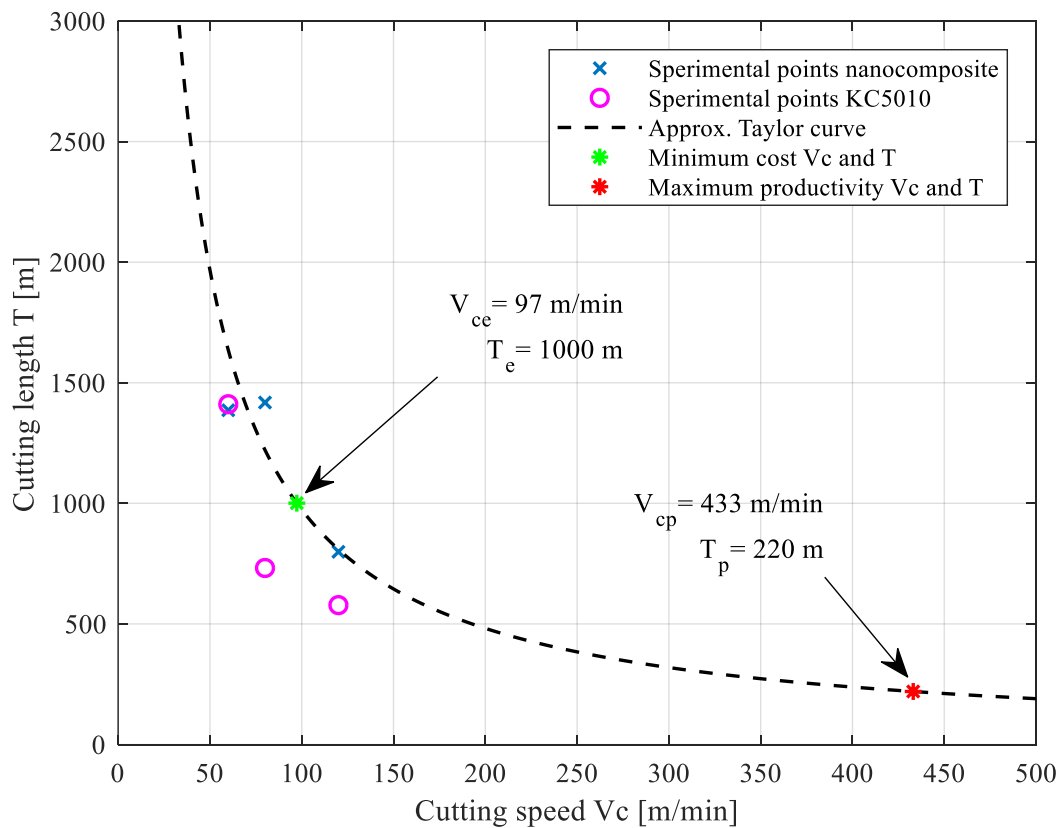


Figure 4.11 – Minimum cost and maximum productivity cutting speeds

From the image, it can be seen that the resultant  $V_{cp}$  is not coherent with the main idea of the project, because the value is too much elevated. Consequently, further

analysis has been focused just on the cost optimization through the experimental test of  $V_{c_e} = 97 \text{ m/min}$ .

#### *4.4.2 Cutting test with the minimum cost cutting speed*

The results of the evaluated minimum cost cutting speed  $V_{c_e} = 97 \text{ m/min}$  are showed in Figure 4.12 (for KC5010) and Figure 4.13 (for the nanocomposite multi-layered coating).

The tool life data for KC5010 are as expected not coherent with the evaluated Taylor's curve; the life of the tool has been particularly short (even shorter than the tests at  $120 \text{ m/min}$ ), due to critical chipping and extreme flank wear. This behaviour could be associated to high forces and at the same time temperature not enough elevated to form resistant tribofilms.

Even the nanocomposite coating achieved worse outcomes than expected. Indeed, as shown in Figure 4.11, the predictive model forecasted a tool life around  $L = 1000\text{m}$ , while in the experimental trial the tool lasted about  $900\text{m}$ . This discrepancy might be associated to the fact that the analytical Taylor's model does not consider the effect of all the tool wear modes: in this research, the most intensive types of wear are not only flank wear and depth-of-cut notching, but strong BUE and chipping are verified. A clear demonstration of that are the microscopic images in Figure 4.13.

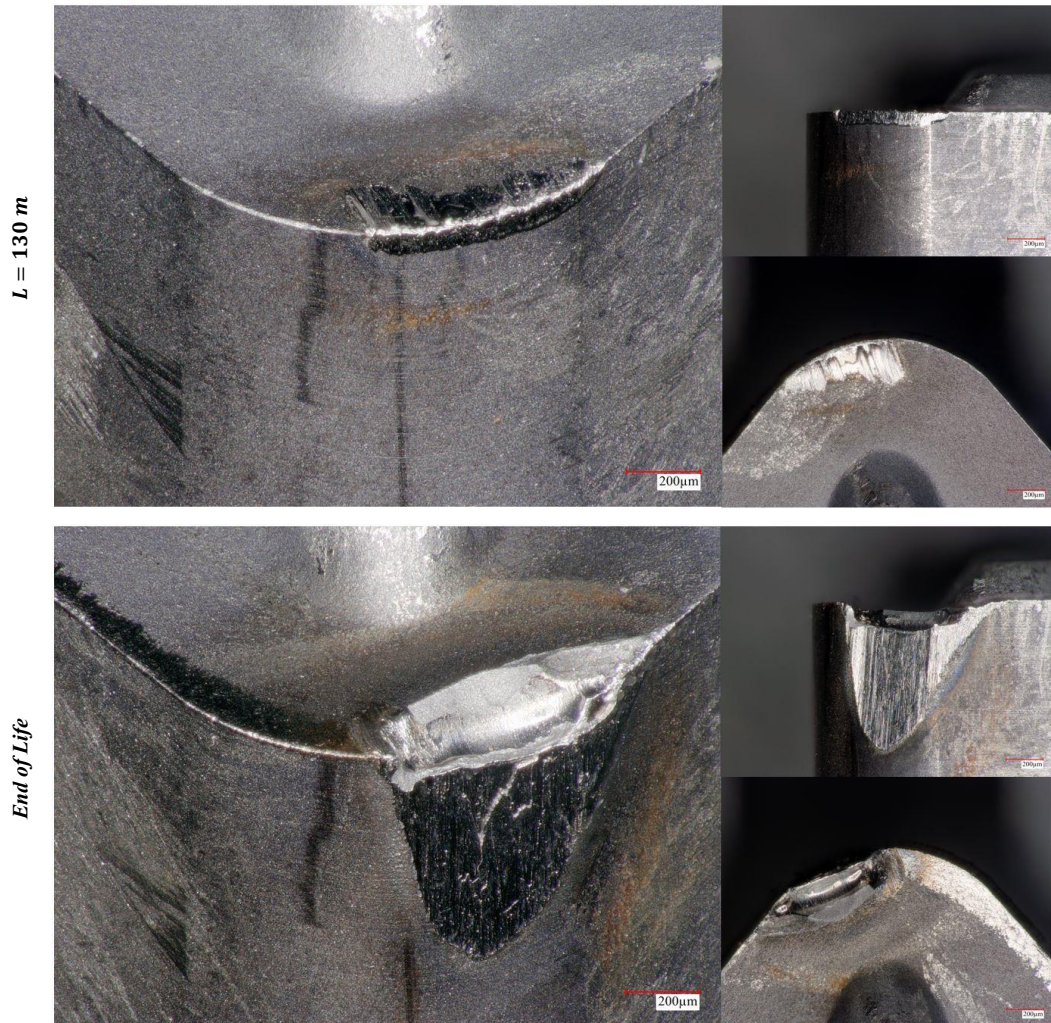


*Figure 4.12 – Tool wear microscopic images for KC5010 coating, obtained with 200x magnification, for cutting speed  $V_c = 97$  m/min*

*Results and Discussion*  
*4.4 Optimization of cutting parameters*

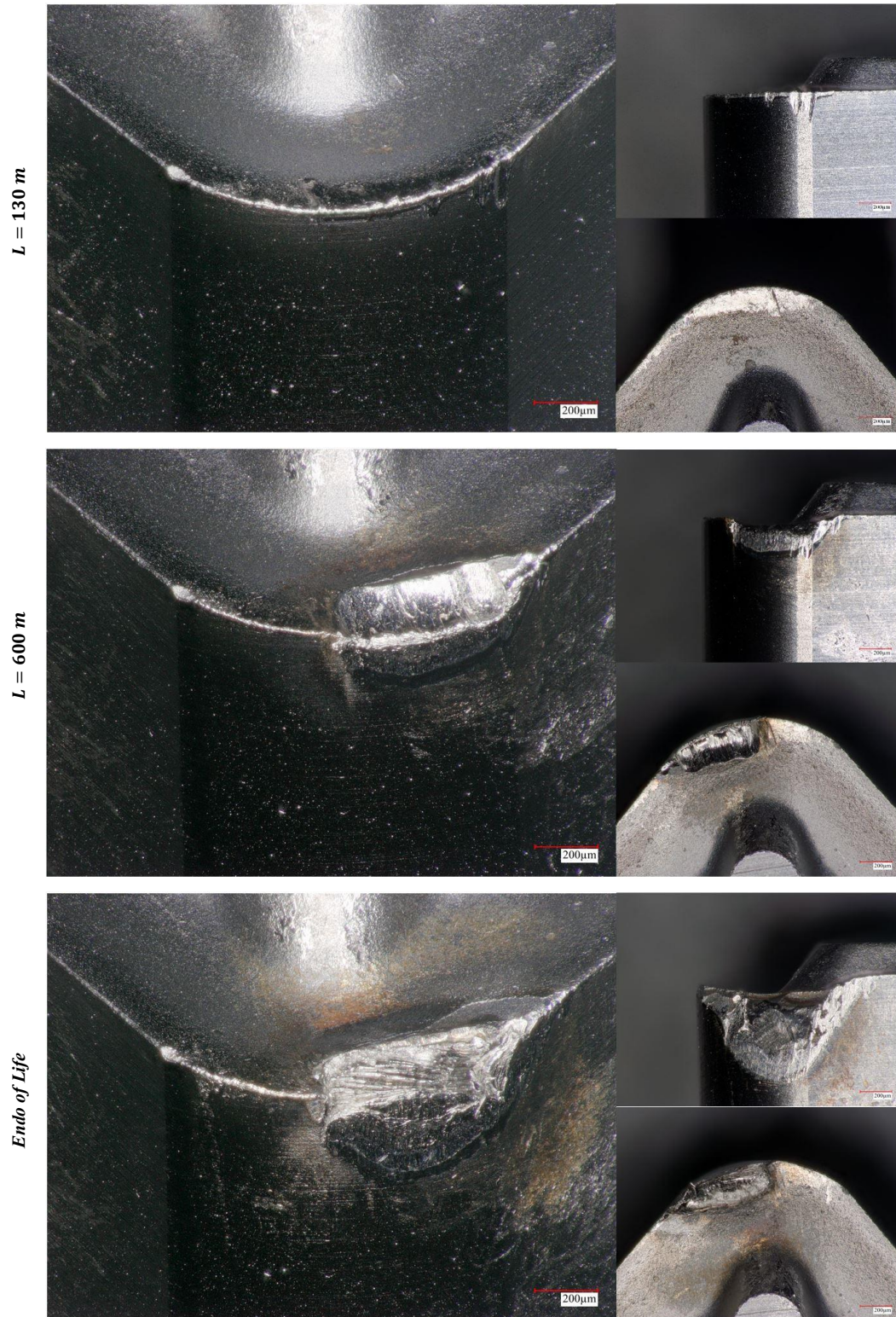


Figure 4.13 – Tool wear microscopic images for the multi-layered nanocomposite coating, obtained with 200x magnification, for cutting speed  $V_c = 97$  m/min

## 4.5 Evaluation of performance and comparison

### 4.5.1 Tool Wear Rate TWR

Figure 4.14 has been obtained by a Matlab third-order interpolation of all the available TWR values in a range between 0 and 900m of cutting length. Coherently with the tool life curves (Figure 4.19), in this range, the best behaviour has been observed for the slowest cutting speed  $V_c = 60 \text{ m/min}$  and TWR tends to increase raising up  $V_c$ . Moreover, it is worth noticing that the TWR, according to the tool life curves, has an initial part (low  $L$ ) in which it is high, then it decreases correspondently with the steady zone of the tool life trend and finally, before the corner reaches the end of life, the TWR peaks again.

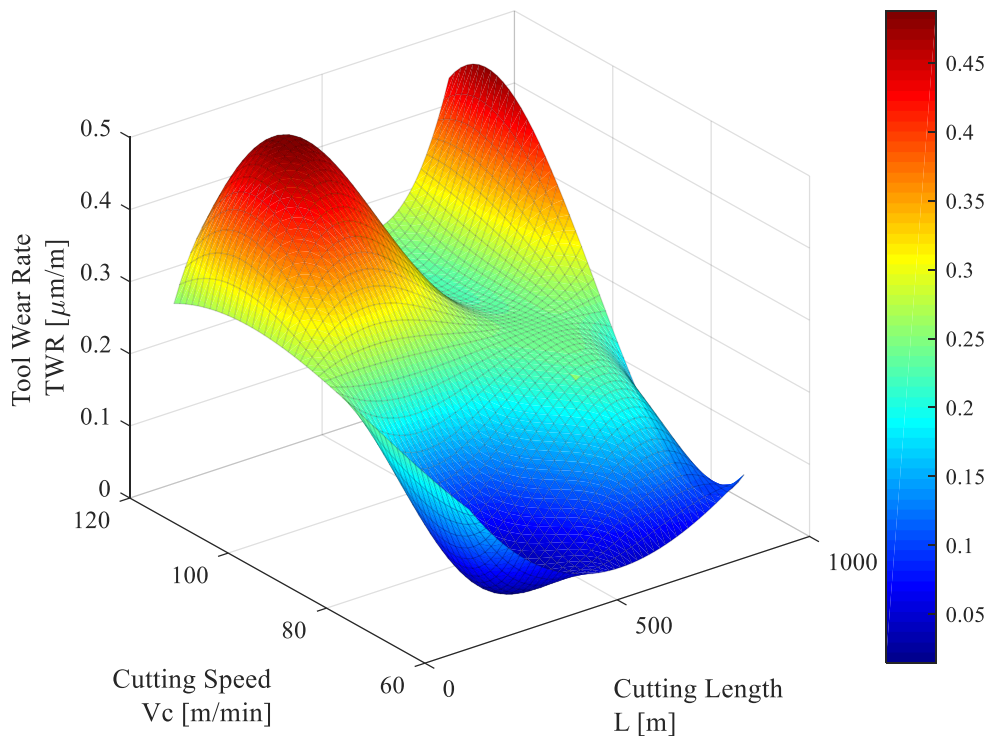


Figure 4.14 – Tool Wear Rate TWR [ $\mu\text{m/m}$ ] variation along the tool life, based on the variation of Cutting Speed [ $\text{m/min}$ ] for the nanocomposite multi-layered coating

It is not possible to extend this surface to higher cutting length, because there would not be data for the cases in which the tool life is already ended at  $L = 900\text{m}$ . Thus, to have a complete vision about the parameter, this figure must be associated to the Table 4.3, because it considers the whole tool life and thus the average TWR, instead

of only the outcome of a restricted zone. It is noticeable that at 80  $m/min$ , the TWR is the lowest among all the tests, with a value of 0.19  $\mu m/m$ , while  $V_c = 120 m/min$  is the less convenient in this analysis.

$V_c \left[ \frac{m}{min} \right]$	<b>60</b>	<b>80</b>	<b>97</b>	<b>120</b>
$MRR \left[ \frac{mm^3}{min} \right]$	1838	2450	2971	3675
$TWR_{avg} \left[ \frac{\mu m}{m} \right]$	0.22	0.19	0.30	0.33

*Table 4.3 – Average values of TWR for TiAlCrN/TiCrAl52Si8N, based on the variation of cutting speed*

### 4.5.2 Index of Performance *IP*

As described in the previous chapter, TWR is not enough to establish the best cutting speed. In fact, if related to a  $V_c$  extremely limited, a low value of TWR could be not interesting for the process, because it involves a leak in productivity. Therefore, in this paragraph, it has been related to the MRR, defining the ratio between the two parameters as the index of performance *IP*.

Similarly to what has been done for the TWR, a Matlab interpolation model has been developed also for *IP* and the result is displayed in Figure 4.15. Even for this parameter, the surface shape is as expected coherent with the successively displayed tool life curve in Figure 4.19: in the range between  $L = 0m$  and  $L = 900m$ , increasing the cutting speed, the flank wear is in every point higher in comparison to the local  $V_{B_B}$  of the curve at lower  $V_c$ .

In Figure 4.16, a full view of *IP* can be observed. It is now clear that having higher TWR does not mean to have a better machining process. Indeed, while in terms of average tool wear rate the condition of  $V_c = 120 m/min$  is 50% worse than the case of  $V_c = 60 m/min$ , the former results to be more than 30% better by comparing its *IP* to the latter's one. Even from this point of view, as well as from the previous observations on microscopic images and TWR, 80  $m/min$  seems to be the best choice.

From Figure 4.16 it is also worth noticing that the effect of the nanocomposite coating is more incident at higher cutting speeds (IPs are significantly greater than the benchmark KC5010), because in these cases the temperature is high enough to activate the formation of protective tribofilms and spinodal decomposition.

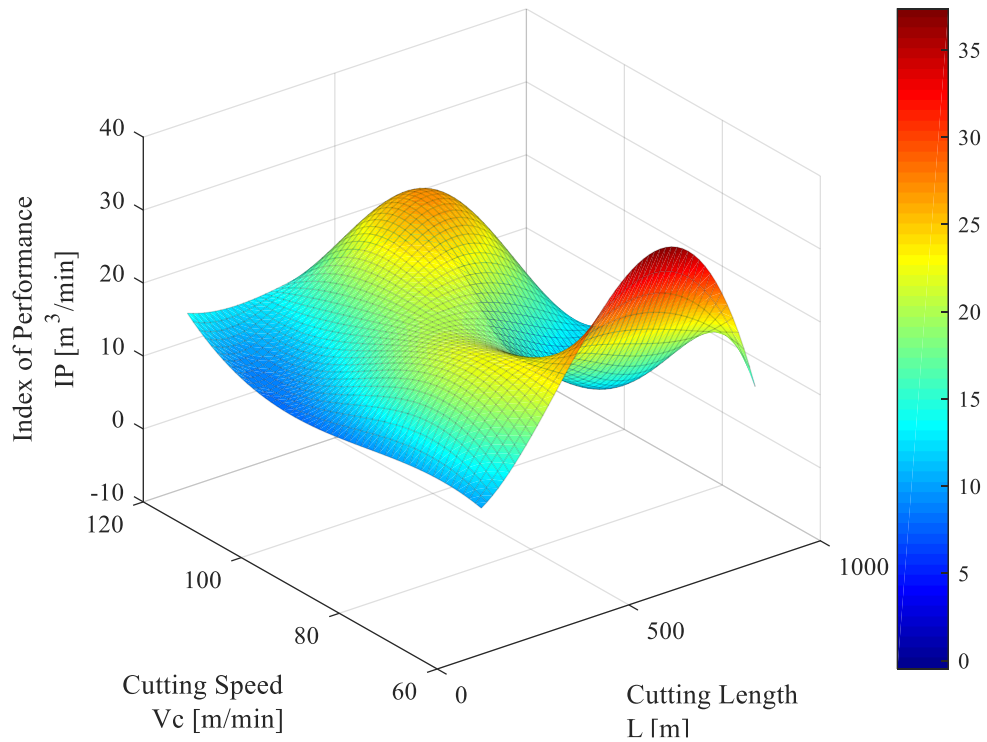


Figure 4.15 – Index of Performance IP [ $m^3/min$ ] variation along the tool life, based on the variation of Cutting Speed [ $m/min$ ], for the nanocomposite multi-layered coating

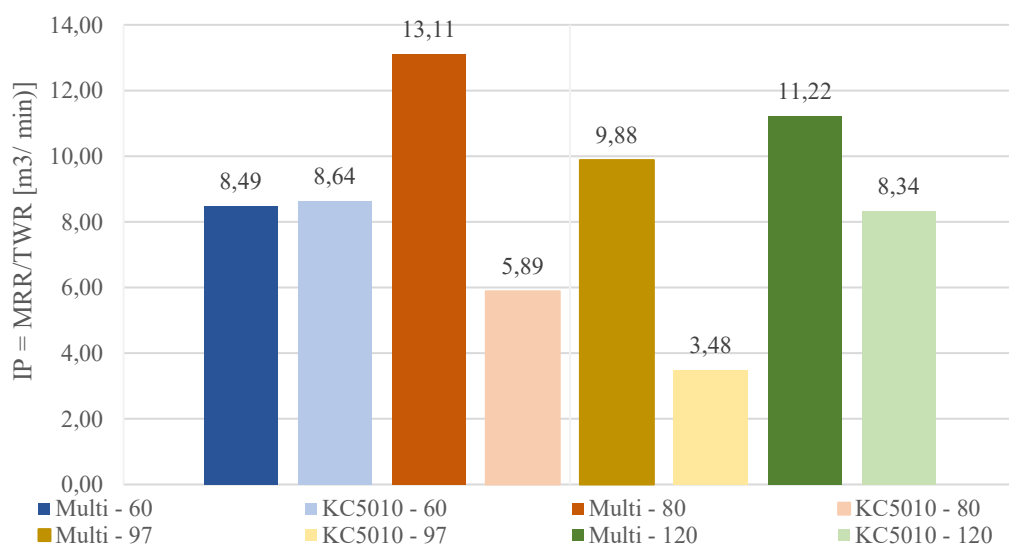


Figure 4.16 – Average values of IP for TiAlCrN/TiCrAl52Si8N, based on the variation of cutting speed

### 4.5.3 TCCL and CCR

#### 4.5.3.1 Tool Chip Contact Length TCCL

As shown in Figure 4.17, the nanocomposite coating has given better results in terms of TCCL. This confirms that the coating has therefore improved lubrication characteristic in comparison with the commercial KC5010.

Furthermore, the main tendency is decreasing in both cases, demonstration of faster and more effective tribofilms development, as much as the temperature (in consequence of the cutting speed) is increasing, with the effect of a reduction in the sticking and sliding areas [21].

The only one exception is for the nanocomposite coating, in which the TCCL at 120 *m/min* is greater than when  $V_c = 97 \text{ m/min}$ , probably because of the higher cutting forces that could lead in more extended abrasion.

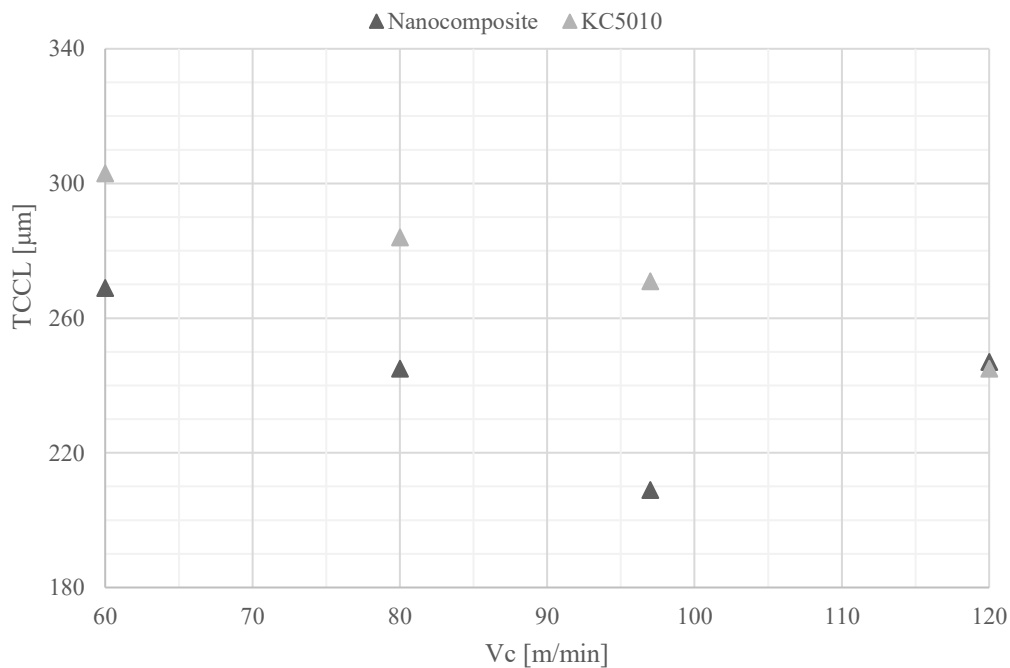


Figure 4.17 – TCCL comparison at different cutting speed between KC5010 and nanocomposite coating

#### 4.5.3.2 Chip Compression Ratio CCR

Since from the previous comparisons it resulted the most convenient for the finishing process, the CCR has been only evaluated for the tests at  $V_c = 80 \text{ m/min}$ .

The thickness of the chip was pretty irregular for both KC5010 and the nanocomposite coatings, therefore,  $d_{re}$  has been calculated as an average of 5 values, measured as shown in the following Figure 4.18:

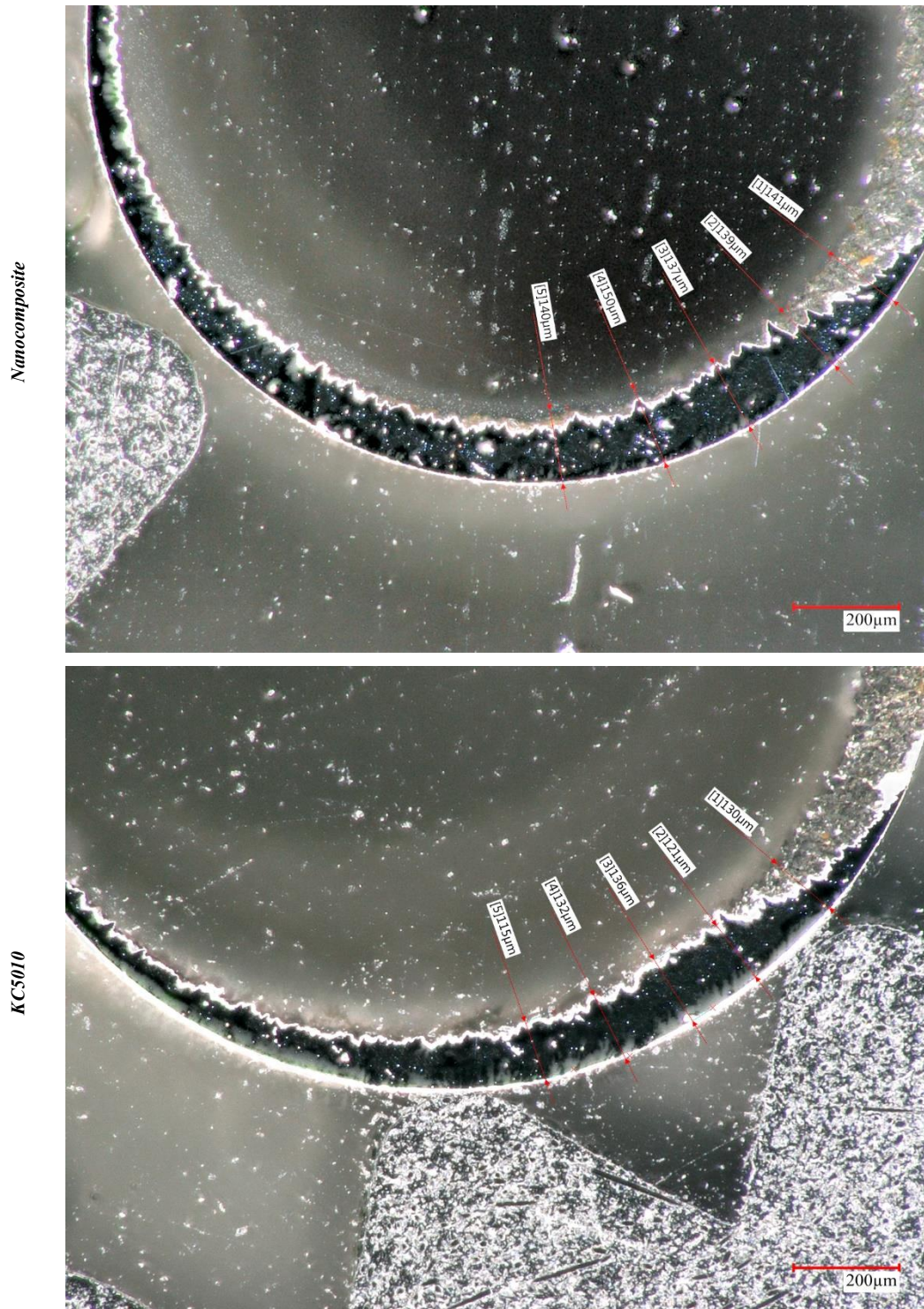


Figure 4.18 –  $d_{re}$  measurement

The outcome is displayed in Table 4.4:

	$d_{re} [\mu m]$	$CCR$
<i>Nanocomposite</i>	141.4	0.57
<i>KC5010</i>	126.8	0.51

*Table 4.4 – CCR results*

As expected,  $CCR_{nanocomposite} > CCR_{KC5010}$ . This result could be interpreted justifying the  $CCR$  variation with the difference in the lubricity of the coatings (theoretically greater for the nanocomposite coating). Higher lubricity might be related to resultant improved machining, with reduced deformation of both the tool body and the surface of the workpiece. Thus, since having less plastic deformation leads in thicker chip (and so  $CCR$  closer to 1), the  $CCR$  values give the information that hard machining is improved while using nanocomposite coatings, with positive influence also on work hardening, one of the major issues during machining of Inconel DA 718.

#### *4.5.4 Tool life curves*

The final and most employed comparison method for machining operations is the tool life curves, plotted in Figure 4.19 below. The trend can be generally divided into three areas: a first zone in which the concavity of the curve is downward oriented, followed by a steady trend with low tool wear rate and in turn followed by the last zone where the TWR increase (upward oriented tendency), leading to the ending of the life.

The best representation of what described above is the curve for the nanocomposite coating at 60 *m/min*. At 80 *m/min*, the trend is not well divided in the three areas and in the steady zone the TWR is higher, but the final result is slightly improved with respect to the 60 *m/min* test. Given that the curves at 97 *m/min* and at 120 *m/min* are comparable, employing the former method for further analysis is not required.

Regarding the comparison between KC5010 and TiAlCrN/TiCrAl52Si8N, there is an advantage of using the nanocomposite structure, that is greater for high-speed machining.

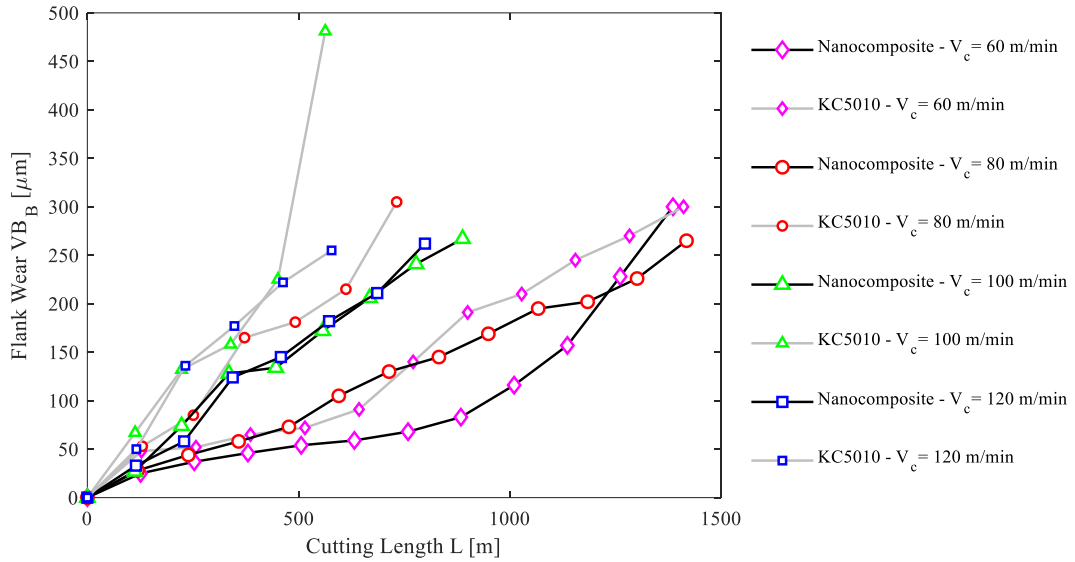


Figure 4.19 – Tool life curves comparison between KC5010 and TiAlCrN/TiCrAl52Si8N

$V_c \left[ \frac{m}{min} \right]$	60	80	97	120
$MRR \left[ \frac{mm^3}{min} \right]$	1838	2450	2971	3675
$L_{eol} [m]$	1386	1418	888	799

Table 4.5 – Cutting length at the end of life (maximum tool life) for TiAlCrN/TiCrAl52Si8N, based on the variation of cutting speed

#### 4.5.4.1 Predictive model for Flank Wear

Considering the wide sort of data extrapolated from the experimental procedure, the punctual points for flank wear have been fitted with a three-dimensional surface, according to the general equation:

$$VB_B = a_1 + a_2 * L^{a_3} * V_c^{a_4}$$

In Figure 4.20, the result of the modelling is shown:

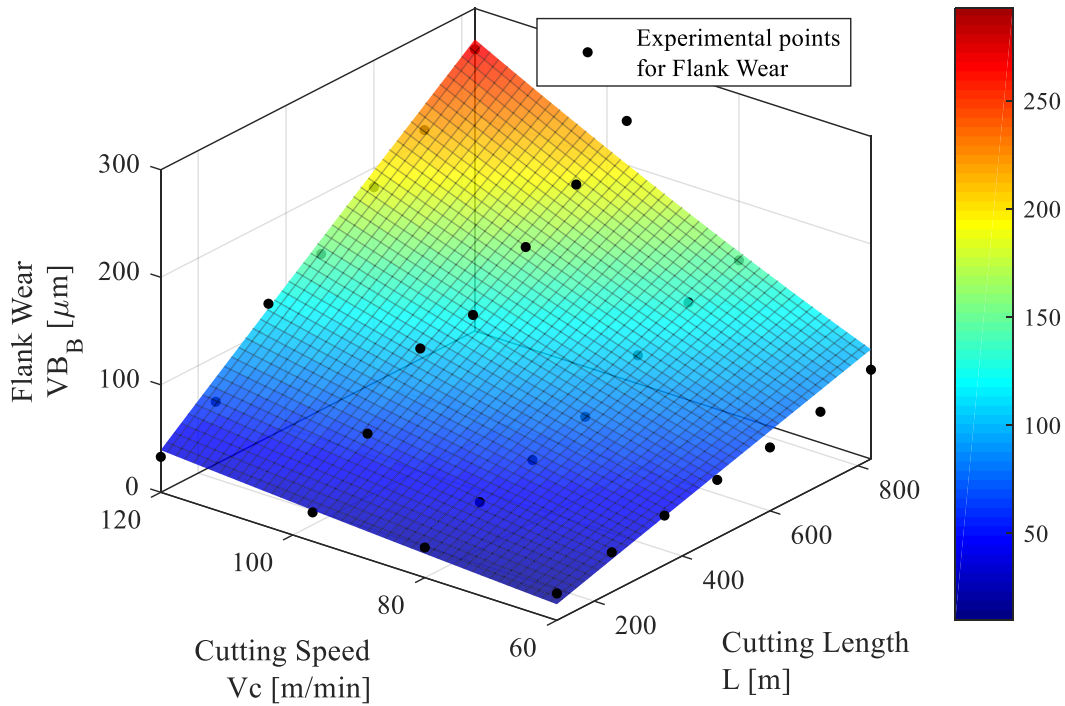


Figure 4.20 – Fitting for the predictive model of the Flank Wear experimental data for the nanocomposite coating at different cutting speed

The resultant equation of the predictive model for the nanocomposite coating for carbide inserts during hard turning of Inconel DA718 under finishing cutting conditions is:

$$VB_B = 0.3383 + 4.245 * 10^{-4} * L^{0.9811} * V_c^{1.414}$$

The R-square for the fitting procedure is higher than 93%, confirming the reliability of the study.

#### 4.5.5 Final Considerations

A 2-ways Analysis of Variance (ANOVA) and a Student’s t-test were performed on the tool life, the TWR, the IP and the TCCL, to statistically confirm the better response of the nanocomposite coating than the KC5010. However, the level of significance of these tests were around  $\alpha = 15\%$ , which means that it is possible to state that the use of the nanocomposite coating confers better properties to carbide tools in comparison to the KC5010 coating, with an accuracy of 85%. To obtain a

lower level of significance, a wider sort of data and repetitive trials are needed: this is one of the proposals for the future work.

However, using the available data, it is worthwhile that the usage of a multi-layered nanocomposite coating implies improvements for hard machining of Inconel DA 718. Indeed, as displayed in the summary graphs in Figure 4.21, both punctually and on average, KC5010 have had lower tool life and IP and higher TWR and TCCL in respect to the nanocomposite architecture.

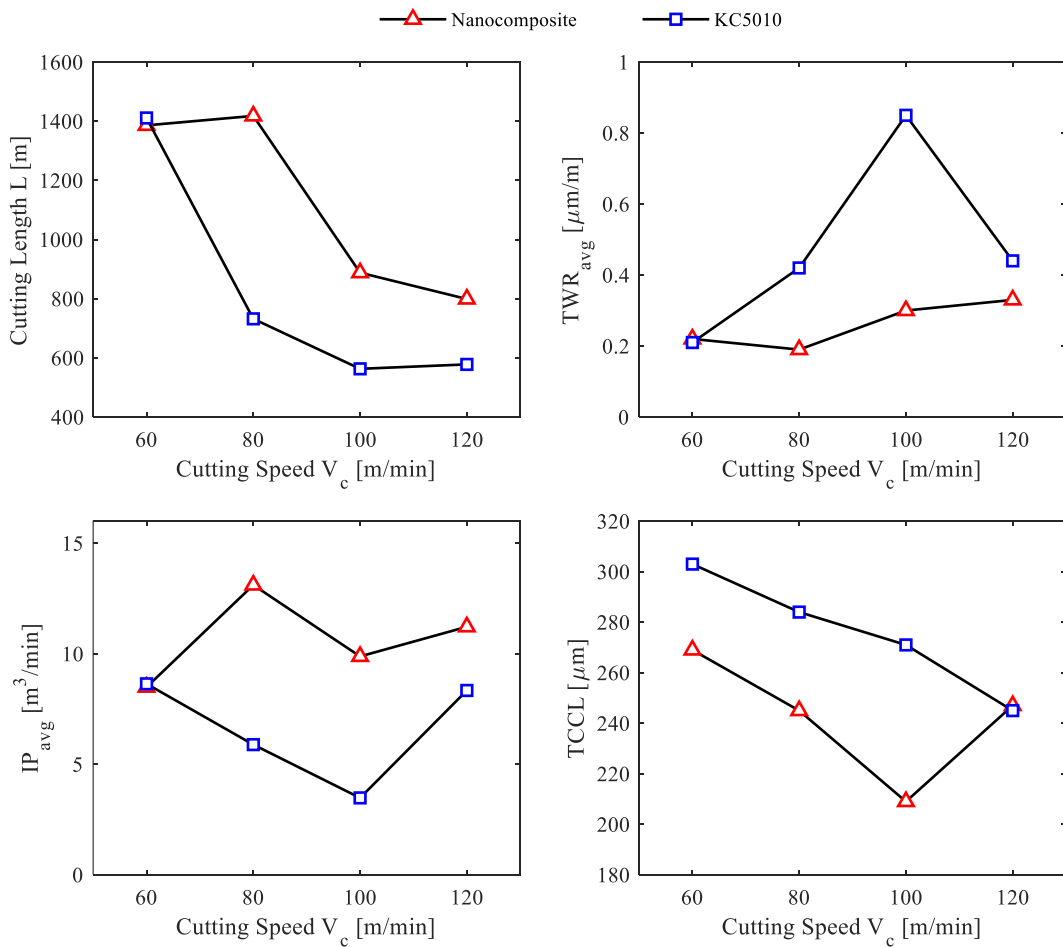


Figure 4.21 – Comparison of performance between nanocomposite and KC5010, varying the cutting speed

Moreover, considering that the coefficient of variation CV (Table 4.6) is significantly limited for the nanocomposite structure than for the benchmark, the former has shown more stability during the variation of the cutting conditions. This is an important advantage of the studied system, because it can be applied in a wide range of applications, without a great loss of performance.

## Results and Discussion

### 4.5 Evaluation of performance and comparison

	$\sigma$	$\mu$	$CV$	
<i>Tool Life [m]</i>	325	1123	0.29	Multi
	401	821	0.49	KC5010
<i>TWR [<math>\mu\text{m}/\text{m}</math>]</i>	0.07	0.26	0.25	Multi
	0.27	0.48	0.56	KC5010
<i>IP [<math>\text{m}^3/\text{min}</math>]</i>	1.97	10.68	0.18	Multi
	2.41	6.59	0.37	KC5010
<i>TCCL [<math>\mu\text{m}</math>]</i>	24.84	243	0.10	Multi
	24.35	276	0.09	KC5010

Table 4.6 – Standard deviation, mean, and coefficient of variation calculated between tests at different  $V_c$  for some of the comparison parameters

## 4.6 Three-Dimensional Tool Wear Analysis

In this section, the results of the FVM study using the best cutting speed of  $V_c = 80 \text{ m/min}$  are showed. It is a proposal as an alternative of the flank wear ISO methodology to investigate the evolution of the tool degradation.

During the tests execution it has been noticed that the limit of this 3D method is that, because of imperfection during the scanning and small undesired scraps on the tool-tip, the values measured from the software could be slightly altered. In any case, these issue does not affect the general graphical trends of 3D volume wear and BUE.

### 4.6.1 3D Volume Wear

In Figure 4.22, the 3D volume wear for both the studied systems is plotted. There are two curves per coating: one representing the 3D volume wear evolution in respect of the original unworn corner  $V_v$  and the other related to the sum of the partial values of the valleys volume between the subsequent passes  $V_{v_{discr}}$ .

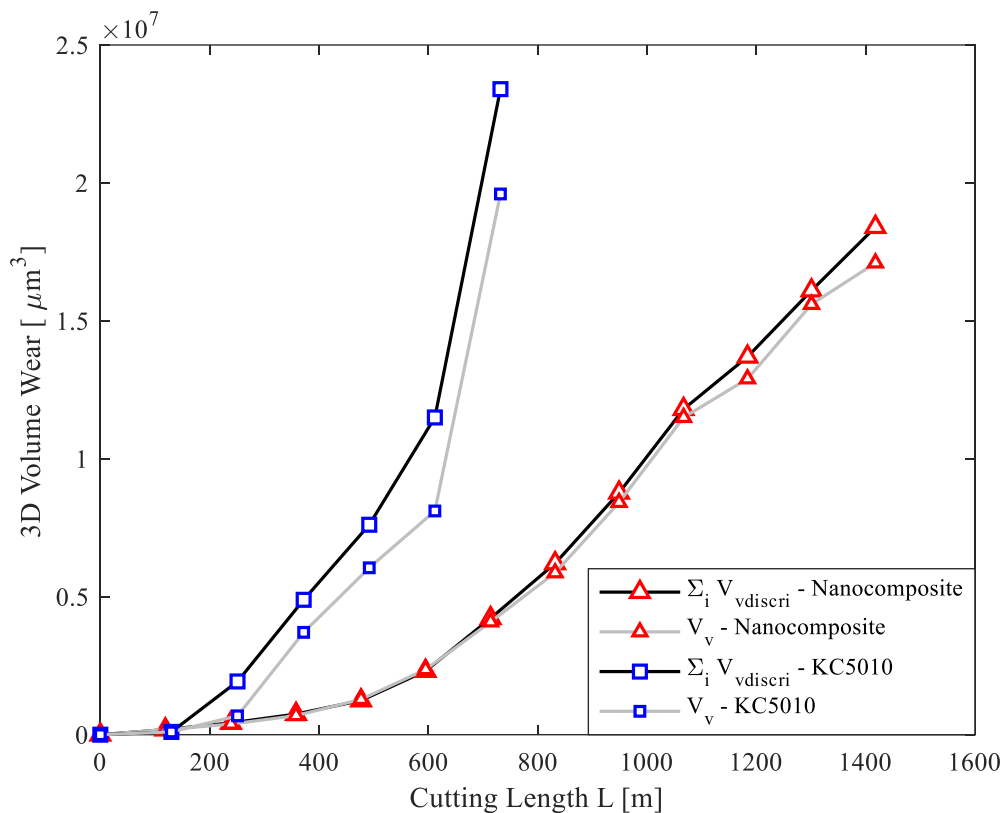


Figure 4.22 – 3D volume wear evolution along the tool life for KC5010 and TiAlCrN/TiCrAl52Si8N

Worthwhile is that the end of life is reached for both the coatings when  $V_v$  is between  $1.7 * 10^7$  and  $2.4 * 10^7$ . It can be explained thinking about the structure of the two inserts and the evolution of the degradation of the inserts: they are both formed by the same carbide substrate, thus, once the coating is abraded, the cratering on the rake face is developed similarly. This evidence suggests that, for carbide tools to machine Inconel DA 718, a 3D wear end of life criteria could be established, independently from the selected coating structure.

It can be noticed that the difference between the incremental and the absolute curves is not significant, but the incremental one gives more accurate results. To explain that, it is necessary to think about a condition in which the tool-tip is close to reach the end of life: in this case, there would be a high 3D volume wear and an eventual BUE over the worn area that might not exceed the surface limit of the fresh corner. Therefore, the BUE would have a reducing effect on the 3D volume wear measured quantity. In fact, as shown in the graph, the curves of  $V_v$  are positioned behind the curves of  $\sum V_{v_{discr_i}}$ , that is thus more accurate.

#### ***4.6.1.1 Comparison between 3D Volume Wear and Flank Wear***

In the following representation, a comparison between the flank wear and the 3D volume wear is traced for both the coated tools.

It is noteworthy that the two methods to describe the tool life have different tendencies. Indeed, while as described before the flank wear tool life curve can be divided into three areas with different trends, the 3D volume wear keeps increasing with higher inclination until the end of life.

Moreover, the growth of the 3D wear is more regular than the flank wear, that is strongly variable for machining hard materials, since the tool life is limited. Hence, by tracking this measure, it could be probably possible to predict more accurately the tool life in hard turning. However, as mentioned before, more tests are needed to establish a limit in the 3D volume wear correspondent to the end of life.

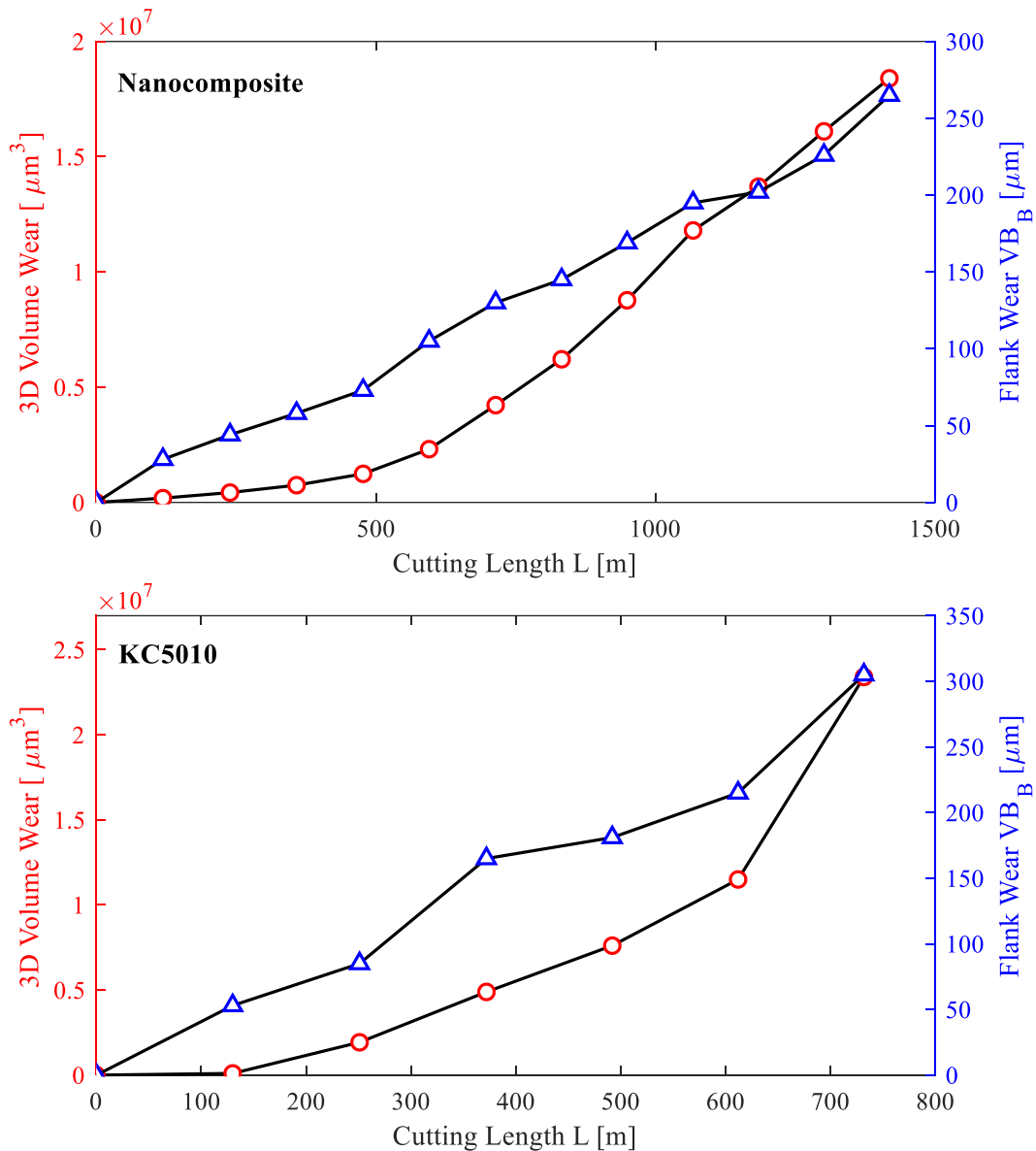


Figure 4.23 – Comparison between flank wear and 3D volume wear trends for the nanocomposite and the KC5010 coatings

#### 4.6.1.2 Curves Fitting with exponential curves

From Figure 4.23, it has been noticed that the 3D tool wear trends might resemble exponential or quadratic curves. Thus, curves fitting has been performed utilizing the Curve Fitting Matlab tool, obtaining poor results for the quadratic case (not shown in this document) and interesting outcomes for the exponential analyses.

The fitting is shown in the following Figure 4.24. From the graph, it is worth noticing that the 3D volume wear grows following trends well approximate by

exponential curves, with different coefficients of the function for the two considered coating structures. Indeed, in both the cases, the evaluated R-square, a measure of how much reliably the model describes the experimental data, is higher than 95%.

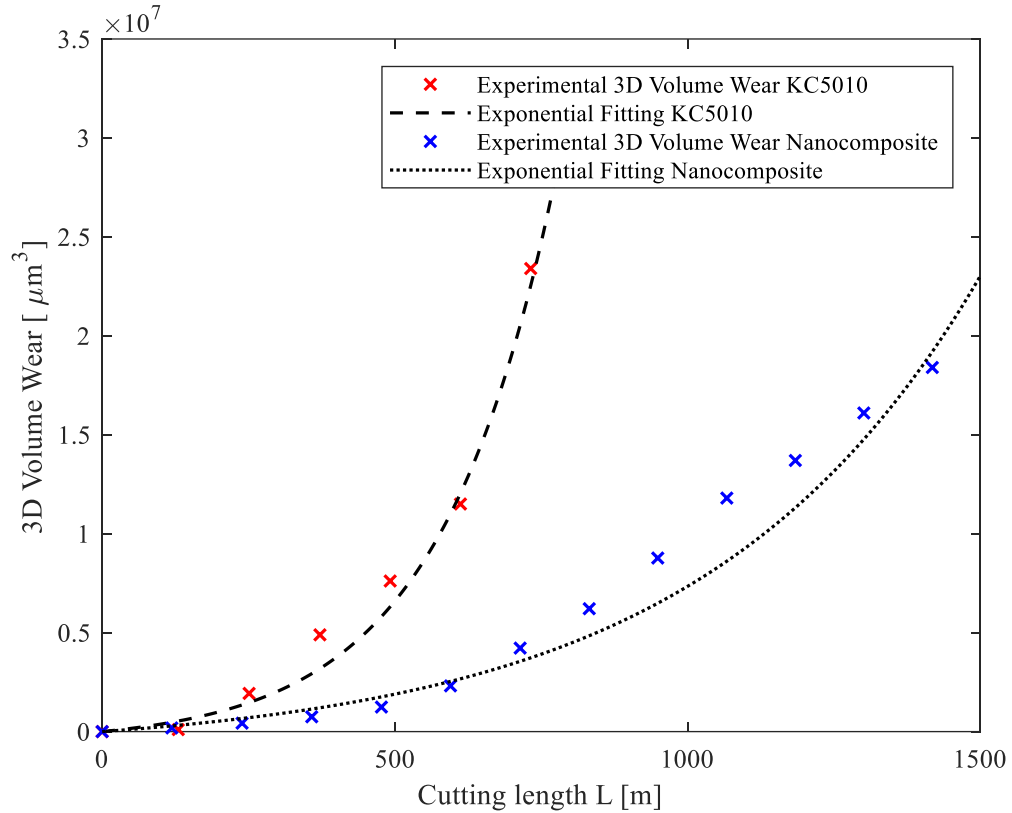


Figure 4.24 – 3D Volume Wear exponential fitting for the Nanocomposite and KC5010 coated tools

Considering a general starting exponential equation passing from the origin in the form:

$$y = a * (e^{bx} - 1)$$

In which  $y$  is the 3D volume wear and  $x$  is the cutting length, the coefficients  $a$  and  $b$  extracted from the fitting procedure are showed in Table 4.7:

	$a$ [ $\mu\text{m}^3$ ]	$b$
Nanocomposite	$1.007 * 10^6$	0.002115
KC5010	$5.759 * 10^5$	0.005044

Table 4.7 – Values of the coefficients  $a$  and  $b$  for the fitting with exponential curves of the experimental data

More cutting tests and 3D wear analyses are needed in order to find a wide range of coefficients of the exponential curves at different cutting speeds and with different coatings. In this way, a predictive and complete model about the tool life could be developed, allowing to improve productivity or minimize the costs of an Inconel DA 718 turning operation.

Another interesting result that could be investigated is to determine if there is an analytical law able to describe the variation of the parameter  $a$  and  $b$ , based on the cutting speed change.

### *4.6.2 Built-Up Edge*

In Figure 4.25, the built-up edge diagrams are plotted for both KC5010 and TiAlCrN/TiCrAl52Si8N. To express this quantity, the values of  $V_p$  have been ignored in favour of the incremental values between subsequent passes  $V_{p_{discr}}$  and its sum  $\sum V_{p_{discr_i}}$ . Indeed, the BUE evolution is an instable phenomenon consisting in a continuous adhesion of material from the workpiece that detaches afterwards, carrying off part of the tool body: tracking it in respect to the unworn tool tip surface could result in filtering this effect because it would not consider the amount of material already attached and detached during the previous passes. Furthermore, the effect already described at page 75 could lead in errors in the trends. The measure is in any case an approximation, since BUE is not tracked instant-by-instant and evaluating the real modification is not possible with the available technologies.

Demonstration of the BUE instability are the curves of the incremental peaks volume over the previous pass delimiting surface, that are changing frequently their tendencies.

Tracing the summation of  $V_{p_{discr}}$ , highlights the difference in the total amount of material adhered along the tool life on the KC5010 tool in comparison to the nanocomposite one, also if the cutting length to arrive to the end of life has been a way longer (approximately 1400m) for the nanocomposite instead of the KC5010 (about 700m). Almost the double of material has adhered on the benchmark: this

confirms the better lubricity of the nanocomposite coatings and the probably lower temperature reached during the cutting process.

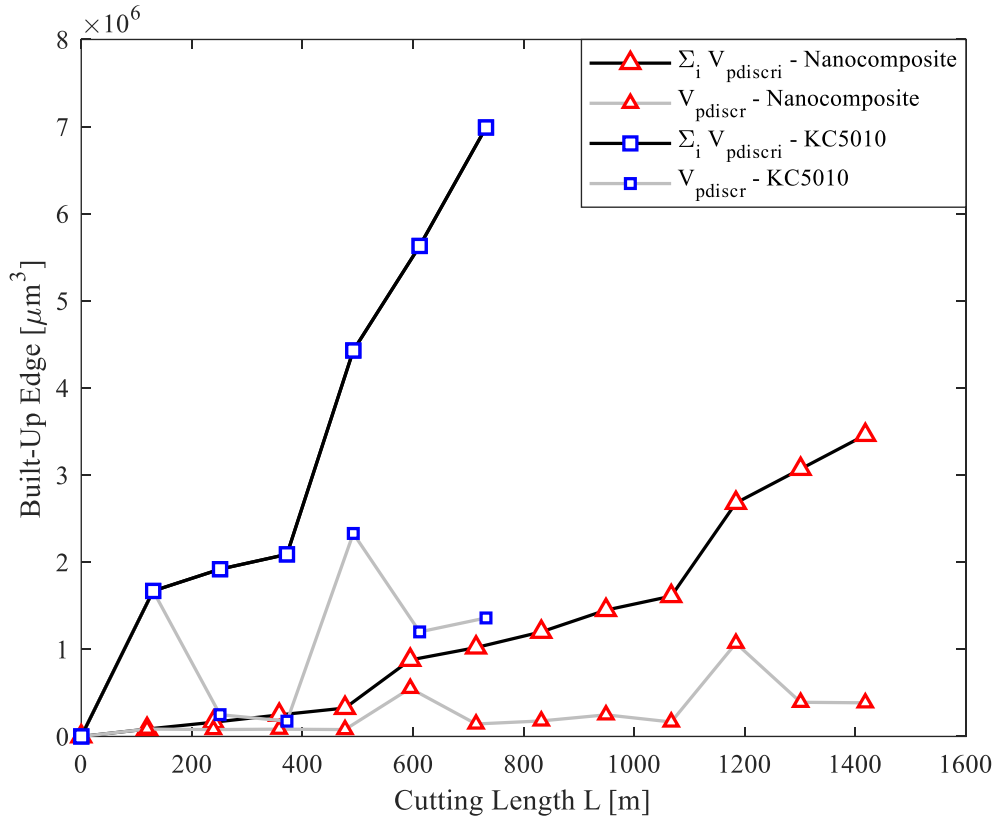


Figure 4.25 – BUE evolution along the tool life for KC5010 and TiAlCrN/TiCrAl52Si8N

### 4.6.3 3D Figures

In the following pages, the 3D images captured with the FVM and post-processed with the Alicona software are displayed.

To obtain the deviation in respect to the original (green) surface, every 3D model has been overlapped on the unworn body. Because of that, the BUE can be clearly seen in red just in the first example (tool wear after the first pass), while in the following images, the BUE is in any case under the reference surface, so it is part of the blue or green area. To distinguish between chipping and built-up edge in the figures, they should be substituted with the ones related to the incremental study, losing, however, the absolute referential green surface representing the unworn tool-tip.

4.6.3.1  $L = 130m$

Since Figure 4.26, representing the superficial condition after the first pass, the behaviour of the two system has been widely different. In fact, after  $L = 130m$ , there has been a small amount of BUE over the nanocomposite coating, while on the KC5010 coating, the BUE has been the main developed tool wear mode.

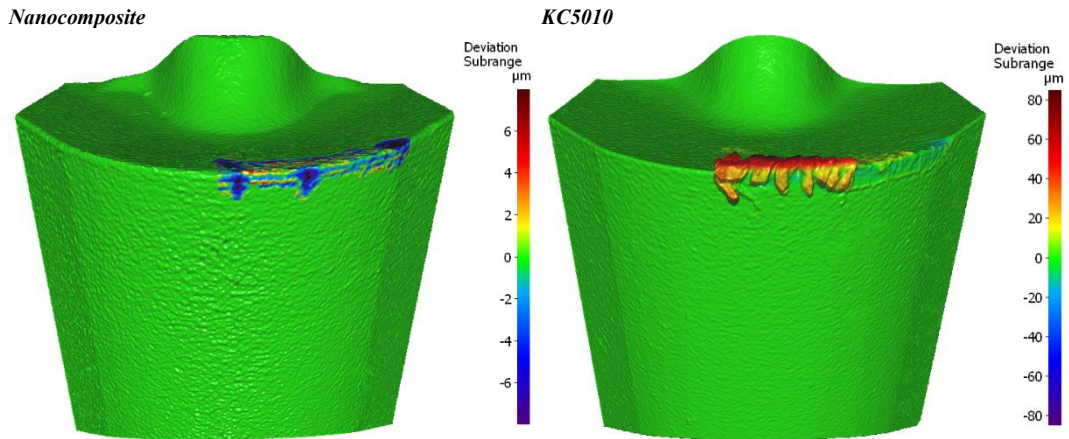


Figure 4.26 – 3D figures of the worn coated tools after  $L = 130m$

4.6.3.2  $L = 600m$

After 600m of cutting length, as shown in Figure 4.27, the valleys on the KC5010 system have been much more developed than on the nanocomposite, with holes deep up to  $150\mu m$  versus roughly  $7\mu m$  for the multi-layered structure. This confirms the better tool protection guaranteed by the nanocomposite system from the three-dimensional wear described above by Figure 4.22.

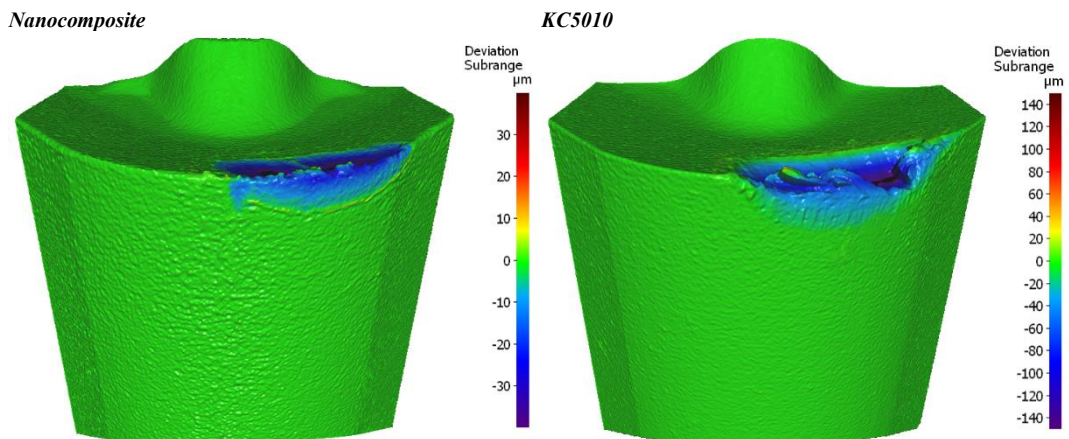
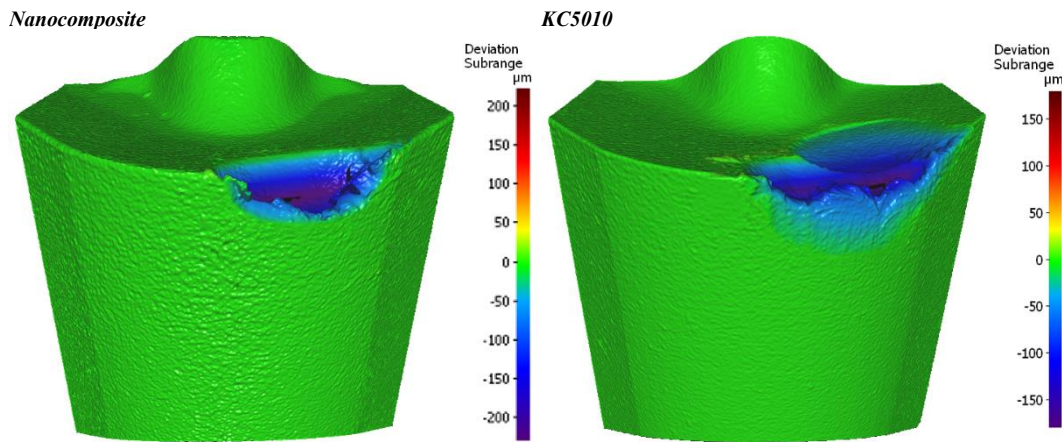


Figure 4.27 – 3D figures of the worn coated tools after  $L = 600m$

**4.6.3.3 End of Life**

At the end of the life, since the coatings are at that point no longer effective and the substrate for both the tested inserts is the same tungsten carbide, the two corners behaved similarly. As an example, the deepest part of the crater has been around  $200\mu\text{m}$  in both cases and the shape of the worn area is comparable. One exception is that the KC5010 coating has been delaminated because of the adverse cutting conditions (wide flat blue area on the tool on the right part of Figure 4.28).



*Figure 4.28 – 3D figures of the worn coated tools at end of tool life*

**4.6.4 Analysis at  $V_c = 120\text{ m/min}$**

Since at cutting speed  $80\text{ m/min}$  the studied results are interesting, the same procedure for the 3D volume wear has been applied at  $V_c = 120\text{ m/min}$ . This condition has been selected because the calculated IP is the second best for the nanocomposite coating, after  $V_c = 80\text{ m/min}$ .

**4.6.4.1 3D Volume Wear**

Figure 4.29 shows that at high cutting speed the behaviour of the two different systems is similar, probably because, since the tribological conditions are critical due to the high cutting forces and temperatures, the presence of the coating influences less the tool duration, as it is early abraded during the first phase of the process. Because of that, the 3D wear might be just a function of tool geometry and substrate, that is identical for the two architectures. For the nanocomposite coating,

the results are plotted just until about  $L = 700m$ , because in the next pass a critical failure occurred and therefore the end of life value is altered.

As happened also for lower  $V_c$ , the end of life corresponds for both the corner to a 3D incremental volume wear of  $\sum V_{v_{discr_i}} \cong 2.00 * 10^7 \mu m^3$ . It suggests that this limit, after an eventual future work of validation, could be employed to determine the end of life using the explained methodology.

Moreover, worthwhile is that the KC5010 architecture seems to have a slight better response on the 3D wear, while considering the ISO 3685 for the flank wear measurement, the nanocomposite showed improved behaviour (Figure 4.19). This will be deeper investigated through the EDS analysis in the following section.

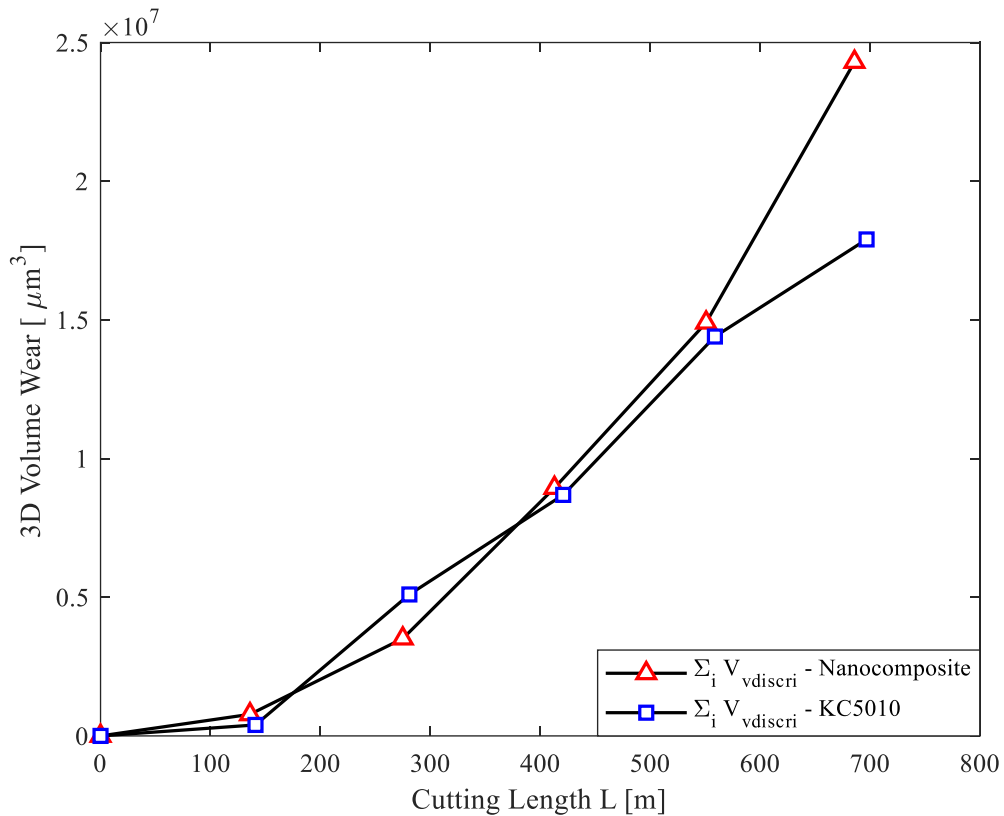


Figure 4.29 – 3D Volume Wear tool life curves at  $V_c = 120 m/min$

#### 4.6.4.2 Curves Fitting with exponential curves

As well as the previous study, the evolution of the  $V_v$  resembles an exponential curve for both the tool tips. Hence, an exponential fitting model has been developed and the graphical product is shown in Figure 4.30.

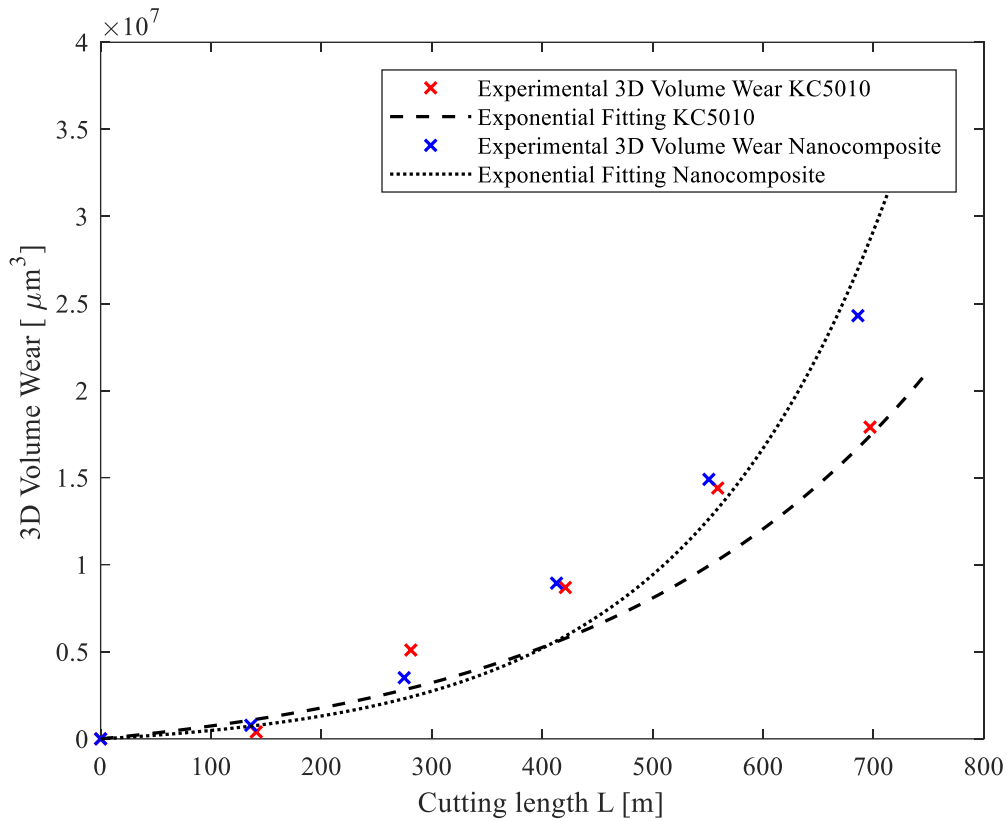


Figure 4.30 – 3D Volume Wear exponential fitting for the coated tools at  $V_c = 120$  m/min

The  $a$  and  $b$  coefficients of the fitting procedure are displayed in Table 4.8. They have the same order of magnitude, also in comparison to the previous analysis. However, since the amount of data is limited, more research is needed for finding a relation between the cutting speed and the parameters of the fitting curve, allowing to develop a predictive model for the three-dimensional wear.

	$a$ [ $\mu\text{m}^3$ ]	$b$
Nanocomposite	$6.713 \times 10^5$	0.005420
KC5010	$1.858 \times 10^6$	0.003355

Table 4.8 –  $a$  and  $b$  coefficients for the exponential curves fitting of the experimental data at  $V_c = 120$  m/min

#### 4.6.4.3 3D Figures

Figure 4.31 presents the merging between the unworn inserts and their condition after different passes along the tool life.

As discussed above, the behaviour of the two corners is pretty similar and the worn areas have almost the same geometry. The differences are caused by random effects or could be either justified by the type of wear observed in the two systems. The higher lubricity of the nanocomposite material is demonstrated by the inferior presence of BUE phenomenon for all the steps. Moreover, the nanocomposite architecture is more brittle. Thus, the major tool wear mode is clearly chipping.

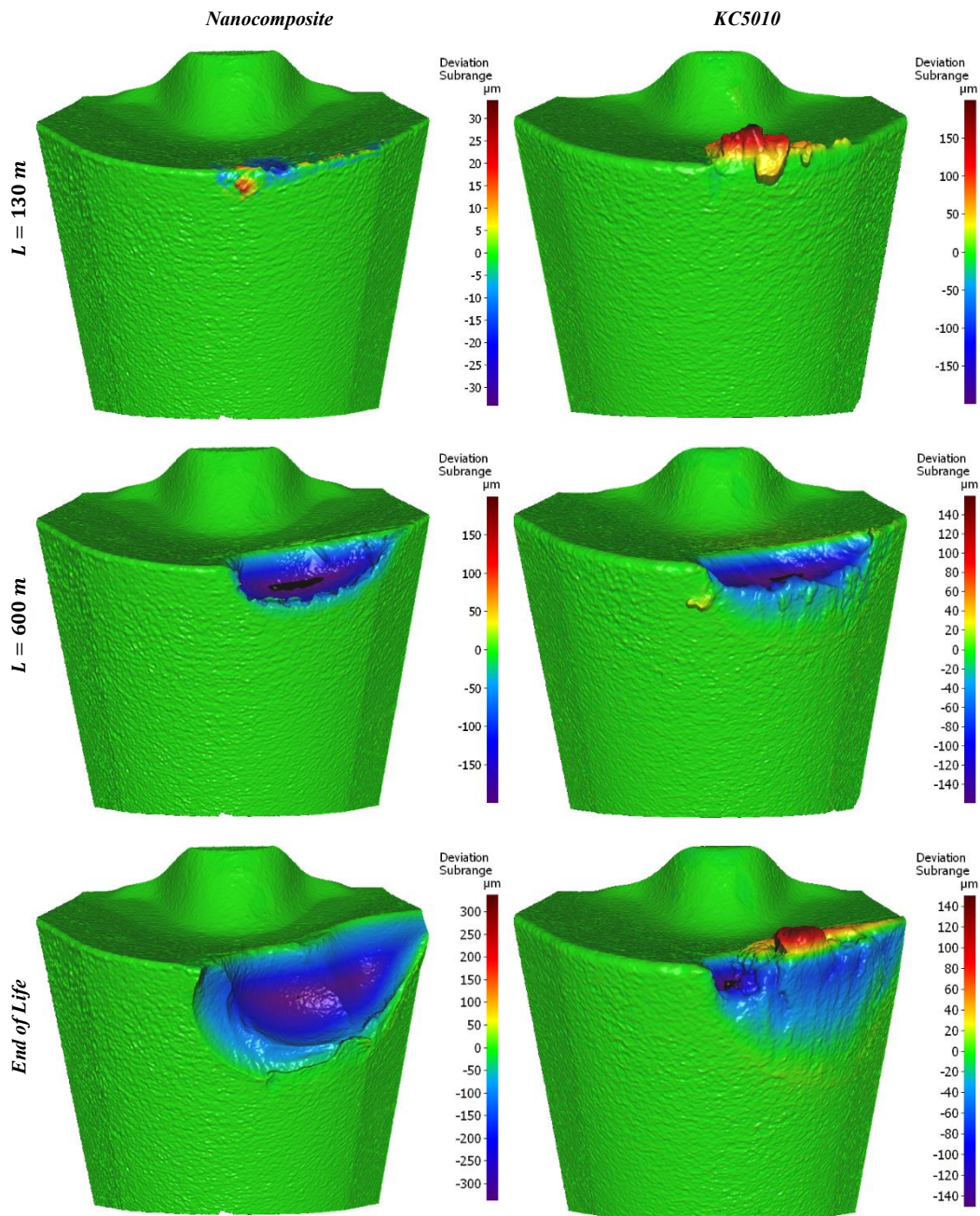


Figure 4.31 – 3D figures of the worn at  $V_c = 120$  m/min

## 4.7 Scanning Electron Microscope (SEM) analysis

### 4.7.1 Tool-tips at the End of Life

From Figure 4.32, an SEM investigation of the tool-tips shows that the main difference between the two architectures is that the KC5010 tends to favour the adhesion of the workpiece on the worn areas, while nanocomposite, that confers higher lubricity to the system, is more liable to chipping wear mode.

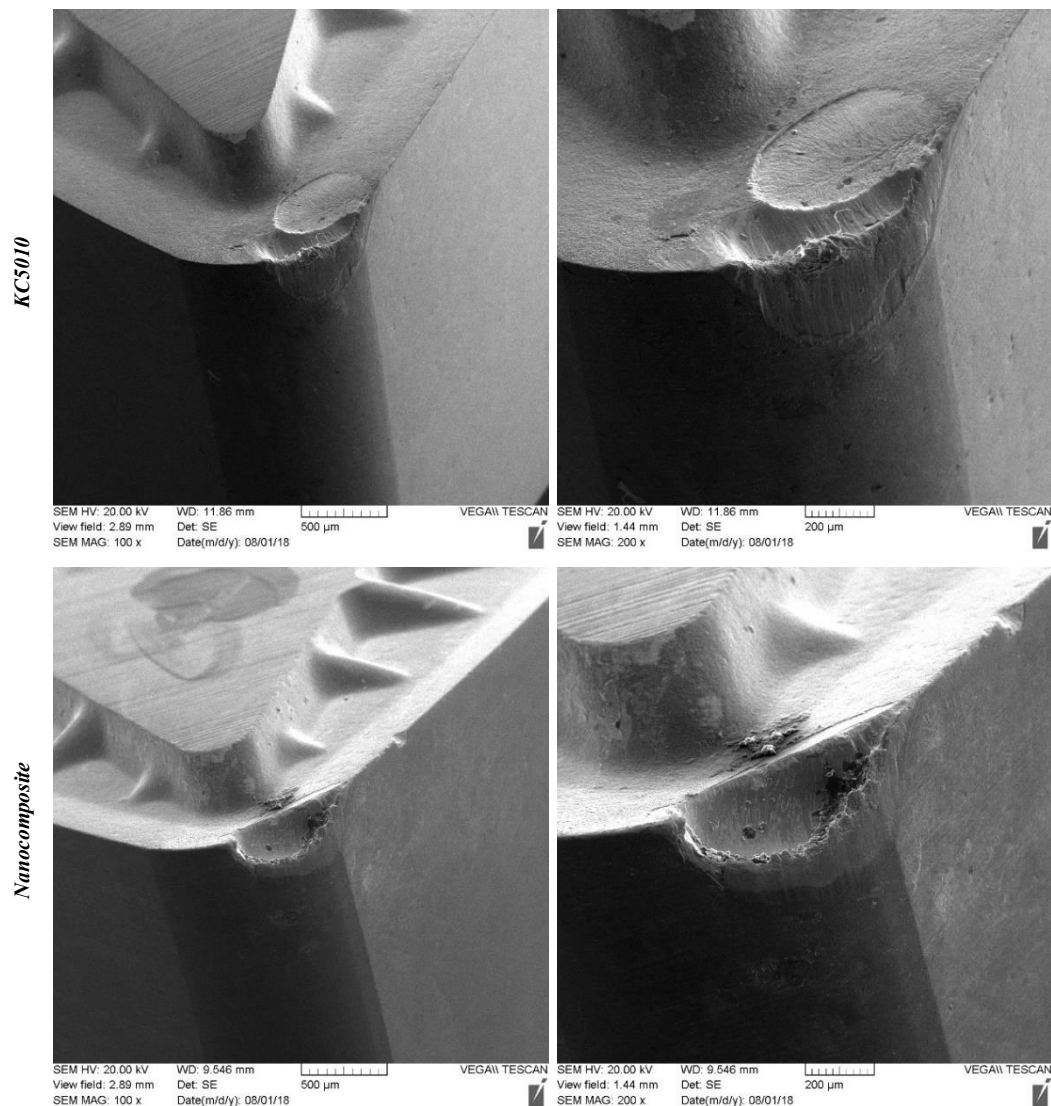


Figure 4.32 – SEM images with two different magnification at the end of life at  $V_c = 80$  m/min

At high cutting speed (Figure 4.33), the outcome is similar (delamination and BUE for KC5010 and chipping for nanocomposite), but in this case, the studied coating has reached the end of life because of critical failure of the tool corner.

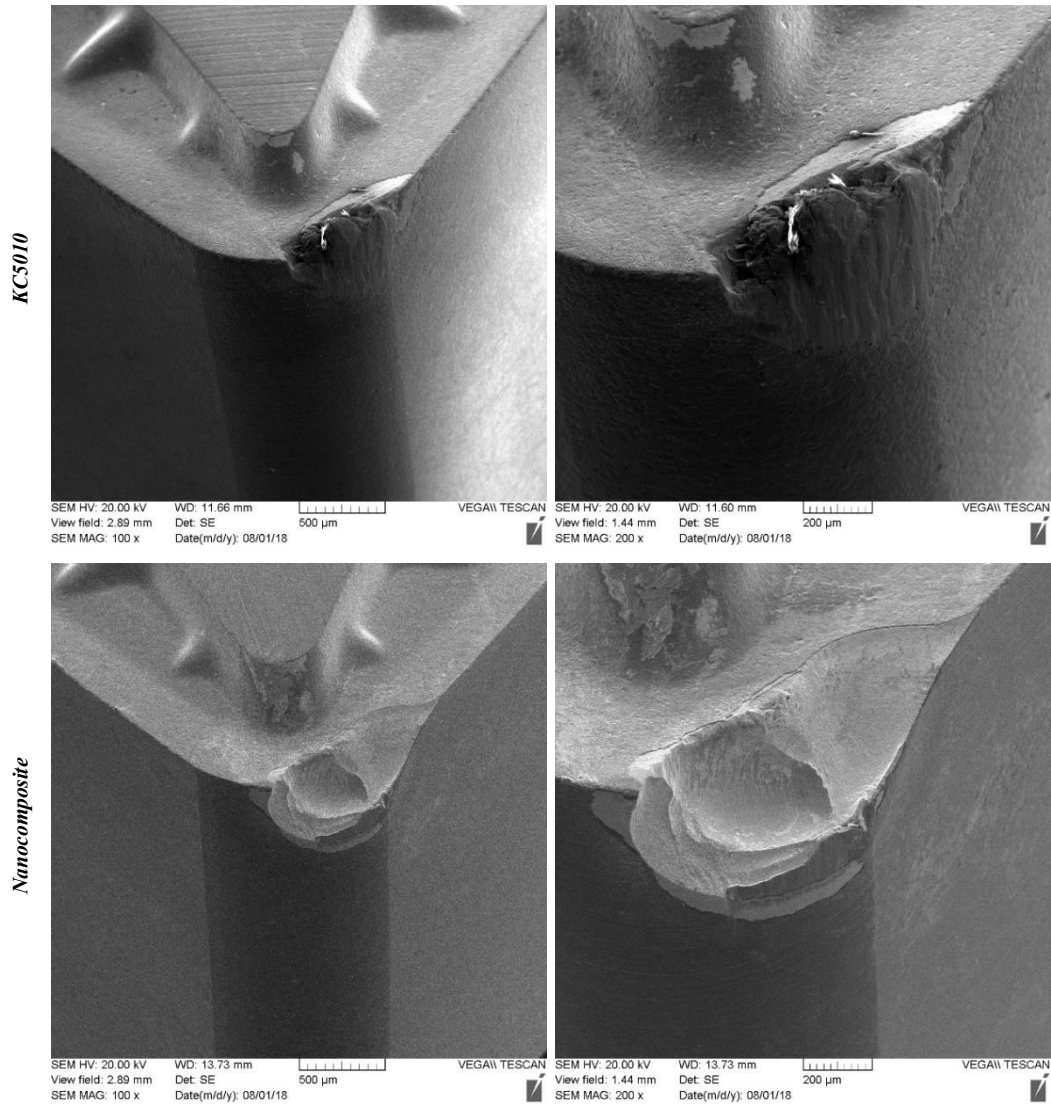


Figure 4.33 – SEM images with two different magnification at the end of life at  $V_c = 120$  m/min

## 4.7.2 EDS Analysis

### 4.7.2.1 $V_c = 80$ m/min

Considering  $V_c = 80$  m/min in Figure 4.34 and Figure 4.35 (spectroscopies of the tool tips in Figure 4.32), the nanocomposite coating property of developing more

## Results and Discussion

### 4.7 Scanning Electron Microscope (SEM) analysis

effective and widely distributed tribofilms is immediately noticeable from the larger amount of O, Al e Ti around the worn area in respect to the KC5010. Moreover, CrO takes part of the tribofilms of the nanocomposite coating, while in the KC5010 architecture, chromium is situated only in the abraded area, due to the great quantity of adhered Inconel over the corner. Strong adhesion over the KC5010 insert is also confirmed by the detected amount of Ni, higher than in the nanocomposite case. The presence of W on the analysed surfaces is low (probably due just to diffusion and/or EDS errors), because the substrate containing W is covered by the coatings and the adhered material. As well as W, the figures suggest that Ti and Ni atoms might be migrating due to the high temperatures of the cutting processes.

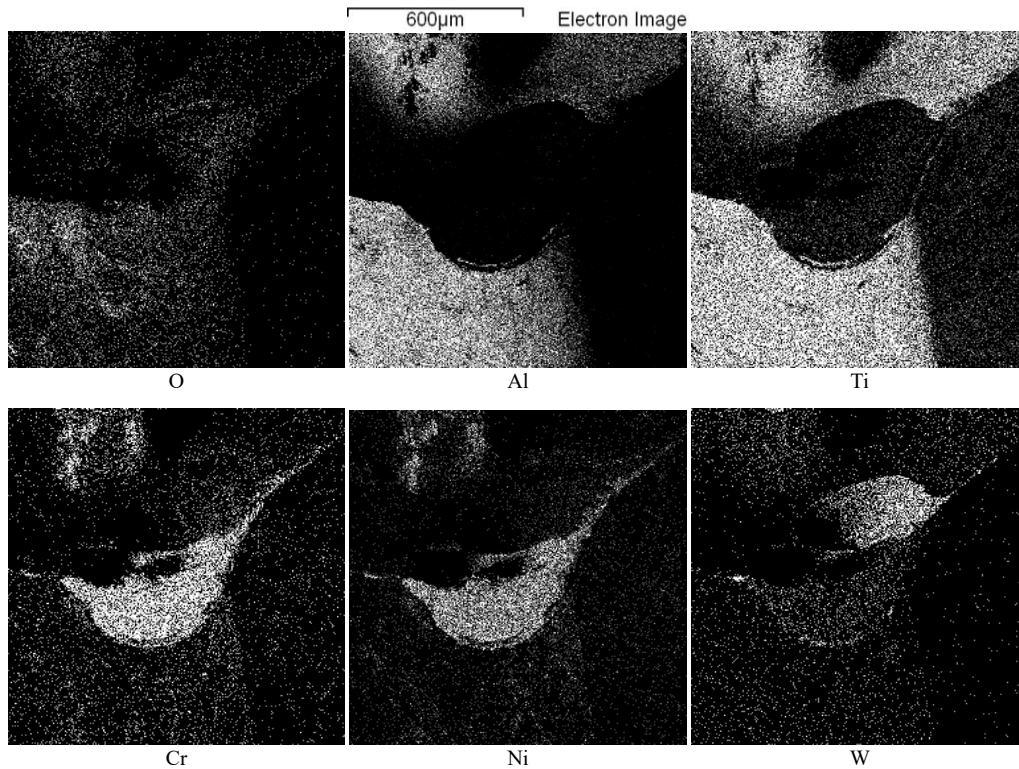


Figure 4.34 – EDS analysis at the end of life for KC5010 at  $V_c = 80$  m/min

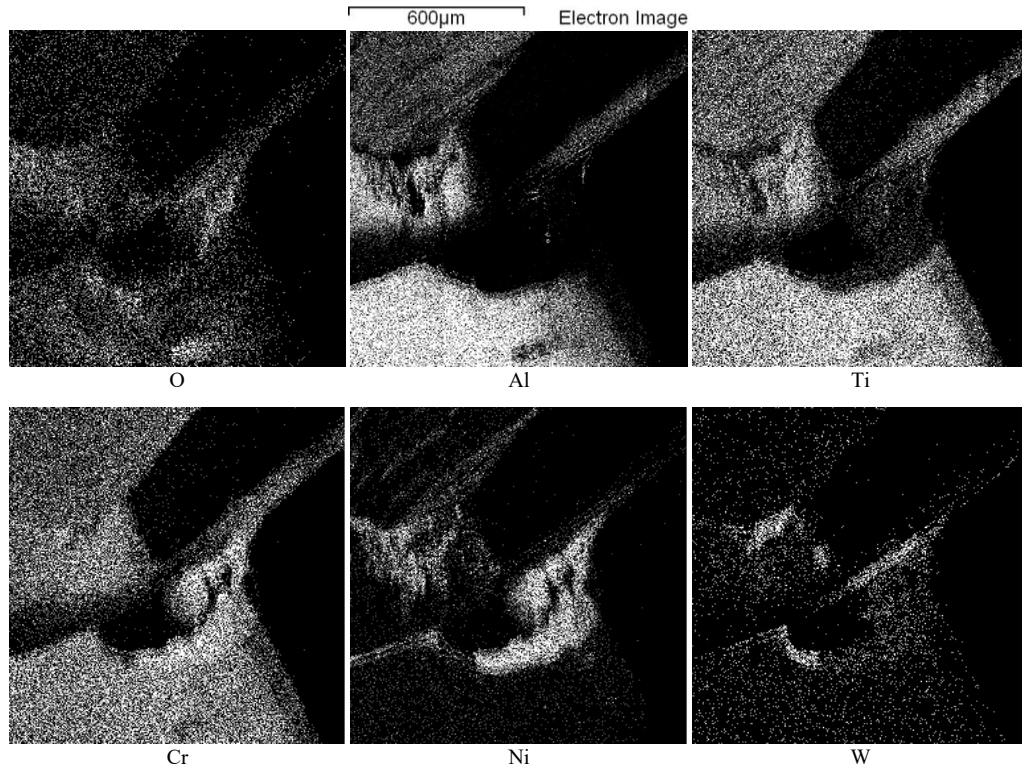


Figure 4.35 – EDS analysis at the end of life for nanocomposite at  $V_c = 80 \text{ m/min}$

**4.7.2.2  $V_c = 120 \text{ m/min}$**

The EDS analysis of the high-speed machining of Figure 4.33 is represented in Figure 4.36 and Figure 4.37. The results are analogue to the previous investigation, with the difference that, for the nanocomposite, in the worn areas there is less evidence of Cr and Ni, while W is the main chemical element. This discrepancy is justified by the way of life ending, which for high speed has been reached through critical failure, with the consequence of obtaining the substrate on the superficial area.

As explained in the paragraph describing the 3D tool life curves for  $V_c = 120 \text{ m/min}$ , KC5010 had worse results than showed, but the curve is altered from the BUE adhered on the already chipped zones, causing a reduction in the 3D volume wear measured quantity. The proof of this explanation is the great amount of chromium and nickel detected with EDS, symptoms of Inconel adhesion on the tool-tip.

**Results and Discussion**

**4.7 Scanning Electron Microscope (SEM) analysis**

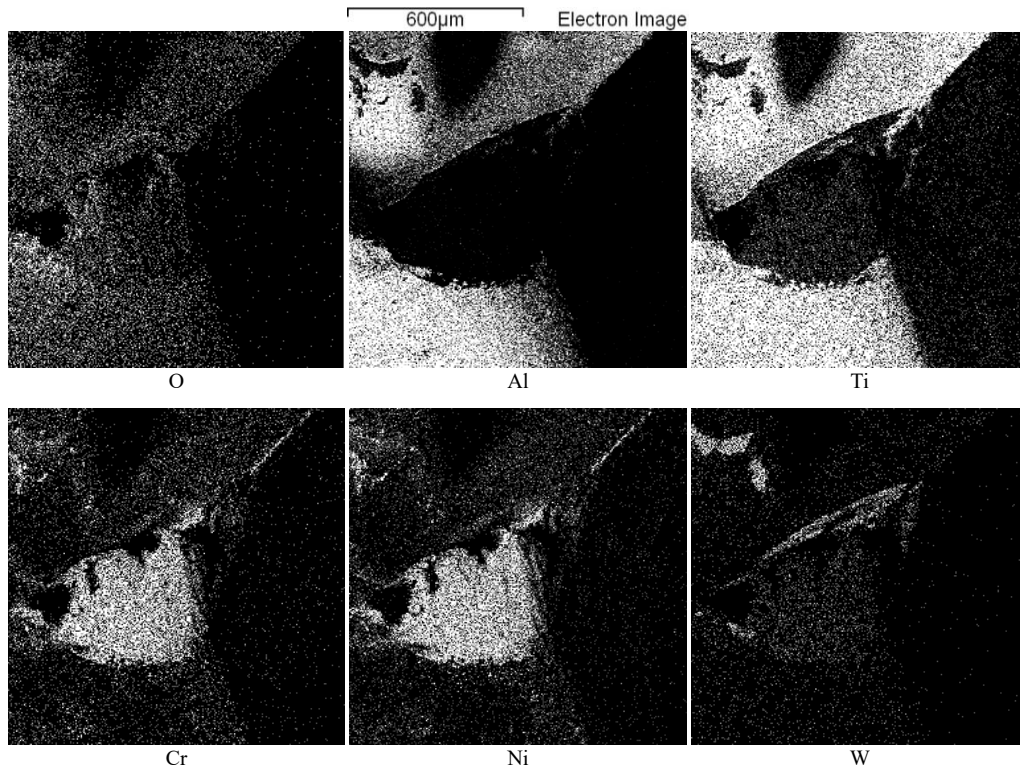


*Figure 4.36 – EDS analysis at the end of life for KC5010 at  $V_c = 120$  m/min*

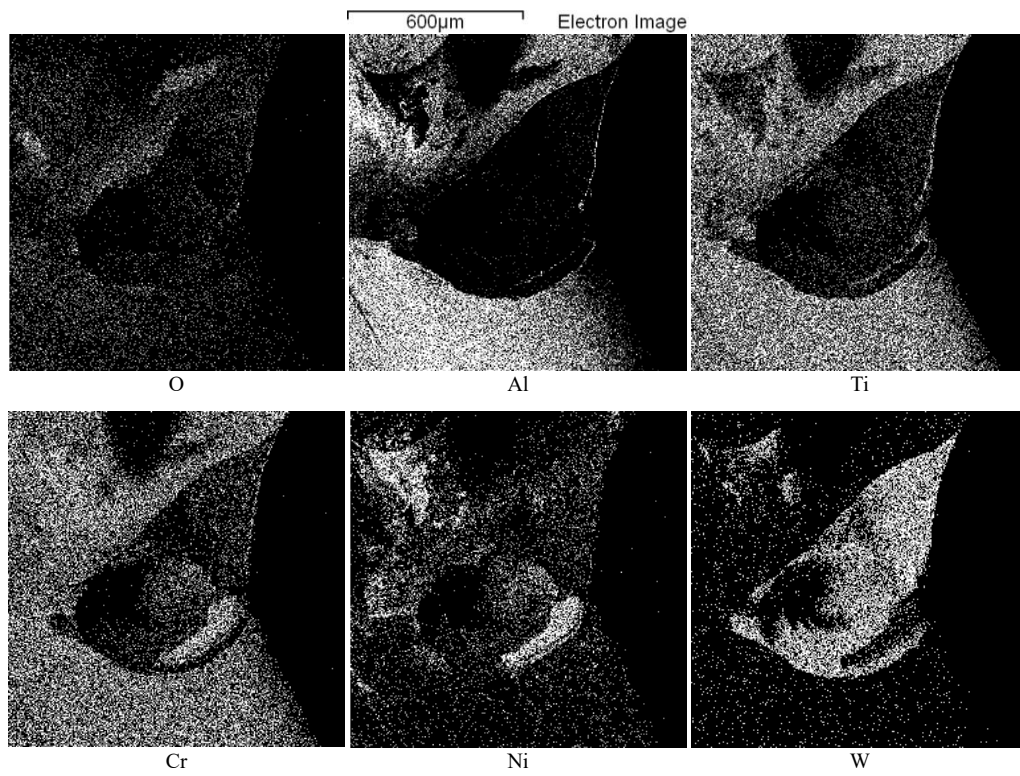


*Figure 4.37 – EDS analysis at the end of life for nanocomposite at  $V_c = 120$  m/min*

## Chapter 5: Conclusion

The first part of the study was focused on the analysis of the performance. Overall, using the multi-layered nanocomposite coating for carbide tools gives an advantage in comparison to the commercial KC5010 architecture. Moreover, considering finishing cutting parameters, the cutting speed of  $V_c = 80 \text{ m/min}$  is the most performing for hard-turning of Inconel DA 718. Basing on this preliminary section, the main findings can be summarized as:

- The roughness of the machined workpieces followed a trend that can be distinguished in three areas, based on the wear condition of the tool;
- Moving to high-speed machining, the tool wear evolution tends to be very sharp and to lose the dependence from the cutting speed and the selected coating, because the coating is abraded fast, without conferring protective properties;
- The use of the nanocomposite coating ensures higher indexes of performance than utilizing the KC5010, with the best outcomes at  $V_c = 80 \text{ m/min}$ ;
- The high lubricity of the TiAlCrN/TiCrAl<sub>5</sub>Si<sub>8</sub>N system is shown not only by the better results in term of performance and tool life, but also because of the reduced sticking and sliding areas and the higher chip compression ratio;
- A predictive model for flank wear under the cutting conditions considered in the study has been formulated.

The second part of the research is based on the analysis of three-dimensional wear parameters with advanced microscopical technologies. The principal outcomes are summed up in the following list:

- A new 3D volume wear discrete evaluation methodology has been defined, considering that the absolute parameter  $V_v$ , referred to the unworn tool corner, implies the introduction of a discontinuity error, filtering the BUE and confusing the adhesion of material with the chipping of the insert;

## Conclusion

### 4.7 Scanning Electron Microscope (SEM) analysis

---

- Independently from the coating, for machining Inconel DA 718 with carbide tools, the volumetric tool wear increases exponentially, reaching the end of life when  $\sum V_{v_{discr_i}}$  is around  $2 * 10^7 \mu m^3$ ;
- SEM observations and EDS analysis confirmed that KC5010 has less lubricity than the nanocomposite structure, because of the high amount of built-up edge on the tool-tip. Conversely, TiAlCrN/TiCrAl52Si8N is more fragile than the benchmark; indeed, the principal tool wear mode is in this case chipping.

## Chapter 6: Future Works

The following suggestions are recommended to researchers as future work to expand this study:

- Adding to the optimization model for machining costs and productivity based on the Taylor's equation also the effect of chipping and adhesion of material (BUE), in order to obtain coherent  $V_{cp}$  and  $V_{ce}$  and the associated tool lives. Furthermore, it is important to calibrate the model on the experimental results, so that it could be employed from companies also to predict the best cutting parameters when the boundary conditions (i.e. costs, time) are changing;
- Examine the evolution of the three-dimensional wear parameters (chipping and BUE) using etching to remove the BUE after every pass. By comparing the values of  $V_v$  and  $V_p$  before and after the etching procedure, it will be possible to trace accurate curves and confirm the outcomes of the traditional measurement;
- Executing more repetitive tests, to validate the positive effects of nanocomposite coatings using ANOVA with low significance level. Moreover, more data can be useful also to verify the correlation between  $V_{BB} = 300\mu m$  and  $\sum V_{v_{discr_i}} = 2 * 10^7 \mu m^3$ , so to propose a new standardized definition of end of life, in addition to what is nowadays considered in the ISO 3685 normative;
- Verify if, applying the same measurements for the 3D volume wear, also other coatings lead to an exponential growth and if the parameters  $a$  and  $b$  of the fitting are related to the cutting speed variation.



# References

- [1] J. Cantero, J. Díaz-Álvarez, M. Miguélez e N. Marín, «Analysis of tool wear patterns in finishing turning of Inconel 718,» *Wear*, vol. 297, p. 885–894, 2013.
- [2] R. M'Saoubi, D. Axinte, S. Soo, C. Nobel, H. Attia, G. Kappmeyer, S. Engin e W. Sim, «High performance cutting of advanced aerospace alloys and composite materials,» *CIRP Ann.*, n. 64, p. 557–580, 2015.
- [3] S. Sui, J. Chen, E. Fan, H. Yang, X. Lin e W. Huang, «The influence of Laves phases on the high-cycle fatigue behavior of laser additive manufactured Inconel 718,» *Mater. Sci. Eng. A.*, vol. 695, pp. 6-13, 2017.
- [4] A. Thakur e S. Gangopadhyay, «State-of-the-art in surface integrity in machining of nickel-based super alloys,» *Int. J. Mach. Tools Manuf.*, n. 100 , p. 25–54, 2016.
- [5] J.-T. Baek, W.-S. Woo e C.-M. Lee, «A study on the machining characteristics of induction and laser-induction assisted machining of AISI 1045 steel and Inconel 718,» *J. Manuf. Process.*, n. 34 , p. 513–522, 2018.
- [6] D. Ulutan e T. Ozel, «Machining induced surface integrity in titanium and nickel alloys: A review,» *Int. J. Mach. Tools Manuf.*, n. 51, p. 250–280, 2011.
- [7] W. Grzesik, P. Niesłony, W. Habrat, J. Sieniawski e P. Laskowski, «Investigation of tool wear in the turning of Inconel 718 superalloy in terms of process performance and productivity enhancement,» *Tribol. Int.*, n. 118, p. 337–346, 2018.

- [8] S. Olovsjö e L. Nyborg, «Influence of microstructure on wear behaviour of uncoated WC tools in turning of Alloy 718 and Waspaloy,» *Wear*, n. 282–283, p. 12–21, 2012.
- [9] R. M'Saoubi, T. Larsson, J. Outeiro, Y. Guo, S. Suslov, C. Saldana e S. Chandrasekar, «Surface integrity analysis of machined Inconel 718 over multiple length scales,» *CIRP Ann*, n. 61, p. 99–102, 2012.
- [10] E. Ezugwu, «Key improvements in the machining of difficult-to-cut aerospace superalloys,» *Int. J. Mach. Tools Manuf.*, vol. 45, p. 1353–1367, 2005.
- [11] D. Zhu, X. Zhang e H. Ding, «Tool wear characteristics in machining of nickel-based superalloys,» *Int. J. Mach. Tools Manuf.*, p. 60–77, 2013.
- [12] V. Bushlya, J. Zhou e J. Ståhl, «Effect of Cutting Conditions on Machinability of Superalloy Inconel 718 During High Speed Turning with Coated and Uncoated PCBN Tools,» *Procedia CIRP*, n. 3, pp. 370-375, 2012.
- [13] G. Fox-Rabinovich, K. Yamamoto, M. Aguirre, D. Cahill, S. Veldhuis, A. Biksa, G. Dosbaeva e L. Shuster, «Multi-functional nano-multilayered AlTiN/Cu PVD coating for machining of Inconel 718 superalloy,» *Surface and Coatings Technology*, vol. 204, n. 15, pp. 2465-2471, 2010.
- [14] G. Dosbaeva, S. Veldhuis, K. Yamamoto, D. Wilkinson, B. Beake, N. Jenkins, A. Elfizy e G. Fox-Rabinovich, «Oxide scales formation in nano-crystalline TiAlCrSiYN PVD coatings at elevated temperature,» *Int. J. Refract. Met. Hard Mater.*, n. 28 , p. 133–141, 2010.
- [15] M. Salio, T. Berruti e G. D. Poli, «Prediction of residual stress distribution after turning in turbine disks,» *Int. J. Mech. Sci.* , n. 48 , p. 976–984, 2006.

- [16] R. Arunachalam, M. Mannan e A. Spowage, «Residual stress and surface roughness when facing age hardened Inconel 718 with CBN and ceramic cutting tools,» *Int. J. Mach. Tools Manuf.* , n. 44, p. 879–887, 2004.
- [17] A. Sharman, J. Hughes e K. Ridgway, «An analysis of the residual stresses generated in Inconel 718TM when turning,» *J. Mater. Process. Technol.*, n. 173, pp. 359-367, 2006.
- [18] A. Madariaga, J. Esnaola, E. Fernandez, P. Arrazola, A. Garay e F. Morel, «Analysis of residual stress and work-hardened profiles on Inconel 718 when face turning with large-nose radius tools,» *Int. J. Adv. Manuf. Technol.*, n. 71, p. 1587–1598, 2014.
- [19] S. Soo, S. Khan, D. Aspinwall, P. Harden, A. Mantle, G. Kappmeyer, D. Pearson e R. M'Saoubi, «High speed turning of Inconel 718 using PVD-coated PCBN tools,» *CIRP Ann.*, n. 65 , p. 89–92, 2016.
- [20] M. Chowdhury, S. Chowdhury, K. Yamamoto, B. Beake, B. Bose, A. Elfizy, D. Cavelli, G. Dosbaeva, M. Aramesh, G. Fox-Rabinovich e S. Veldhuis, «Wear behaviour of coated carbide tools during machining of Ti6Al4V aerospace alloy associated with strong built up edge formation,» *Surf. Coatings Technol.*, pp. 319-327, 2017.
- [21] J. Yuan, G. S. Fox-Rabinovich e S. C. Veldhuis, «Control of tribofilms formation in dry machining of hardened AISI D2 steel by tuning the cutting speed,» 2017.
- [22] B. Beake, J. Endrino, C. Kimpton, G. Fox-Rabinovich e S. Veldhuis, «Elevated temperature repetitive micro-scratch testing of AlCrN, TiAlN and AlTiN PVD coatings,» *Int. J. Refract. Met. Hard Mater.* , n. 69 , p. 215–226, 2017.

- [23] B. Beake e G. Fox-Rabinovich, «Progress in high temperature nanomechanical testing of coatings for optimising their performance in high speed machining,» *Surf. Coatings Technol.*, n. 255 , p. 102–111, 2014.
- [24] G. Dosbaeva, S. Veldhuis, A. Elfizy, G. Fox-Rabinovich e T. Wagg, «Microscopic Observations on the Origin of Defects During Machining of Direct Aged (DA) Inconel 718 Superalloy,» *Journal of Materials Engineering and Performance*, 2009.
- [25] SAE International, “SAE Aerospace Material Specifications AMS 5xxx,” 2018. [Online]. Available: <https://www.sae.org/publications/collections/content/dlibstd-ams/>.
- [26] Special Metals Corporation, «Publication Number SMC-045,» U.S.A., 2007.
- [27] D. Deng, R. L. Peng, H. Brodin e J. Moverare, «ScienceDirect,» 14 December 2017. [Online]. Available: <https://www.sciencedirect.com/science/article/pii/S0921509317316416#bib2>.
- [28] United Performance Metals, “UPM,” [Online]. Available: <https://www.upmet.com/products/nickel-alloys/alloy-718>.
- [29] Maher, « Maher Limited 2018,» 2018. [Online]. Available: <https://www.maher.com/media/pdfs/718-datasheet.pdf>.
- [30] Wikipedia, «The Free Encyclopedia,» 24 January 2018. [Online]. Available: <https://en.wikipedia.org/wiki/Inconel>.
- [31] K. Bouzakis, E. Bouzakis, S. Kombogiannis, S. Makrimalakis, G. Skordaris, N. Michailidis, P. Charalampous, R. Paraskevopoulou, R. M’Saoubi, J. C. Aurich, F. Barthelmä, D. Biermann, B. Denkena, D. Dimitrov, S. Engin, B. Karpuschewski, F. Klocke, T. Özel, G. Poulachon, J. Rech, V. Schulze, L.

Settineri, A. Srivastava, K. Wegener, E. Uhlmann e P. Zeman, «Effect of cutting edge preparation of coated tools on their performance in milling various materials,» *CIRP journal of manufacturing science and technology*, vol. 7, n. 3, pp. 264-273, 2014.

- [32] L. Settineri, M. G. Faga e B. Lerga, «Properties and performances of innovative coated tools for turning Inconel,» in *International journal of machine tools & manufacture*, Elsevier, 2008, pp. 815-823.
- [33] A. Biksa, K. Yamamoto, G. Dosbaeva, S. Veldhuis, G. Fox-Rabinovich, A. Elfizy, T. Wagg e L. Shuster, «Wear behavior of adaptive nano-multilayered AlTiN/MexN PVD coatings during machining of aerospace alloys,» *Tribology International*, 2010.
- [34] A. R. C. Sharman, J. I. H. e K. Ridgway, «Workpiece Surface Integrity and Tool Life Issues When Turning Inconel 718™ Nickel Based Superalloy,» *Machining Science and Technology*, pp. 399-414, 2004.
- [35] A. Inspektor e P. A. Salvador, «Architecture of PVD coatings for metalcutting applications: A review,» *Surface & Coatings Technology*, n. 257, pp. 138-153, 2014.
- [36] F. Barthelmä, H. Frank, M. Schiffler e A. Bartsch, «Hard coatings to improve the machining of nickel based materials,» *CIRP Conference on High Performance Cutting*, n. 46, pp. 294-298, 2016.
- [37] Y. Chen, H. Du, M. Chen, J. Yang, J. Xiong e H. Zhao, «Structure and wear behavior of AlCrSiN-based coatings,» *Applied Surface Science*, n. 370, pp. 176-183, 2016.
- [38] S. Veprek e M. J. Veprek-Heijman, «Industrial applications of superhard nanocomposite coatings,» *Surface & Coatings Technology*, n. 202, pp. 5063-5073, 2008.

- [39] M. A. Xavior, M. Manohar, P. Jeyapandiarajan e P. M. Madhukar, «Tool Wear Assessment During Machining of Inconel 718,» *Procedia Engineering*, vol. 174, pp. 1000-1008, 2017.
- [40] W. Grzesik, *Advanced Machining Processes of Metallic Materials*, Elsevier, 2017.
- [41] M. C. Shaw, *Metal cutting principles*, Oxford, 2004.
- [42] Walter Tools, «Walter Tools Wear Optimization App,» 2018. [Online]. Available: <https://www.walter-tools.com/SiteCollectionDocuments/woa/index.html#turning/turningIso>.
- [43] W. Reynolds, «Okuma Crown CNC Lathe,» Hamilton, 2004.
- [44] Optimax Imaging Inspection Measurement, «ALICONA INFINITE FOCUS G5,» 2018. [Online]. Available: <http://www.optimaxonline.com/non-contact-metrology-3d-surface-characterisation/37/alicona-infinitefocus-g5>.
- [45] TESCAN Digital Microscopy Imaging, «Scanning Electron Microscope VEGA II,» Brno.
- [46] Kennametal, «ISO Carbide Insert,» [Online]. Available: <https://www.kennametal.com/en/products/20478624/47535256/63745063/63745065/63840303/63840318/55735598/100003623.html>.
- [47] KOBELCO Advanced Coating Industry, «KOBELCO PVD TECHNOLOGY,» 2018. [Online]. Available: <https://www.pvd-coating-kobelco.com/products/aip.html>.
- [48] KENNAMETAL Inc., «Grades,» May 2018. [Online]. Available: <https://www.kennametal.com/en/products/20478624/556249/3925999/4283287/100002780/grades.html.html>.

- [49] S. Zhang, D. Sun, Y. Fu e H. Du, «Recent advances of superhard nanocomposite coatings: a review,» *Surface and Coatings Technology*, vol. 167, n. 2-3, pp. 113-119, 2003.
- [50] Commonwealth Oil Corporation, «CommCool HD,» 2010. [Online]. Available: <http://commonwealtheoil.com/products/semi-synthetic-coolants/commcool-hd/>.
- [51] J. A. P. M. Q. Meng, «Calculation of optimum cutting conditions for turning operations using a machining theory,» *International Journal of Machine Tools & Manufacture*, n. 40, pp. 1709-1733, 2000.
- [52] A. P. Kulkarni e V. G. Sargade, «Characterization and Performance of AlTiN, AlTiCrN, TiN/TiAlN PVD Coated Carbide Tools While Turning SS 304,» *Materials and Manufacturing Processes*, n. 30:6, pp. 748-755, 2015.
- [53] Kennametal, «Kenclamp Toolholders,» 2018. [Online]. Available: <https://www.kennametal.com/en/products/20478624/47535256/63745063/63745069/63840393/63840463/100004558.html?orderNumber=1875199>.
- [54] CustomPartNet, «Machining Cost Estimator,» 2018. [Online]. Available: <http://www.custompartnet.com/estimate/machining/>.
- [55] Z. Wang, D. Zhou, Q. Deng, W. Xie e G. Chen, «TMS,» 2010. [Online]. Available: [http://www.tms.org/superalloys/10.7449/2010/Superalloys\\_2010\\_343\\_349.pdf](http://www.tms.org/superalloys/10.7449/2010/Superalloys_2010_343_349.pdf).